AN ABSTRACT OF THE DISSERTATION OF

Waduge Jayani Jayasuriya for the degree of Doctor of Philosophy in Mechanical Engineering presented on August 23, 2022.

Title: Computational Modeling of Smoldering Combustion in Wildland Fuels

Abstract approved: _____

Kyle E. Niemeyer

Smoldering combustion in wildland fires is a critical phenomenon that needs in-depth study because it can initiate with weaker ignition sources, can persist for long periods, is difficult to suppress, and can transit to flaming combustion. Cellulose, hemicellulose, and lignin are the major organic constituents within biomass, in varying proportions based on the type of fuel. The goal of this study is to computationally model and analyze smoldering combustion in mixtures of these constituents that represent real forest fuels. Smoldering combustion is modeled using a kinetic scheme that involves kinetic parameters and thermophysical properties. These data can vary depending on the source and the experimental setup used for measurements. Variations in input parameters significantly impact the output calculations. An uncertainty analysis estimated uncertainties associated with these inputs while a sensitivity analysis identified which parameters have higher influence on outputs. Kinetic properties are highly sensitive to the behavior of smoldering combustion and uncertainties associated with them are lower. In contrast, physical properties have higher uncertainties associated and are less sensitive to smoldering behavior. Further, fuel composition, density, oxygen concentration, and moisture content affect smoldering behavior, including propagation speed and peak temperature. Increases in lignin content decrease the propagation speed, while increasing hemicellulose content raises the propagation speed due to variations in rates of pyrolysis. Peak temperature rises with both increasing lignin and hemicellulose content, caused by the formation of ash. When the density of a mixture increases, propagation speed decreases and peak temperature rises. Accurately modeling smoldering in a given fuel requires

characterizing whether moisture content causes expansion. In the context of smoldering ignition, radiative heat sources and hot metal particles can ignite a fire. Chemical kinetics drive the ignition via radiation, while physical properties drive ignition from conduction. Thus, fuels with varying physical and chemical characteristics will behave differently under different ignition sources. The insights gained from the model and these studies act as a novel framework for predicting smoldering combustion of forest fuels in wildland fires.

Computational Modeling of Smoldering Combustion in Wildland Fuels

by

Waduge Jayani Jayasuriya

A DISSERTATION

submitted to

Oregon State University

in partial fulfillment of
the requirements for the
degree of

Doctor of Philosophy

Presented August 23, 2022
Commencement June 2023

Doctor of Philosophy dissertation of Waduge Jayani Jayasuriya presented on August 23, 2022.

APPROVED:

Major Professor, representing Mechanical Engineering

Head of the School of Mechanical, Industrial, and Manufacturing Engineering

---

Dean of the Graduate School

I understand that my dissertation will become part of the permanent collection of Oregon State University libraries. My signature below authorizes release of my dissertation to any reader upon request.

Waduge Jayani Jayasuriya, Author

ACKNOWLEDGEMENTS

First and foremost, I would like to thank Dr. Kyle Niemeyer for giving me the opportunity to undertake this research study. I am sincerely grateful for his guidance and support throughout my journey as a graduate student. To me, he has been an excellent role model as a researcher, a teacher, and a leader. I also thank Mr. Benjamin Smucker and Dr. David Blunck from Oregon State University for supporting with their experimental studies. I express my gratitude to all the members of Niemeyer Research Group who helped and encouraged me at crucial times. I also thank my committee for reviewing my work and providing helpful guidance.

I owe the greatest gratitude to my parents, and my sister. I thank them for everything I am now. None of these would be possible without my husband, Dilan Senaratne. I thank him for being there with me for everything and for being an amazing father to our son, Denith.

This research was supported by the Strategic Environmental Research and Development Program (SERDP) award RC-2651 under contract number W912HQ-16-C-0045.

TABLE OF CONTENTS

TABLE OF CONTENTS (Continued)

Page

TABLE OF CONTENTS (Continued)

Page

LIST OF FIGURES

Figure Page

LIST OF FIGURES (Continued)

Figure Page

LIST OF FIGURES (Continued)

Figure Page

LIST OF FIGURES (Continued)

Figure Page

LIST OF TABLES

LIST OF APPENDIX FIGURES

Figure Page

LIST OF APPENDIX FIGURES (Continued)

Figure Page

LIST OF APPENDIX FIGURES (Continued)

Figure Page

LIST OF APPENDIX TABLES

Chapter 1: Introduction

Smoldering combustion is slow, low-temperature, flameless burning of porous fuels. The core of any combustion process is a global exothermic reaction that releases heat. Depending on which chemical species (gaseous and solid products) is oxidized, the dominant mode is determined as smoldering or flaming. If the oxidation occurs in the solid phase, smoldering is dominant; if the oxidation occurs in the gas phase, then flaming dominates. Smoldering combustion is one of the leading causes of wildland fires, and contributes to destruction of vegetation, emissions of global greenhouse gases, and other human/ecological hazards [5]. Smoldering can penetrate much deeper into organic soil than flaming combustion, damaging plants' ability to regrow [6]. Even though the spread rate of smoldering is slower than of flames, it can burn for a longer periods of time, making it more difficult to suppress. Smoldering can be initiated with weaker ignition sources and can transition to flaming combustion, and can persist at much lower oxygen concentrations. Smoldering also emits more pollutants than flaming, due to incomplete combustion at lower temperatures [7, 8].

For these reasons, it is important to understand smoldering combustion of forest fuels to better assess the risks associated with wildland fires. An extensive model that can represent any fuel based on its composition and simulate smoldering combustion will assist the analysis of smoldering fires. In addition, an uncertainty analysis together with a sensitivity study will help to increase the accuracy of model predictions in smoldering combustion in wildland fuels.

The behaviour of smoldering combustion is impacted by a wide variety of factors such as fuel composition, density, oxygen concentration, moisture content, inorganic content, and wind speed. Natural fuels like wood, peat, coal, and forest litter can sustain a smoldering fire because of their porous nature. The composition of these fuels differ depending on their anatomy and chemistry. However, the woody fuels are comprised of three common major constituents: cellulose, hemicellulose, and lignin. Each component has different characteristics when it comes to pyrolysis and oxidation [9–11], so the differences in composition can affect the smoldering behavior of different fuels.

Major pathways of initiation of a smoldering ignition are a radiant heat source, hot metal particle, firebrand, self-heating, or transition from a flaming fire. In relation to radiant heat sources, smoldering can ignite at lower radiation heat fluxes. Hot metal particles generated from power lines, mechanical cutting, bullets, and friction in railroads can cause local ignitions that may grow into large fires [12, 13]. Firebrand or ember ignition can cause a secondary fire or spread an existing fire more intensely [14]. So understanding and estimating risks of initiation of fires requires investigating on smoldering ignition via these pathways.

The overall goal of this work is to computationally model and study smoldering combustion of forest fuels in wildland fires. I addressed four specific objectives to provide a framework for achieving the overall goal:

1. How does smoldering combustion occur in real forest fuels? To answer this research question, a deep analysis on smoldering of real fuels is needed considering physical properties of fuels, chemical kinetics of reactions, and environmental parameters. A computational model that can simulate smoldering combustion of any forest fuel based on its composition serves this purpose.

2. How do chemical kinetic parameters and thermophysical properties affect smoldering combustion? To address this conduct uncertainty and sensitivity analysis.

3. How do physical and environmental conditions affect smoldering behavior? To answer this analyze how fuel composition, density, moisture content and oxygen concentration affect smoldering behavior.

4. How does smoldering combustion initiate? To address this, investigate smoldering ignition via radiation and conduction of real forest fuels.

The structure of this dissertation is as follows. First, the current state of knowledge is summarized as it applies to this work (Chapter 2). A literature review specific to each objective is contained in the corresponding manuscripts. The results of this effort are then presented in manuscript form, followed by the overall conclusions, and suggestions for future work. The first manuscript presents the experimentally validated computational model for smoldering combustion of cellulose and hemicellulose mixtures and analyzes the roles of density, fuel composition, oxygen concentration, and moisture content on smoldering behaviour (Chapter 3). The second manuscript presents the experimentally validated

computational model that simulates real fuels as mixtures of cellulose, hemicellulose, and lignin, and analyzes the smoldering behaviour (Chapter 4). The third manuscript analyzes uncertainty and sensitivity of chemical kinetic parameters and thermophysical properties used in the model (Chapter 5). The fourth manuscript investigates ignition of smoldering combustion via radiation and ignition using the developed model (Chapter 6). Chapter 7 summarizes the conclusions of each manuscript. Appendix A presents the experimental and computational analysis of the influence of lignin on smoldering propagation, which includes the details of the experimentally validated model.

It is anticipated that this work will provide insights and a basis to accurately predict behaviour of smoldering combustion and ignition of forest fuels in wildland fires. The developed model has the flexibility to simulate any fuel as a mixture of cellulose, hemicellulose and lignin based on its composition. The detailed uncertainty analysis will help to bound the uncertainty in computed results from the model. The sensitivity analysis quantitatively analyzes the influence of input parameters to identify the level of the influence on output estimates. For the parameters that have significant effects on simulation results, their uncertainties should be given higher priority in computational models. The developed model and the results of this work help better understand and predict smoldering phenomena in wildfires. Thus, this work assists to close a significant gap in the current knowledge of smoldering combustion of forest fuels in wildland fires.

Chapter 2: Background

This chapter discusses the background and motivation of this work in further depth than the manuscripts presented later in this dissertation. Here, a general overview of smoldering combustion as a threat in wildfires and the current state of knowledge and predictive capabilities is communicated. Each manuscript includes a relevant and more detailed literature review pertaining to the specific objective of the chapter.

2.1 Smoldering in wildfires

In wildfires, smoldering can happen in thick fuels like wood logs and in forest-bed fuels like duff or peat. Thick fuels exhibit residual smoldering combustion, where combustion takes place days after a flaming fire has passed. Smoldering in forest bed fuels is more dangerous and can be severe. In general, up to 50% or more of the total burned biomass during wildfires are due to smoldering combustion [15, 16].

Smoldering fires occur with some frequency worldwide. One of the most studied and well known large smoldering wildfire took place in Indonesia in 1997 and led to an extreme haze event. The smoke covered large parts of South-East Asia, Australia, and China [17]. In July 2006 another megafire occurred in Rothiemurchus, Scotland, where the flaming fire was extinguished within three days while smoldering lasted for more than 40 days [1]. In recent years, the Louise Creek Coal Seam 2018 Fire near Healy, Alaska-which burned 1,900 acres was sparked by a smoldering coal seam. In 2020, the Archie Creek Fire in Oregon burned nearly 140,000 acres. Some smoke was visible from smoldering stumps and logs within the fire perimeter until extinguished by rain [18]. Another characteristic of smoldering fires is that they can continuously burn for years. The best example is the Burning Mountain in New South Wales, Australia, which is a large coal seam that has been smoldering for more than 6000 years [6]. These examples show that smoldering wildfires have brought catastrophic impacts from the past to today, highlighting the importance of expanding the understanding in the area to minimize risks and hazards.

Smoldering combustion can occur in surface and ground fuels within forest fuel beds.

Forest fuel beds consist of three layers: the top (litter) layer, middle (fermentation) layer, and bottom (humus) layer. Twigs, needles, and leaves mostly comprise the litter layer, where smoldering can initiate. Thick fuels like tree branches or logs can lay on the top layer, which can also smolder. Larger smoldering fires occur in duff and peat fuels, which are present in fermentation and humus layers [19]. The major common organic constituents of these fuels are cellulose, hemicellulose, and lignin [20]. In a typical lignified cell, cellulose represents an important structural element that is surrounded by other substances that function as matrix (hemicellulose) and encrusting (lignin) materials. The composition of these constituents within a fuel varies significantly depending on the fuel source [21]. The major constituent of duff and peat is lignin, where as hemicellulose dominates twigs and needles. In contrast, cellulose makes up around 50% of softwood and hardwood.

Each component has different characteristics when it comes to pyrolysis and oxidation. Gani and Naruse discussed pyrolysis and combustion characteristics of cellulose and lignin for several types of biomass [9]. They identified two stages during burning: (1) cellulose decomposition and (2) lignin decomposition for pyrolysis, and then combustion of its char. They concluded that the amounts of cellulose and lignin in biomass play major roles in pyrolysis and char oxidation. Yang, using a thermogravimetric analysis, identified that hemicellulose and cellulose pyrolyze earlier than lignin [22]. In addition, lignin produces the highest solid residue during pyrolysis. Dorez et al. found that natural fibers with a higher composition of lignin yield more char, and have higher effective heat of combustion, and higher activation energy of combustion [11]. These studies show that the three constituents have different and unique characteristics when it comes to pyrolysis and oxidation. Since smoldering combustion represents the combined effects of pyrolysis and oxidation reactions, fuels with different composition could exhibit differences in smoldering behavior. An extensive study on smoldering behaviour incorporating all three constituents that represent mixtures of real fuels will be beneficial to enhance understanding and provide estimates of smoldering wildfires.

2.2 Smoldering combustion and modeling

Smoldering has the core global exothermic reaction that releases heat similar to other combustion processes. Hence, the oxidation mostly takes place in the solid phase in

smoldering. First the solid undergoes pyrolysis, resulting gaseous and solid products. Then, both the pyrolysate and char oxidize. Char oxidation involves solid and gaseous species and is a heterogeneous reaction. This occurs on the char produced by pyrolysis, which leads to smoldering combustion. Char is a carbon-rich porous material that has a high surface-to-volume ratio and a high heat of reaction. With the availability of oxygen, oxidation processes release heat for a self-sustaining smolder. Ash (a mineral-rich residue) is left after occurrence of the fire [15]. Kinetic schemes to represent smoldering combustion can vary depending on the complexity a numerical model can handle and the level of accuracy expected [15]. Figure 5.2 shows three kinetic schemes that are commonly used. These schemes lack the ability of representing smoldering combustion of a given forest fuel as a mixture of cellulose, hemicellulose, and lignin.

(I) 3-step scheme

$$\text{biomass} \cdot \nu_{w,dr}\text{H}_2\text{O} \rightarrow \text{biomass} + \nu_{w,dr}\text{H}_2\text{O(g)}$$
$$\text{biomass} \rightarrow \nu_{\alpha,pp}\alpha\text{-char} + \nu_{g,pp}\text{gas}$$
$$\alpha\text{-char} + \nu_{O_2,\alpha o}\text{O}_2 \rightarrow \nu_{a,\alpha o}\text{ash} + \nu_{g,\alpha o}\text{gas}$$

(II) 5-step scheme

$$\text{biomass} \cdot \nu_{w,dr}\text{H}_2\text{O} \rightarrow \text{biomass} + \nu_{w,dr}\text{H}_2\text{O(g)}$$
$$\text{biomass} \rightarrow \nu_{\alpha,pp}\alpha\text{-char} + \nu_{g,pp}\text{gas}$$
$$\text{biomass} + \nu_{O_2,po}\text{O}_2 \rightarrow \nu_{\beta,po}\beta\text{-char} + \nu_{g,po}\text{gas}$$
$$\beta\text{-char} + \nu_{O_2,\beta o}\text{O}_2 \rightarrow \nu_{a,\beta o}\text{ash} + \nu_{g,\beta o}\text{gas}$$
$$\alpha\text{-char} + \nu_{O_2,\alpha o}\text{O}_2 \rightarrow \nu_{a,\alpha o}\text{ash} + \nu_{g,\alpha o}\text{gas}$$

(III) 9-step scheme

$$\text{biomass} \cdot \nu_{w,dr}\text{H}_2\text{O} \rightarrow \text{biomass} + \nu_{w,dr}\text{H}_2\text{O(g)}$$
$$\text{H} \rightarrow \nu_{\alpha,hp}\alpha\text{-char} + \nu_{g,hp}\text{gas}$$
$$\text{C} \rightarrow \nu_{\alpha,cp}\alpha\text{-char} + \nu_{g,cp}\text{gas}$$
$$\text{L} \rightarrow \nu_{\alpha,lp}\alpha\text{-char} + \nu_{g,lp}\text{gas}$$
$$\text{H} + \nu_{O_2,ho}\text{O}_2 \rightarrow \nu_{\alpha,hp}\beta\text{-char} + \nu_{g,hp}\text{gas}$$
$$\text{C} + \nu_{O_2,co}\text{O}_2 \rightarrow \nu_{\alpha,cp}\beta\text{-char} + \nu_{g,cp}\text{gas}$$
$$\text{L} + \nu_{O_2,lo}\text{O}_2 \rightarrow \nu_{\alpha,lp}\beta\text{-char} + \nu_{g,lp}\text{gas}$$
$$\beta\text{-char} + \nu_{O_2,\beta o}\text{O}_2 \rightarrow \nu_{a,\beta o}\text{ash} + \nu_{g,\beta o}\text{gas}$$
$$\alpha\text{-char} + \nu_{O_2,\alpha o}\text{O}_2 \rightarrow \nu_{a,\alpha o}\text{ash} + \nu_{g,\alpha o}\text{gas}$$

Figure 2.1: Different kinetic schemes proposed for biomass smoldering [23]

Kinetic parameters and thermophysical properties that are used by a model play an important role for accurately predicting smoldering behaviour due to their impacts on energy balances and chemical equilibrium [24]. These kinetic parameters and thermophysical property values can have different ranges depending on the source and the experiments used to determine them. Computed quantities such as propagation speed and peak temperature will also vary with parameter ranges in input parameters. Therefore, conducting uncertainty analysis is important to identify the effects of these parameters on smoldering behavior, and bound the uncertainty of computed results. Anca-Couce [20]

reviewed chemical kinetic schemes and multi-scale modeling of lignocellulosic biomass pyrolysis using 10 chemical kinetic models, but did not consider the differing effects of these models/model parameters on outputs. Anca-Couce et al. [25] earlier studied kinetics and reaction heats of smouldering of pine wood, providing input parameters that are needed to model smoldering of pine wood. However, they did not examine the uncertainly associated with these parameters. Similarly, a number of studies [26, 27] focused on finding kinetic schemes and parameters that represent smoldering combustion, but to my knowledge none have focused on the uncertainties associated with these parameters and the impacts of these uncertainties. Thermochemical properties that are chosen for a particular kinetic scheme can vary depending on the source of information or experimental setup where these are measured [28–32]. With varying input parameters, the computed outputs are uncertain, hence an uncertainty analysis can bound the variations in output parameters.

While identifying uncertainties associated with kinetic parameters and thermophysical properties is important, it is also important to quantitatively analyze the influence of these different parameters. A sensitivity analysis can be used to identify the level of the influence on output estimates. High priority should be given to the uncertainties of parameters that have significant effects on simulation results. Such parameters should be measured accurately and uncertainties must be captured more precisely. A local sensitivity analysis can be used to study the sensitivity relative to change of a single parameter value, while a global analysis can be used to examine the sensitivity with regard to the entire parameter space. Yuan et al. [33] developed a computational model to simulate self-heating ignition for coal origins. They conducted a local sensitivity analysis using a one-at-a-time method to assess the significance of kinetic and physical parameters on ignition temperature. They found that activation energy has the highest impact on ignition temperature and suggested that activation energy should be optimized when considering measurement of uncertainty. Hence, an uncertainty analysis together with a sensitivity study will help to accurately predict smoldering combustion in wildland fuels.

2.3 Smoldering behavior

General parameters used to characterize smoldering are temperature, spread rate, and power of combustion. The peak temperatures for smoldering are in the range of 450 °C to

700 °C, compared to around 1500 °C for flaming. The spread rate is around 1 mm/min, which is two orders of magnitude slower than flame spread. The effective heat of combustion is in the range from 6 to 12 kJ/g, where it is 16–30 kJ/g for flaming. These values are very general and change depending on the chemical nature of the smoldering fuel, which encourages examining the behavior of different types of fuels [15].

In addition to fuel composition, other major parameters that include the behavior of smoldering include density, moisture content, oxygen supply, and inorganic content [34–37]. Natural density of fuels also differs based on their anatomy. For example, cotton is mainly composed of cellulose, and smoldering propagation speed in cotton varies 2–4 mm/min over the density range 5–10 kg/m^3 [25]. In contrast, smoldering in peat which is a mixture of cellulose, hemicellulose, and lignin, propagates at speeds of 0.083–0.333 mm/min for densities of 130–180 kg/m^3 [38]. The substantial variance in smoldering propagation between these fuels shows its dependence on fuel composition and density. Hartford observed through experiments that the probability of sustained combustion drops with increases in the bulk density of organic soil [39]. Chen, Rein, and Liu studied the relationship between bulk density and critical moisture content, and observed a nearly linear decrease in critical moisture content with increases in organic bulk density of peat moss [36]. Mulky and Niemeyer numerically observed a decrease in propagation speed and an increase in peak temperature with density for cellulose and hemicellulose mixtures [1]. Smucker et al. experimentally saw similar trends for cellulose and hemicellulose mixtures [40]. However, real woody fuels contains large amount of lignin, so its important to incorporate lignin in models.

Moisture content is expressed as a percentage, defined in dry basis as mass of water in the fuel divided by mass of the dry fuel. It is an important governing parameter for ignition and spread of smoldering, since porous media like woody fuels can hold moisture from 10% to as high as 300% [5, 41]. Huang and Rein reported an increase in spread rate with moisture content for peat [38]. Peat expands with addition of water, which they took into account, but most woody fuels do not expand with moisture content, so trends can change for biomass based on its origin.

Another important parameter that needs attention is oxygen supply, since smoldering is limited by diffusion of oxygen from atmosphere into the fuel. For horizontal spread in peat smoldering fires, Yan and Fujita found that increases in mass fraction of oxygen transitions the charring to surface glowing combustion in the upper surface of a peat

layer [42]. For upward and downward smoldering, Huang and Rein found the flow of water vapor and pyrolysis gases across the peat layer impacts oxygen diffusion [43]. Huang and Rein identified an interdependency between oxygen concentration and fuel moisture in smoldering of peat fires [34]. As moisture content increases, greater increases in oxygen concentration are needed to achieve ignition and prevent extinction. However, such a study has not yet been conducted for more-general mixtures of cellulose, hemicellulose, and lignin. It is evident that fuel composition, density, moisture content, and oxygen supply impact smoldering behavior, and thus understanding the parameters that control smoldering in woody fuels requires studying their effects.

2.4 Smoldering ignition

Smoldering ignition can be initiated by a radiant heat source, hot metal particle, firebrand, by self-heating or from a flaming fire. In relation to radiant heat sources, we know that smoldering can ignite at lower radiation heat fluxes. For polyurethane foam the critical radiation heat flux for smoldering ignition is $7\,\mathrm{kW/m^2}$, while for flaming ignition it is $30\,\mathrm{kW/m^2}$ [44]. Jones et al. developed a method to evaluate the risk of smoldering ignition based on the activation energy for pyrolysis and a characteristic temperature from thermogravimetric analysis for different biomass types, and ranked these from low to high risk [45]. However, they did not discuss the minimum ignition heat fluxes or exposure times of different heat fluxes—these two parameters drive smoldering ignition. For polyurethane foam a few studies have examined the minimum ignition heat fluxes and exposure times of different heat fluxes [44, 46]. Anderson, Sleight, and Torero observed a self-sustained smolder with a heat flux of 6.1–$6.8\,\mathrm{kW/m^2}$ while Hadden et al. reported a minimum heat flux of $7\,\mathrm{kW/m^2}$ for polyurethane foam, indicating the sample size also plays a role [44, 46]. Gratkowski, Dembsey, and Beyler conducted a similar study for plywood and found a minimum ignition flux of $7.5\,\mathrm{kW/m^2}$ for an 18 mm thick maple plywood block [47]. Most of these studies focused on materials not relevant to wildland fires.

Spot ignition by firebrands and metal particles is another common and important ignition pathway. Firebrand or ember ignition can cause a secondary fire or spread an existing fire more intensely [14]. Some well-known fires that started off by firebrand spot ignition include the 1998 Florida wildfires, 2007 Witch Greek fire, and 2015 Butte fire

[14, 48]. Hot metal particles generated from power lines, mechanical cutting, bullets, and friction in railroads can cause local ignitions that may grow into large fires. Examples of fires started by particles produced by powerlines or rebar cutting/welding include the 2007 Witch Creek and Guejito fires [12], the 2011 Bastrop County Complex wildfire in Texas [49] and the Taylor Bridge fire in Washington [13]. For global context, in recent years many fires in New Zealand and Australia have been ignited by hot particles [50, 51].

In the context of spot ignition there are number of studies done for natural fuels, however these experimental studies mostly focus on flaming ignition [52–57]. There are limited number of studies of smoldering ignition of natural fuels. Most of them are based on experimental work focused on a specific experimental setup. A validated numerical model can simulate a number of scenarios by changing the natural fuel, material of the ignition source, fuel density, and fuel moisture content which will be helpful in estimating spot ignition risks. Wang et al. studied smoldering, flaming ignition, and smoldering-to-flaming transition of pine needles for various moisture contents by hot large stainless steel particles [48]. They developed an empirical correlation for ignition temperature, moisture content, and particle diameter. Urban et al. experimentally studied smoldering ignition of a grass blend powder by hot steel and aluminum particles accompanied by a simplified numerical study [58]. They found that decreases in particle size require increased temperature to ignite, and the energy from melting allows aluminum particles to ignite at lower temperatures. However, this experiment was only done for one specific grass blend fuel. For their modelling effort they developed a one-dimensional, three-step reaction model, which is solved with an implicit finite-volume scheme using adaptive time stepping. Both of the above modelling efforts have their limitations due to the simplifications and assumptions. However, they provide useful experimental data which can be used as a guidance to verify other relevant numerical models in hot-particle smoldering ignition. A computational study that models both radiant and conductive ignition of real fuels and analyzes smoldering ignition based on fuel composition will be helpful in estimating risks in smoldering ignition.

2.5 Gas emissions

Preheating, evaporation, pyrolysis, and oxidation are the main reaction steps of smoldering [59, 60]. Preheating and evaporation occurs in a temperature below 100 °C, and the emission is only large quantities of water vapor. Pyrolysis occurs at temperatures above 200 °C and in the absence of oxygen, forming char and emitting volatile organic species, CO_2, CO, and water vapor. Significant amounts of CO_2 and CO are released in the exothermic char oxidation with a temperature over 350 °C.

Emissions from smoldering fires are weakly buoyant, so wind easily drives them to migrate long distances [61]. The emissions are comprise of incomplete combustion gases and aerosols containing significant quantities of particulate matter (PM). These aerosols ranges from ultrafine particles (aerodynamic diameter $\leq 0.1\,\mu m$) to PM_1 ($\leq 1\,\mu m$), $PM_{2.5}$ ($\leq 2.5\,\mu m$) and PM_{10} ($\leq 10\,\mu m$) [62]. Carbon emissions are important when it comes to global climate change and the carbon budget balance. For example, the 1997 Southeast Asia extreme peat fire event released carbon emissions equivalent to 13–40% of the mean annual global carbon emissions from fossil fuels of that year. Fire particles are also important considerations for local air quality and health, since these small particles can damage lungs. These facts show the importance of estimating the emissions from smoldering fires to provide a better understanding about the impacts on global climate change, the carbon budget balance, and human health. There are only limited methods available for measuring and estimating emissions from smoldering.

Rein, Cohen, and Simeoni conducted experiments of shallow and strong smoldering fronts in boreal peat under laboratory conditions to study emissions of the CO and CO_2 at steady state burning conditions. The CO yield in dry base is 17% g/g and the CO_2 yield 42% g/g. The CO and CO_2 total yield is 59% g/g, and the CO to CO_2 ratio is on average 0.43. They also studied the impact of moisture content and found that high moisture content produces more CO_2 but the same CO yield compared to dryer peat [59]. Hu et al. conducted an experimental study to estimate steady and transient gas and particle emissions from smoldering combustion of peat [60]. They identified CO_2, CO, CH_4, and NH_3 as the four most predominant gas species emitted in the steady stage based on mass flux measurements. Incorporating the mass loss rate, they calculated the transient emission factors of both gas and particle species. Density and inorganic content can also impact the level of emissions. Hu, Cui, and Rein found that peat with

high inorganic content releases lower gas fluxes, specifically CH_4 and NH_3 [63]. Also they saw that increasing bulk density decreased both gas and particle emissions without significantly altering the smoke composition. These information shows that smoldering emissions have characteristic differences depending on the fuel type and condition.

Capturing the released gas species in a smoldering fire and calculating total emissions is the next important study in this context. The total emissions (E_T) can be approximated using,

$$E_T = A \times B \times C \times EF \ , \tag{2.1}$$

where A is annual burnt area (m^2 $year^{-1}$), B is the total fuel load (g dry matter m^{-2}), C is burning efficiency and EF is the emission factor, defined as the mass of the species emitted per mass of dry fuel consumed. EF for species i can be calculated as

$$EF_i = \frac{\dot{m}_i''}{\dot{m}''} \ , \tag{2.2}$$

where $\dot{m}_i''$ is the mass flux of the released species i and $\dot{m}''$ is the total mass loss rate (fuel consumption rate) of the dry fuel. Hu et al. [61] compiled EFs of peat fire gas species that are commonly reported in literature, where 20% of them are field work and rest are laboratory scale studies. They concluded that EF varies considerably in the literature and is highly sensitive to unknown field variables. Experimental studies that capture emissions from smoldering of other forest fuels not seen in literature. This emphasizes that the complexity of natural smoldering fires makes capturing emissions a challenge. Hence more experimental and theoretical studies and a multidisciplinary research approach are needed to enhance the fundamental understanding before a computational model can be developed to capture emissions from smoldering forest fires.

All the above information shows that smoldering combustion in wildland fires can result catastrophic impacts on environment, human life, and human health. Modeling smoldering combustion and studying smoldering behaviour, ignition, and emissions will help to understand, estimate, and mitigate associated hazards and risks.

Chapter 3: Smoldering combustion in cellulose and hemicellulose mixtures: Examining the roles of density, fuel composition, oxygen concentration, and moisture content

Waduge Jayani Jayasuriya, Tejas Chandrashekhar Mulky, and Kyle E. Niemeyer

This study was initiated by Tejas C. Mulky. My contributions to this work included updating the computational model, running simulations, processing the output data, analyzing the results, and preparing the manuscript.

Combustion Theory and Modelling
Vol. 26, 831-855, 2022.
https://doi.org/10.1080/13647830.2022.2071170

3.1 Abstract

Smoldering combustion plays a key role in wildfires in forests, grasslands, and peatlands due to its common occurrence in porous fuels like peat and duff. As a consequence, understanding smoldering behavior in these fuels is crucial. Such fuels are generally composed of cellulose, hemicellulose, and lignin. Here we present an updated computational model for simulating smoldering combustion in cellulose and hemicellulose mixtures. We used this model to examine changes in smoldering propagation speed and peak temperatures with varying fuel composition and density. For a given fuel composition, increases in density decrease the propagation speed and increase mean peak temperature; for a given density, increases in hemicellulose content increase both propagation speed and peak temperature. We also examined the role of natural fuel expansion with the addition of water. Without expansion, addition of moisture content reduces the propagation speed primarily due to increasing (wet) fuel density. However, with fuel expansion similar to that observed in peat, the propagation speed increases due to the overall drop in fuel density. Finally, we studied the influence of fuel composition on critical moisture content of ignition and extinction: mixtures dominated by hemicellulose have 10% higher critical moisture content due to the increase in peak temperature.

3.2 Introduction

Wildland fires lead to human, environmental, and ecological hazards. Global climate change has and will continue to cause increases in the occurrence of droughts, which will in turn lead to an increasing frequency of wildland fires [64, 65]. Combustion in wildland fires, in general, is dominated by either flaming or smoldering combustion. Both types of combustion have different characteristics and can be hazardous in their own way, but flaming combustion has historically received more research compared with smoldering. However, as Rein [66] discussed, smoldering combustion has recently become more recognized as a major fire hazard, resulting in increasing interest in understanding this phenomenon.

Compared with flaming combustion, smoldering can persist longer and under conditions that would extinguish flames. This characteristic of smoldering combustion allows it to penetrate deeper into the soil compared with flaming combustion, which generally

causes shallower burns [5, 67]. Thus, smoldering can actually cause greater destruction in affected ecosystems. Smoldering also emits a large number of pollutants such as carbon monoxide (CO), volatile organic compounds, polycyclic aromatic hydrocarbons, and particulate matter, since it operates at lower temperatures than flaming combustion. Smoldering occurs most commonly in porous fuels like peat, woody fuels, muck, and forest duff [65]. Such fuels are abundant in forests, making it important to understand smoldering combustion in these types of fuels. Woody fuels and biomass generally consist of cellulose, hemicellulose, and lignin in varying proportions, which pyrolyze at different temperatures as shown by Ranzi et al. [68, 69]. Yang et al. [70] found that, among the three, hemicellulose pyrolyzes earliest, at temperatures of 220–315 °C, cellulose undergoes pyrolysis at temperatures of 315–400 °C, and finally lignin pyrolyzes at temperatures of 150–900 °C. Anca-Couce et al. [71] showed similar trends in pyrolysis of these three constituents in their thermogravimetric analysis of pine wood. In addition, these fuel constituents produce different amounts of char [34, 72, 73]. Smoldering combustion is generally modeled using a set of global reactions, which include fuel pyrolysis and char oxidation [71, 74]. Differences in fuel composition thus may lead to significant differences in smoldering characteristics. This motivates our detailed study looking into how varying fuel composition affects smoldering characteristics.

Along with fuel composition, the other parameters that could affect smoldering propagation are density and moisture content. Huang and Rein [38] found that increasing the density of peat by 40% reduces the downward propagation speed by approximately 40%. However, no (computational) studies have looked into how changes in density affect smoldering speed and temperatures in fuel mixtures of cellulose and hemicellulose. In contrast, regarding the effects of moisture content, Huang and Rein [38] studied how moisture content affects the propagation speed of peat and observed an increase in downward propagation speed with moisture content, due to expansion of the peat. Recently, Smucker et al. [40, 75] experimentally observed that smoldering propagation speed in mixtures of cellulose and hemicellulose decreases with density, and attributed this to oxygen availability. They also found that propagation speed increases with additional hemicellulose content in fuel, attributed to faster pyrolysis with addition of hemicellulose, from its lower activation energy and higher heat release.

Critical moisture content is the highest moisture content above which smoldering combustion cannot self-sustain. Garlough and Keyes [76] experimentally studied ponderosa

pine duff and found that fuel consumption decreases after reaching critical moisture content of 57 and 102% on the upper and lower duff, respectively. Frandsen showed experimentally that duff's critical moisture content of ignition drops with inorganic content [77, 78]. Huang and Rein [35, 79] found that natural peat's critical moisture contents of ignition and extinction are around 117% and 250%, respectively, but vary significantly depending upon the thickness of wet layer, dry layer, inorganic content, physical properties, and boundary conditions. However, no studies have looked into the influence of the fuel composition on these threshold values.

In our prior work, we found that propagation speed increases as density drops or hemicellulose content increases for mixtures of cellulose and hemicellulose [1]. Based on prior theories in the literature, we hypothesized that oxygen availability causes the sensitivity to density, and that adding hemicellulose increases propagation speed since it pyrolyzes faster. However, that study did not include an in-depth analysis to examine the proposed hypotheses or their fundamental causes. In addition, for validating the model with experimental results, we relied on a fixed temperature boundary condition, which overconstrained the model. Furthermore, our previous treatment of bulk density for validation case may not represent actual experimental conditions: we fixed the bulk density of hemicellulose and changed the bulk density of cellulose to match the mixture bulk density; in experiments, they change together [40, 75, 80]. The model used in that work did not predict ignition for bulk densities of less than $200\,\mathrm{kg/m^3}$ for 100% cellulose, which disagrees with experimental observations [40, 75]. Here, we use a more-appropriate boundary condition at the upper surface, allow the bulk density of the fuel components to vary independently, and updated physical property values (e.g., particle surface area). This study also expands on the analysis of the reasons behind observed trends in propagation speed and peak temperature, confirms the relationship between oxygen availability and density posited for peat by Huang and Rein [38], confirms—and extend to general fuels—the observation by Huang and Rein [38] that moisture content increases downward smoldering in peat, and also examines the impact of fuel composition on critical moisture content of ignition and extinction.

Building on our prior work, this article presents an updated one-dimensional, transient computational model to simulate smoldering combustion in cellulose and hemicellulose mixtures. First, we validate the model against a different experimental configuration that more closely matches the simulation, and use a heat-flux boundary condition. Following

this model validation, we examine the effects of varying density and fuel composition on smoldering propagation speed and peak temperature, and perform an in-depth analysis to explain the observed trends. Next, we investigate the effects of varying moisture content on smoldering propagation speed and temperature, including and excluding the contribution of fuel expansion with the addition of water. Finally, we identify how varying fuel composition affects the critical moisture content of ignition and extinction.

3.3 Computational model

In this article, we study downward propagation of smoldering using a one-dimensional transient model following approaches of past studies [1]. This model was developed using Gpyro [81]. We performed simulations with a spatial cell size (Δz) of 1×10^{-4} m and an initial time step of 0.05 s. We based this selection of cell size on our previous work, where we showed that further increasing resolution has little impact on global quantities of interest [1].

3.3.1 Governing equations

To model smoldering combustion, we use Gpyro v0.700 [81, 82] to solve the transient governing equations: condensed-phase mass conservation (3.1), condensed-phase species conservation (3.2), gas-phase mass conservation (3.3), gas-phase species conservation (3.4), condensed-phase energy conservation (3.5), gas-phase momentum conservation (3.6), and gas-phase energy conservation (3.7); the ideal gas equation of state (3.8) is needed to close the set of equations. Lautenberger and Fernandez-Pello [82] provide more details about Gpyro. For completeness, the governing equations are:

$$\frac{\partial \overline{\rho}}{\partial t} = -\dot{\omega}'''_{fg} \,, \tag{3.1}$$

$$\frac{\partial (\overline{\rho} Y_i)}{\partial t} = \dot{\omega}'''_{fi} - \dot{\omega}'''_{di} \,, \tag{3.2}$$

$$\frac{\partial (\rho_g \overline{\psi})}{\partial t} + \frac{\partial \dot{m}''}{\partial z} = \dot{\omega}'''_{fg} \,, \tag{3.3}$$

$$\frac{\partial (\rho_g \overline{\psi} Y_j)}{\partial t} + \frac{\partial (\dot{m}'' Y_j)}{\partial z} = -\frac{\partial}{\partial z}(\overline{\psi} \rho_g D \frac{\partial Y_j}{\partial z}) + \dot{\omega}'''_{fj} - \dot{\omega}'''_{dj} \,, \tag{3.4}$$

$$\frac{\partial(\overline{\rho}\overline{h})}{\partial t} = \frac{\partial}{\partial z}(\overline{k}\frac{\partial T}{\partial z}) - \dot{Q}'''_{s-g} + \sum_{k=1}^{K}\dot{Q}'''_{s,k} - \frac{\partial \dot{q}''_r}{\partial z} + \sum_{i=1}^{M}((\dot{\omega}'''_{fi} - \dot{\omega}'''_{di})h_i) \ , \tag{3.5}$$

$$\dot{m}'' = -\frac{\overline{K}}{v}\frac{\partial P}{\partial z} \ , \text{ and} \tag{3.6}$$

$$\frac{\partial(\overline{\psi}\rho_g\overline{h_g})}{\partial t} + \frac{\partial(\dot{m}''_z\overline{h_g})}{\partial z} = \frac{\partial}{\partial z}(\overline{\psi}\rho_g D\frac{\partial \overline{h_g}}{\partial z}) + h_{cv}(T - T_g) + \sum_{j=1}^{N}(\dot{\omega}'''_{s,fj} - \dot{\omega}'''_{s,dj})h^*_{g,j} + \dot{Q}'''_{s-g} \ , \tag{3.7}$$

$$P\overline{M} = \rho_g R T_g \ , \tag{3.8}$$

where ρ is the density, M is the number of condensed-phase species; X is the volume fraction; $\dot{\omega}'''$ is the reaction rate; T is the temperature; Y_j is the jth species mass fraction; ψ is the porosity; K is the permeability/number of reactions; h_{cv} is the volumetric heat transfer coefficient; $\overline{M}$ is the mean molecular mass obtained from local volume fractions of all gaseous species; $\dot{q}''_r$ is the radiative heat-flux; $\dot{Q}'''$ is the volumetric rate of heat release/absorption; R is the universal gas constant; D is the diffusion coefficient; h is the enthalpy; P is the pressure; subscripts f, d, i, j, k, s, and g are formation, destruction, condensed-phase species index, gas-phase species index, reaction index, solid, and gas; and * indicates that gas-phase species enthalpy is calculated at condensed phase temperature. The overbars over ρ, ψ, K, and k mean an averaged value weighted by condensed-phase volume fraction, while the overbar over h indicates an averaged value weighted by condensed-phase mass fraction.

3.3.2 Boundary conditions

The top surface ($z = 0$) of the domain was modeled as open to atmosphere while the bottom surface ($z = L$) was modeled as insulated to match the experimental setup, as Figure 3.1 shows. The pressure (P) at the top surface was 1 atm and the ambient temperature was 300 K. On the top surface we set a convective heat transfer coefficient ($h_{c,0}$) as 10 W/m^{2}K using an empirical correlation of $h_{c,z=0} = 1.52 \times T^{1/3}$ where T = 300 K [35]. At the upper surface we also set the mass-transfer coefficient ($h_{m,0}$) at

$0.02\,\mathrm{kg/m^2sec}$ based on previous work [35]. To ignite the sample we provided a heat flux ($\dot{q}''_e$) of $25\,\mathrm{kW/m^2}$ for 20 min at the top boundary to establish self-sustained smoldering, after which we removed the heat flux and established a convective–radiative balance at the top surface (e.g., for $t > 20\,\mathrm{min}$):

$$-\overline{k}\frac{\partial T}{\partial z}\bigg|_{z=0} = -h_{c0}(T_{z=0} - T_\infty) + \overline{\epsilon}\dot{q}''_e - \overline{\epsilon}\sigma(T^4_{z=0} - T^4_\infty)] \,, \tag{3.9}$$

$$-\overline{k}\frac{\partial T}{\partial z}\bigg|_{z=0} = -h_{c0}(T_{z=0} - T_\infty) - \overline{\epsilon}\sigma(T^4_{z=0} - T^4_\infty) \,, \tag{3.10}$$

$$-\left(\overline{\psi}\rho_g D\frac{\partial Y_j}{\partial z}\right)\bigg|_{z=0} = h_{m0}\left(Y_{j\infty} - Y_j|_{z=0}\right) \,, \text{ and} \tag{3.11}$$

$$P|_{z=0} = P_\infty \,. \tag{3.12}$$

We applied these boundary conditions for all simulations, except those looking at the effects of varying moisture content on propagation speed (Sec. 3.4.3) where we set a constant heat flux throughout the simulation to guarantee ignition at higher moisture contents.

For the bottom surface we set a heat-transfer coefficient ($h_{c,L}$) of $3\,\mathrm{W/m^2K}$ to account for losses through the insulation. The mass flux ($\dot{m}''$) was set to zero at the bottom surface. The equations used for boundary conditions on the bottom surface are

$$-\overline{k}\frac{\partial T}{\partial z}\bigg|_{z=L} = -h_{cL}(T|_{z=L} - T_\infty) \,, \text{ and} \tag{3.13}$$

$$-\left(\overline{\psi}\rho_g D\frac{\partial Y_j}{\partial z}\right)\bigg|_{z=L} = 0 \,. \tag{3.14}$$

3.3.3 Chemical kinetics

Gpyro represents heterogeneous reactions as [82]:

$$\mathrm{A}_k + \sum_{j=1}^{N} v'_{j,k}\,\mathrm{gas\,j} \longrightarrow v_{B,k}\,\mathrm{B}_k + \sum_{j=1}^{N} v''_{j,k}\,\mathrm{gas\,j} \,, \tag{3.15}$$

where k represents the reaction number, A_k and B_k are condensed-phase species, $v'_{j,k}$ and $v''_{j,k}$ are the reactant and product stoichiometric coefficients for gas j in reaction k,

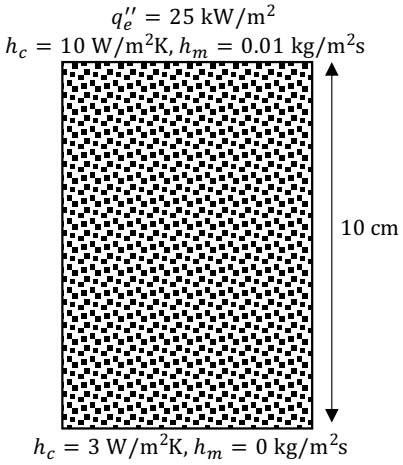

Figure 3.1: Schematic illustration of the one-dimensional computational domain.

$v_{B,k}$ is the stoichiometric coefficient for condensed-phase species B in reaction k, and N is the total number of gas-phase species. The reaction rates are expressed in Arrhenius form:

$$\dot{\omega}'''_{dA_k} = Z_k \frac{(\overline{\rho} Y_{A_k} \Delta z)_{\sum}}{\Delta z} \left(\frac{\overline{\rho} Y_{A_k} \Delta z}{(\overline{\rho} Y_{A_k} \Delta z)_{\sum}} \right)^{n_k} \times \exp\left(-\frac{E_k}{RT}\right) g(Y_{\mathrm{O_2}}) \ , \tag{3.16}$$

where

$$(\overline{\rho} Y_{A_k} \Delta z)_{\sum} = \overline{\rho} Y_{A_k} \Delta z|_{t=0} + \int_0^t \dot{\omega}'''_{fi}(\tau) \Delta z(\tau) d\tau \ , \tag{3.17}$$

Z is the pre-exponential factor, E is the activation energy, n is the order of reaction, subscript dA stands for destruction of species A, and subscripts k, f, and i are reaction index, formation, and condensed-phase species index. In Eq. (3.16), for inert atmosphere $g(Y_{O_2}) = 1$ and when oxygen is available $g(Y_{O_2}) = (1 + Y_{O_2})^{n_{O_2,k}} - 1$ [82].

We represent the smoldering process with a system of global pyrolysis and oxidation reactions [25, 74], using the model developed by Huang and Rein [34, 83] for smoldering of the mixtures of interest. In this model, moist fuel dries, then the dried fuel thermally decomposes to form char by two paths: fuel pyrolysis and fuel oxidation. α-Char forms via fuel pyrolysis while β-char forms from fuel oxidation. Next, α- and β-char oxidize and form ash. The drying and fuel-pyrolysis reactions are endothermic reactions while the

fuel- and char-oxidation reactions are exothermic. When considering 100% cellulose (i.e., neat cellulose) the model contains five global reactions, while for mixtures of cellulose and hemicellulose the model includes 10 global reactions. The full 10-step chemical kinetic model follows:

$$\text{Cellulose} \cdot v_{w,dr}\text{H}_2\text{O} \longrightarrow \text{Cellulose} + v_{w,dr}\text{H}_2\text{O}\,(\text{g}) \tag{R1}$$

$$\text{Cellulose} \longrightarrow v_{\alpha,cp}\,\alpha\text{-Char}_c + v_{g,cp}\,\text{Gas} \tag{R2}$$

$$\text{Cellulose} + v_{O_2,co}\text{O}_2 \longrightarrow v_{\beta,co}\,\beta\text{-Char}_c + v_{g,co}\text{Gas} \tag{R3}$$

$$\alpha\text{-Char}_c + v_{O_2,c\alpha o}\,\text{O}_2 \longrightarrow v_{a,c\alpha o}\text{Ash}_c + v_{g,c\alpha o}\text{Gas} \tag{R4}$$

$$\beta\text{-Char}_c + v_{O_2,c\beta o}\text{O}_2 \longrightarrow v_{a,c\beta o}\text{Ash}_c + v_{g,c\beta o}\text{Gas} \tag{R5}$$

$$\text{Hemicellulose} \cdot v_{w,dr}\text{H}_2\text{O} \longrightarrow \text{Hemicellulose} + v_{w,dr}\text{H}_2\text{O}\,(\text{g}) \tag{R6}$$

$$\text{Hemicellulose} \longrightarrow v_{\alpha,hp}\,\alpha\text{-Char}_h + v_{g,hp}\,\text{Gas} \tag{R7}$$

$$\text{Hemicellulose} + v_{O_2,ho}\,\text{O}_2 \longrightarrow v_{\beta,ho}\,\beta\text{-Char}_h + v_{g,ho}\,\text{Gas} \tag{R8}$$

$$\alpha\text{-Char}_h + v_{O_2,h\alpha o}\text{O}_2 \longrightarrow v_{a,h\alpha o}\text{Ash}_h + v_{g,h\alpha o}\text{Gas} \tag{R9}$$

$$\beta\text{-Char}_h + v_{O_2,h\beta o}\text{O}_2 \longrightarrow v_{a,h\beta o}\text{Ash}_h + v_{g,h\beta o}\text{Gas} \tag{R10}$$

where v is the stoichiometric coefficient; α and β indicate char produced from fuel pyrolysis and fuel oxidation reactions, respectively; and subscripts w, g, O_2, a, c, h, dr, o, p, αo, βo are water, gas, oxygen, ash, cellulose, hemicellulose, drying, oxidation, pyrolysis, α-char oxidation, and β-char oxidation, respectively.

Table 3.1 lists the chemical-kinetic parameters (pre-exponential factor, activation energy, order of reaction, and heat of reaction) for the schemes used here, obtained from Huang and Rein [34]. They developed the model to simulate smoldering of biomass, by optimizing kinetic parameters to match thermogravimetric-analysis measurements using a genetic algorithm [84]. We chose the kinetic parameters based on experiments using low-mineral moss peat (2.1% inorganic content), with oxygen concentrations of 0, 10, and 21 % and heating rates of 10, 20, and 30 K/min; the optimized model showed a minimum error of 5.5% with respect to the experimental measurements. Here, we apply

this model to simulate smoldering in more-general mixtures of cellulose and hemicellulose. We accounted for the consumption of oxygen using the relation $\upsilon_{O_2,k} = \Delta H/(-13.1)$ MJ/kg [35, 85].

Table 3.1: Kinetic parameters for cellulose and hemicellulose model.

Cellulose						
Reaction number	Reaction	$\log Z$ $\log \mathrm{s}^{-1}$	E kJ/mol	ΔH MJ/kg	n –	n_{O_2} –
(R1)	Drying	8.12	67.8	2.26	2.37	–
(R2)	Pyrolysis	11.7	156	0.5	1	–
(R3)	Oxidation	24.2	278	-28.2	1.73	0.74
(R4)	β-char oxidation	7.64	120	-28.8	1.25	0.89
(R5)	α-char oxidation	12.2	177	-27.8	0.93	0.52
Hemicellulose						
Reaction Number	Reaction	$\log Z$ $\log \mathrm{s}^{-1}$	E kJ/mol	ΔH MJ/kg	n –	n_{O_2} –
(R6)	Drying	8.12	67.8	2.26	2.37	–
(R7)	Pyrolysis	6.95	93.8	0.5	0.98	–
(R8)	Oxidation	20.2	294	-20.9	0.47	0.11
(R9)	β-char oxidation	7.64	120	-28.8	1.25	0.89
(R10)	α-char oxidation	12.2	177	-27.8	0.93	0.52

3.3.4 Physical properties

Table 3.1 reports the physical properties of condensed-phase species: solid density ($\rho_{s,i}$), thermal conductivity ($k_{s,i}$), and heat capacity (c_i). For the natural bulk densities of cellulose and hemicellulose (ρ_i), we used the values experimentally measured by Cowan et al. [86]: 175 $\mathrm{kg/m^3}$ and 695.71 $\mathrm{kg/m^3}$, respectively. (Bulk density refers to the density of the species including pores, i.e., total mass divided by total volume, while solid density is the density of the species without any pores.) We calculated the bulk density of char using the correlation $\rho_{\mathrm{char}} \approx \upsilon_{\mathrm{char}} \times \rho_{\mathrm{fuel}}$ [38] and the bulk density of ash using $\rho_{\mathrm{ash}} \approx \mathrm{AC}/100 \times 10 \times \rho_{\mathrm{fuel}}$, where AC stands for ash content [87]. The ash contents of cellulose and hemicellulose are 0.3% and 1.2%, respectively [34, 88, 89]. Following

the studies of Huang et al. [35], we assumed the solid physical properties of fuels do not depend on temperature.

Table 3.2: Thermophysical properties of condensed-phase species, taken from the literature for water [34], cellulose [90], hemicellulose [2, 4, 91], char [34, 92], and ash [34, 92].

Species	Solid density, $\rho_{s,i}$ (kg/m^3)	Thermal conductivity, $k_{s,i}$ ($W/(m\,K)$)	Heat capacity, c_i ($J/(kg\,K)$)
Water	1000	0.6	4186
Cellulose	1500	0.356	1674
Hemicellulose	1365	0.34	1200
Char	1300	0.26	1260
Ash	2500	1.2	880

The effective thermal conductivity of a condensed-phase species is calculated using

$$k_i = k_{s,i}(1 - \psi_i) + \gamma_i \sigma T^3 \,, \tag{3.18}$$

where $k_{s,i}$ is the solid thermal conductivity of species i, ψ_i is the porosity of species i, σ is the Stefan–Boltzmann constant, and γ_i is an empirical parameter for radiation across pores that depends on pore size [82]. The porosity of species i is calculated with

$$\psi_i = 1 - \frac{\rho_i}{\rho_{s,i}} \,. \tag{3.19}$$

Pore size, γ_i, and permeability are calculated for each condensed-phase species at their natural densities using

$$d_{po,i} \approx d_{p,i} = \frac{1}{S_i \times \rho} \tag{3.20}$$

$$K_i = 1 \times 10^{-3} \times d_{p,i}^2 \tag{3.21}$$

$$\gamma_i = 3 \times d_{po,i} \,, \tag{3.22}$$

where ρ is the density of the fuel, S_i is the particle surface area for species i, $d_{p,i}$ is the particle size, K_i is the permeability, and $d_{po,i}$ is the pore size [34, 35, 93, 94]. The particle surface areas of cellulose, cellulose-based ash, hemicellulose, and hemicellulose-based ash are 0.0388, 0.1533, 0.0678, and $0.2712\,m^2/g$, respectively [34, 95–97]. These correlations

apply at the natural densities of the fuels based on the assumption of similar particle and pore size [34, 35]. For cases where we model fuels with specific or varying densities, we assigned this value as the natural density and used Eqs. (3.20)–(3.22) to vary properties with density.

However, when we emulate increases in density due to compression, the particle size $d_{p,i}$ remains constant but pore size $d_{po,i}$ decreases due to the reduction of pore volume. Thus, when validating our model (Section 3.4.1), we used the experimental measurements of Smucker et al. [40, 75] for bulk density; they changed the density of fuels by compressing the samples from their natural density to reach the desired density. To model this compression, we account for the associated changes in pore size ($d_{po,i}$) and radiation parameter (γ_i) by scaling them with change in porosity (ψ), since porosity is directly proportional to the volume occupied by pores. Permeability also changes during compression, which we vary with the Kozeny–Carman equation:

$$K_i \propto \frac{e_i^3}{1+e_i} \,, \tag{3.23}$$

where e_i is the void ratio, related to porosity with $e_i = \psi_i/(1-\psi_i)$.

Unless mentioned otherwise, we ran all simulations with 10% moisture content to account for moisture content already present in natural fuels and moisture absorbed from the atmosphere [34, 38]. The addition of water changes the density of the (wet) fuel, and we accounted for this change using

$$\rho_{\text{wet fuel}} = \rho_{\text{dry fuel}} \times (1 + \text{MC}) \,, \tag{3.24}$$

where MC is the moisture content [35]. To investigate the role of this natural fuel expansion, we considered cases where the fuel expands with moisture content and where it does not; when the fuel does expand, we use the correlation developed for peat by Huang and Rein [38] with the bulk density modified for the fuels considered here. Porosity changes less than 5% with this change in density here, so we consider this adoption justified. The modified correlation is

$$\rho_{\text{dry fuel}} = \frac{200 + 40\text{MC}}{1 + \text{MC}} \,. \tag{3.25}$$

Thermal conductivity (k) and heat capacity (c) also vary with moisture content, and we change those for wet fuels by averaging using volume fraction (X_i) and mass fraction (Y_i), respectively [35, 82]:

$$k_{\text{wet fuel}} = X_{\text{H}_2\text{O}} k_{\text{H}_2\text{O}} + X_{\text{dry fuel}} k_{\text{dry fuel}} \tag{3.26}$$

$$c_{\text{wet fuel}} = Y_{\text{H}_2\text{O}} c_{\text{H}_2\text{O}} + Y_{\text{dry fuel}} c_{\text{dry fuel}} \, . \tag{3.27}$$

3.3.5 Calculation of global quantities

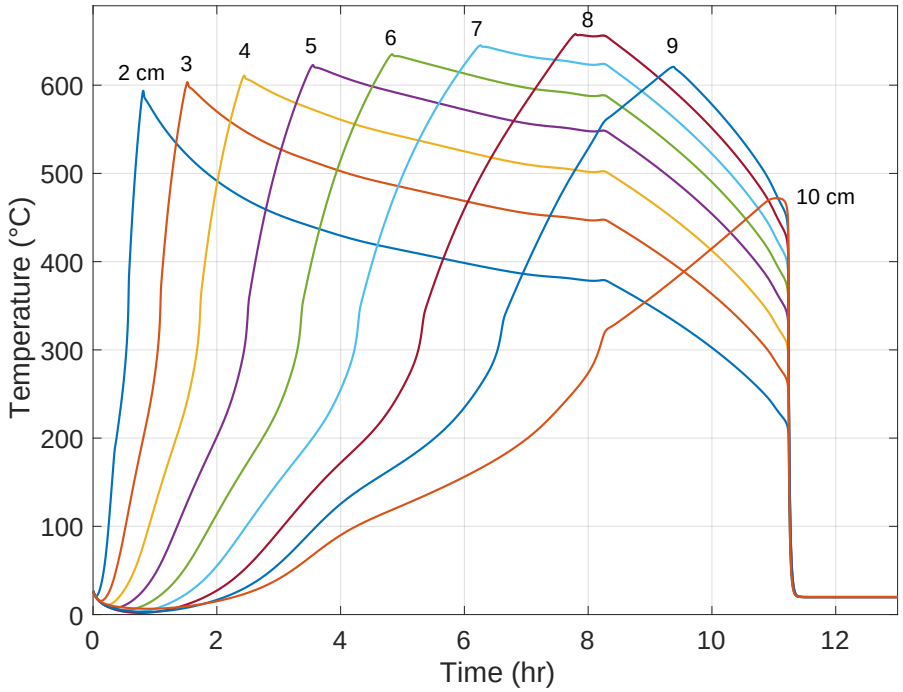

Figure 3.2: Temperature profile with respect to time for a fuel composition of 50 % cellulose at a density of 300 kg/m^3.

The two main parameters of interest in this study are mean propagation speed of smoldering and mean peak temperature. We calculate propagation speed by numerically computing the derivative of depth with respect to time of peak temperature; in other words, the difference between two depths divided by the times when those depths reach their maximum temperature. Figure 3.2 shows an example temperature vs. time profile

that demonstrates how we record the data for calculating these global quantities. This requires selecting a depth interval for evaluating this finite difference; to determine the appropriate interval value for calculating mean propagation speed, starting at 6 cm we systematically reduced the depth interval and examined the effect on calculated mean propagation speed. (A smaller depth interval requires both producing and evaluating more data from the simulations, so we seek a pragmatic choice that affects the results little while reducing the computational burden.) After reducing the depth interval to 1 cm, further reduction negligibly affects propagation speed: reducing from 1 cm to 0.5 cm increases the calculated speed by less than 0.3%. As a result, we chose a depth interval of 1 cm for all cases. The supplementary material shows the effects of reducing depth interval on propagation speed in more detail. We calculated mean peak temperature similarly by averaging the peak temperatures every 1 cm.

3.4 Results and discussion

First, we validated the model by comparing it with experimental measurements of mean propagation speed and mean peak temperature. Then, we varied density and fuel composition to study how these parameters affect smoldering behavior. Next, we examined the effect of moisture content on mean peak temperature and mean propagation speed for 100% cellulose. Finally, we examined how the critical moisture content of ignition and extinction change with fuel composition.

3.4.1 Validation

We validated the computational model using the experimental results of Smucker et al. [40, 75] by comparing two parameters: mean peak temperature and mean propagation speed. The experiments used a one-dimensional reactor box of dimensions $10\,\text{cm} \times 10\,\text{cm} \times 13\,\text{cm}$, with thermocouples placed at 1 cm depth intervals. The top surface of the reactor box was open to atmosphere and the other sides were insulated using a calcium silicate insulation board, and the fuel samples were ignited using a cartridge heater applied until the point of self-sustained smoldering. The supplemental material contains key information about the experimental measurements, and Smucker et al. [40, 75] provide further details about the experimental configuration.

To ensure self-sustained smoldering, we performed our validation simulations using a heat flux of 25 kW/m^2 applied for 20 min at the top surface. However, we found that smoldering behavior was insensitive to the magnitude of the heat flux; doubling it changed the propagation speed by less than 1.8%. This gave us the confidence to use heat flux as the boundary condition to ignite the fuel sample.

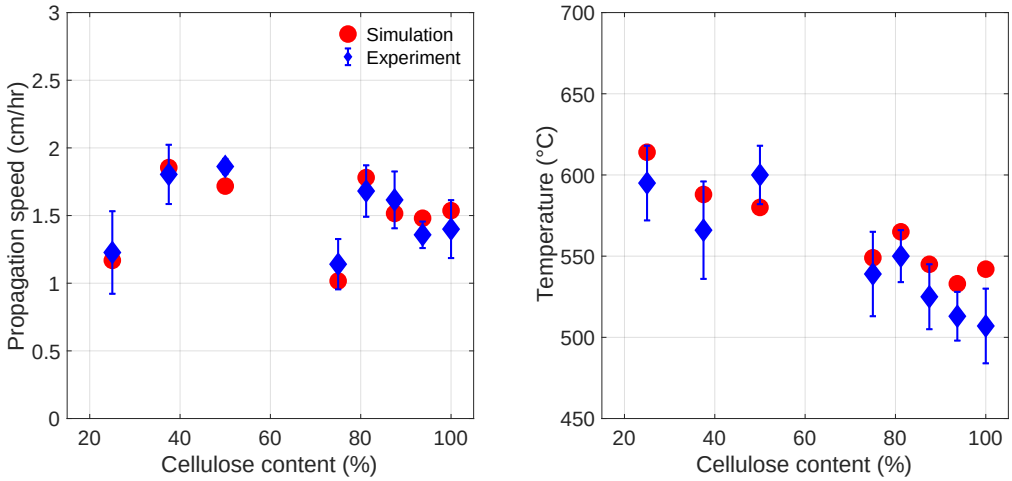

Figure 3.3: Experimental (diamond) and predicted (circle) propagation speeds and mean peak temperatures (filled symbols) for fuel compositions of 25, 50, 75, and 100 % cellulose at densities of 400, 250, 300, and 170 kg/m^3.

We used eight fuel samples with varying fuel composition and density to validate the model: 25, 37.5, 50, 75, 81.2, 87.5, 93.7, and 100 % cellulose, with the remainder hemicellulose, at respective densities of 400, 200, 250, 300, 250, 250, 250, and 170 kg/m^3. They created these mixtures artificially by mixing the two components and then compressing the fuel to achieve a desired density. Figure 3.3 compares the experimental measurements and model calculations of mean propagation speed and peak temperature; the model captures all of the experimentally observed trends, and also agrees well quantitatively. The model overpredicts mean propagation speed for 100% cellulose by 10.8% in the worst case, while the average error in propagation speed for the four mixtures is 8.7%. Similarly, the model overpredicts mean peak temperature for 100% cellulose in the worst case by 6.1%, with the average error at 5.3%. Based on these results, we will use this model for the remaining studies here.

3.4.2 Sensitivity to fuel composition and density

Next, we investigated the effects of density and fuel composition on mean peak temperatures, as Figure 3.4 shows. We artificially created these mixtures to analyze the effects of fuel composition and density on smoldering behavior. We varied fuel density between 200–400 $\mathrm{kg/m^3}$ in increments of 50 $\mathrm{kg/m^3}$ and the fuel composition from 100–25% cellulose in decrements of 25% cellulose, with hemicellulose as the remaining fuel in the mixture. As Figure 3.4 shows, mean peak temperature increases with increasing density.[1] To determine the cause of this temperature dependence, we individually varied the parameters that change when density increases. We found that decreasing value of the empirical parameter for radiation across pores (γ) of the condensed-phase species contributes most to the increase in peak temperatures. Figure 3.5 shows temperature profiles for 100% cellulose at densities of 200, 300, and 200 $\mathrm{kg/m^3}$ but with γ associated with 300 $\mathrm{kg/m^3}$. For the fuel with a density of 200 $\mathrm{kg/m^3}$, when we change only the values of γ for the condensed-phase species to those at 300 $\mathrm{kg/m^3}$, the peak temperatures closely match those of the 300 $\mathrm{kg/m^3}$ fuel, with differences of 1.9% and 1.2% for 2 cm and 3 cm profiles, respectively.

Figure 3.4 also shows that increasing hemicellulose content in the fuel increases mean peak temperature. To explain this, Figure 3.6 shows temperature at varying depths and times for 50% cellulose and 50% hemicellulose at a density of 300 $\mathrm{kg/m^3}$. The peak temperatures in Fig. 3.6 do not occur at the surface of the fuel where oxygen is most available, but instead below the surface. Ash forms at the topmost layer of the fuel, acting as an insulator. According to Eq. (3.20) and (3.22), ash formed from cellulose has a higher γ than ash formed from hemicellulose. This leads to greater losses due to radiation across the pores at higher cellulose content, hence peak temperatures drop with increasing cellulose content.

To test this theory, we ran a simulation with the value of γ of ash from hemicellulose set equal to the γ of ash from cellulose for a fuel mixture with 50% cellulose. In other words, in this case the ash formed from hemicellulose matches that from cellulose, in terms of radiation heat transfer across the pores. Figure 3.7 shows the resulting temperature profiles along with temperature profiles of 50% cellulose and 100% cellulose at density

[1] The calculated peak temperatures differ from those shown in Figure 3.3 due to the different treatment of density, as we discussed in Section 3.3.4.

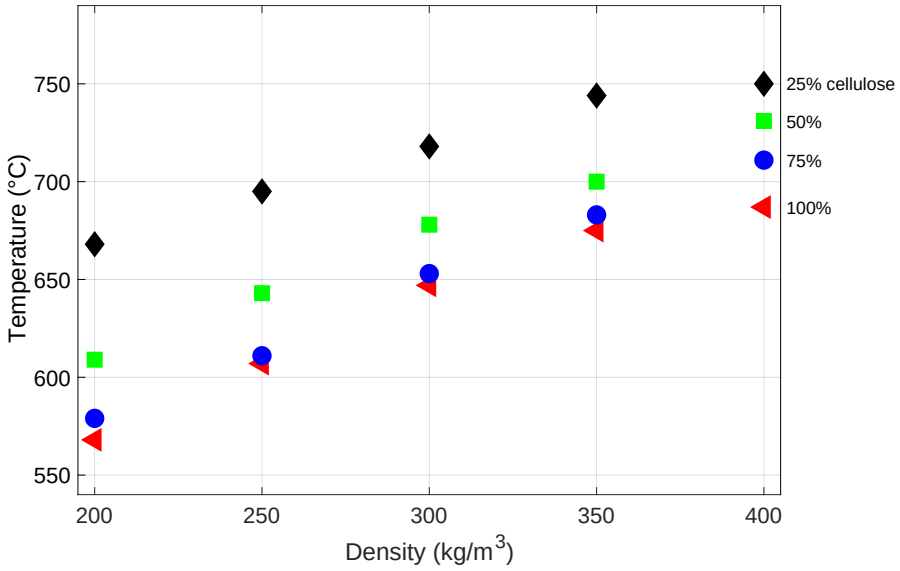

Figure 3.4: Effects of varying density and fuel composition on peak temperature.

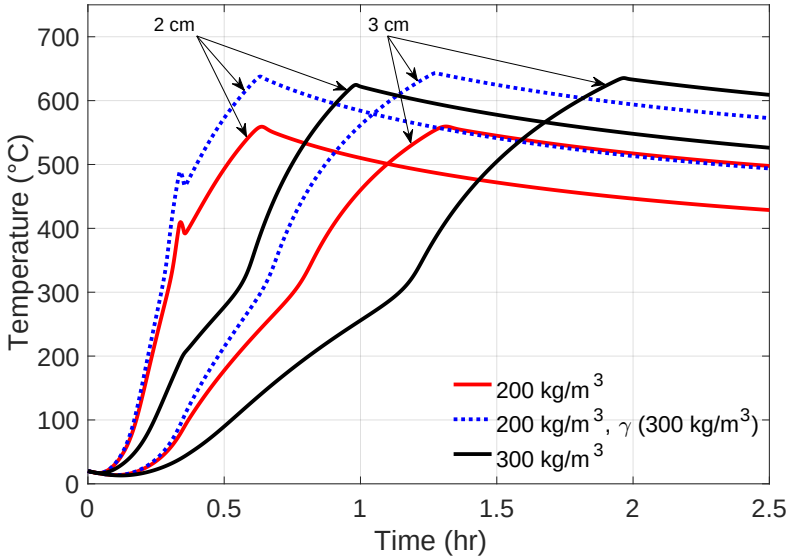

Figure 3.5: Temperature profiles at depths of 2 and 3 cm of 100% cellulose with densities 200 kg/m^3, 300 kg/m^3, and 200 kg/m^3 with the empirical parameter for radiation across pores (γ) of 300 kg/m^3.

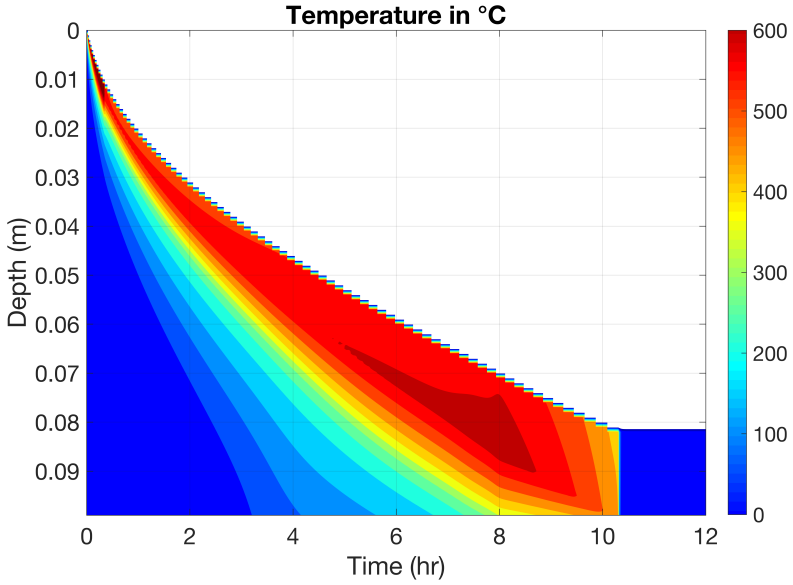

Figure 3.6: Temperature contour varying with depth and time for fuel composition of cellulose 50% and density of 300 kg/m^3

300 kg/m^3. The peak temperature of 50% cellulose matches that of 100% cellulose when γ from hemicellulose matches that of ash from pure cellulose, with differences of 3.9% and 4.4% for 2 cm and 3 cm profiles, respectively.

Our findings show that the physical parameters of condensed-phase species control the observed variations in peak temperature, both as density and fuel composition change. Richter et al. [98] also discussed the larger role that physical properties play in wood charring, compared with reaction kinetics. Charring, which occurs through pyrolysis and heterogeneous oxidation, controls burning behavior and relates to temperature profile (including peak temperature). Figures 3.5 and 3.7 also show that the location of peak temperature does not shift significantly even as its value increases, In Figures 3.5 the shift is 0.6% and 2.3% for 2 and 3 cm profiles, and in Figures 3.7 the shift is 3.1% and 2.3% for 2 and 3 cm profiles, respectively. This indicates that the change in peak temperature does not notably affect propagation speed.

Next, we consider the effects of density and fuel composition on mean propagation speed, shown in Figure 3.8. Propagation speed increases with increasing hemicellulose content and decreases with increasing density. To understand the role of fuel composition,

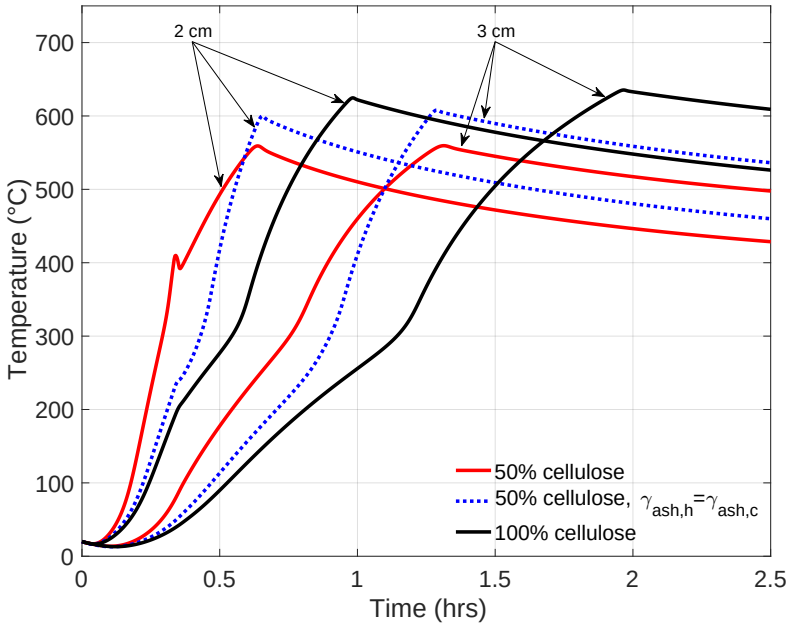

Figure 3.7: Temperature profiles at depth 2 and 3 cm for fuels with density 300 kg/m^3 and fuel composition of 50% cellulose, 100% cellulose, and 50% cellulose with the parameter for radiation across pores of ash coming from hemicellulose set equal to that from cellulose ($\gamma_{\text{ash,h}} = \gamma_{\text{ash,c}}$).

Figure 3.9 shows reaction rates of fuel with hemicellulose along the depth at 4000 s. Hemicellulose pyrolyzes faster than cellulose, so that a given time its pyrolysis occurs deeper than fuels with a higher proportion of cellulose. The fuel shrinks faster, providing earlier access to oxygen ultimately leading into faster propagation speed. To examine the role of density, Figure 3.10 shows the reaction rates and condensed-phase species mass fractions at 4 cm below the surface for 100% cellulose at densities of 200 kg/m^3 and 300 kg/m^3. The reaction rates of lower density fuel are higher and less spaced out compared to higher density fuel. This means more time is required for fuel to convert to char and ash as observed in the mass fractions of Fig. 3.10. This comes from the increased density of the fuel, which means more mass in a given volume converts to char and ash. As a result, the fuel shrinks, delaying access to oxygen for the char formed.

Across all fuel compositions, the propagation speed decreases by a factor of two when the density of fuel increases proportionally from 200 kg/m^3 to 400 kg/m^3 (i.e., doubles).

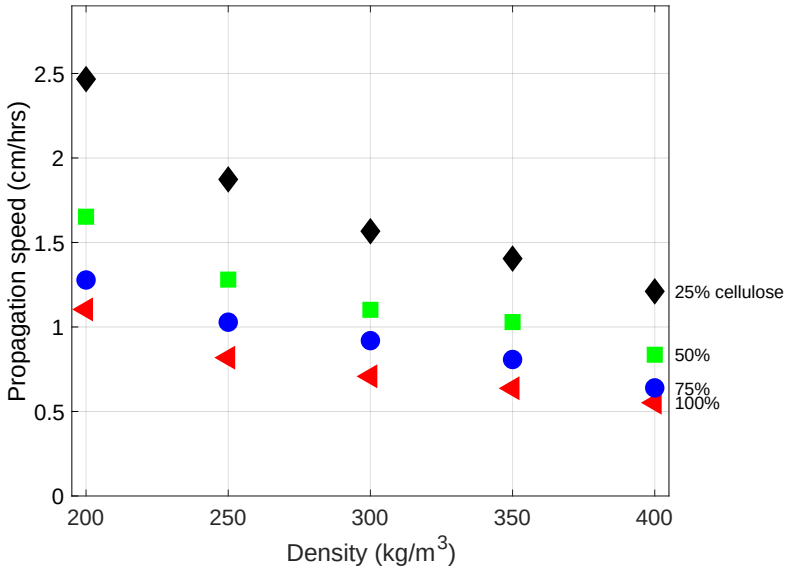

Figure 3.8: Effects of varying density and fuel composition on propagation speed.

Huang and Rein [38] discussed an inverse relation between oxygen concentration and density. To further examine the dependence of oxygen concentration, we increased oxygen concentration, and density simultaneously, by the same factor. The oxygen supply was increased via mass fraction of (diffusing) oxygen. For example, if the density increases by a factor of 1.5, from 200 $\mathrm{kg/m^3}$ to 300 $\mathrm{kg/m^3}$, then oxygen mass fraction increased to 0.348 for 300 $\mathrm{kg/m^3}$. This was done for all densities and fuel compositions shown in Fig. 3.8. Figure 3.11 shows that when mass fraction of oxygen (Y_{O_2}) increases by the same factor as density (ρ) the propagation velocities (S) remains constant, confirming the $S \propto Y_{O_2}/\rho$ relationship posed by Huang and Rein [38]. We performed a similar analysis of increasing oxygen supply with density for peak temperatures, shown in Figure 3.12; peak temperature increases with oxygen content.

To model how propagation speed and peak temperatures quantitatively scale with all the controlling variables, we performed linear regression of the data shown in Figs.3.4, 3.8, 3.11, and 3.12. We used the Matlab function `regress()`, where the independent variables are mass fraction of cellulose ($Y_{\mathrm{cellulose}}$), density (ρ), and oxygen concentration (Y_{O_2}) and the dependent variables are velocity (S) and peak temperature (T). The

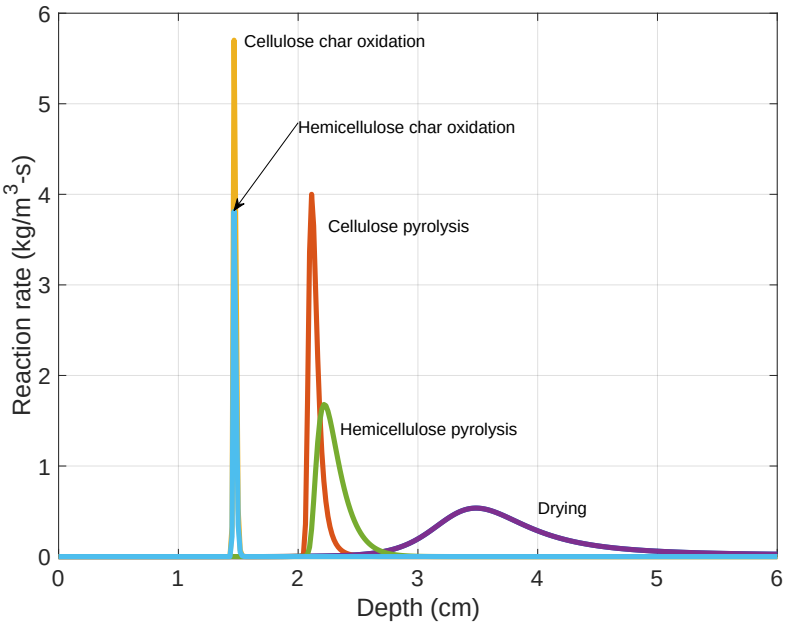

Figure 3.9: Reaction rates of cellulose and hemicellulose drying, pyrolysis, and oxidation for 50% cellulose and 50% hemicellulose at density 300 kg/m^3 along the depth at 4000 s.

resulting equations are:

$$S = 685.08 \times \frac{Y_{O_2}^{0.9892}}{\rho^{0.9464} \times Y_{\text{cellulose}}^{0.5865}} \quad \text{and} \tag{3.28}$$

$$T = 272.28 \times \frac{\rho^{0.2500} \times Y_{O_2}^{0.3921}}{Y_{\text{cellulose}}^{0.0835}} \, . \tag{3.29}$$

The goodness of fit (R^2) values for both equations are approximately 0.99. In the fit for propagation speed, Eq. (3.28), the power of fuel density (ρ) and mass fraction of oxygen (Y_{O_2}) are 0.9464 and 0.9892, respectively, which are both close to 1.0—confirming the $S \propto \frac{Y_{O2}}{\rho}$ relationship discussed earlier. As demonstrated by Eq. (3.29), peak temperature is more sensitive to oxygen supply than to density.

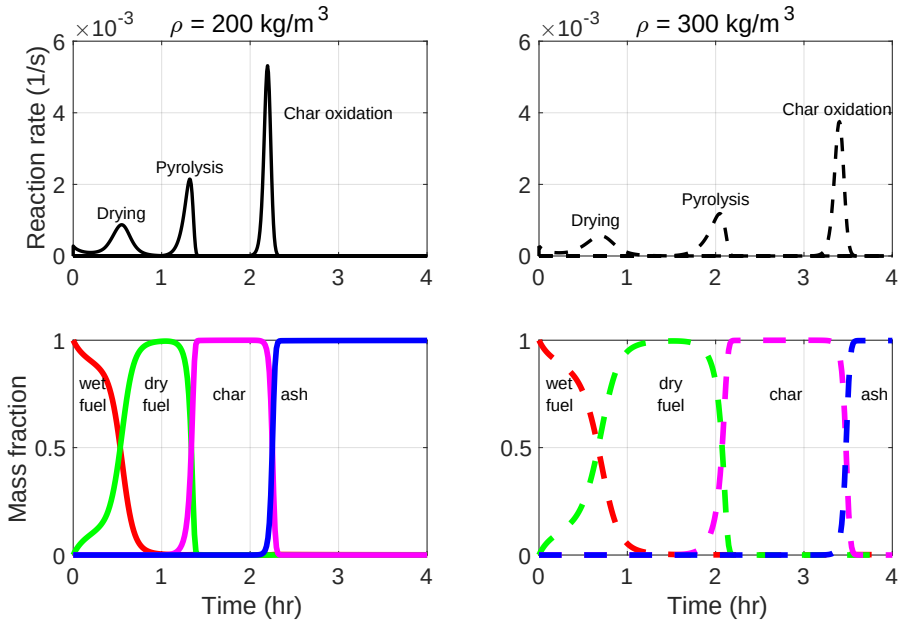

Figure 3.10: Reaction rates of drying, pyrolysis, and char oxidation (top) and mass fractions of wet fuel, dry fuel, char, and ash (bottom) of 100 % cellulose with density 200 and 300 $\mathrm{kg/m^3}$.

3.4.3 Effect of moisture content on propagation speed

Next, we look into how moisture content affects the propagation speed and peak temperatures of smoldering, considering cases both with and without the natural expansion with water. We investigated cases without expansion because while some prior studies of peat reported expansion with addition of water [38], most woody fuels have no reported expansion.

Figure 3.13 shows the effect of increasing moisture content on propagation speed and peak temperature in expanding and non-expanding fuels. Moisture content is increased from 10% to 70% in increments of 20% for 100% cellulose. Peak temperature drops with increasing moisture content with and without expansion, while propagation speed shows opposite trends: increasing with expansion and decreasing without expansion.

When the fuel does not expand, i.e., all the water added to the fuel sample occupies the pores, the propagation speed decreases with increasing moisture content. In contrast, when the fuel expands, i.e., addition of water increases the total volume of the fuel,

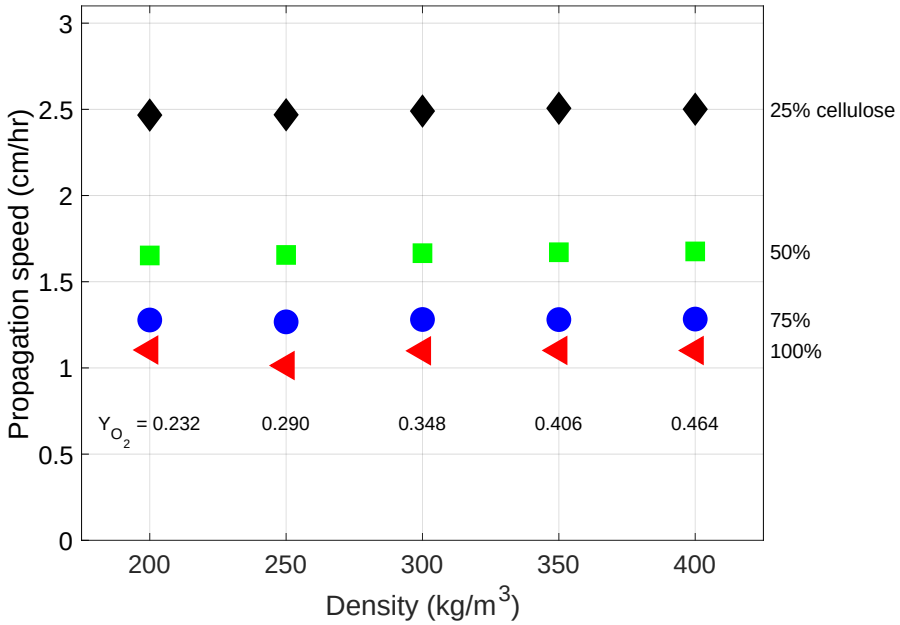

Figure 3.11: Propagation speed when oxygen availability is linearly increased with density, where the value of Y_{O_2} indicates the value of mass fraction of oxygen used for the respective density.

propagation speed increases with moisture content.

Without expansion, when water is added to the fuel the thermal conductivity, heat capacity, and wet fuel bulk density increase. In addition, when moisture content of the fuel increases, the drying becomes more endothermic, which increases the associated heat of reaction. To examine which parameters contribute most to reduce speed and temperature with moisture content, we analyzed the affect of each parameter individually as shown in Fig. 3.14. To do this, we set the value of each parameter that changes on addition of moisture content to the value for 70% moisture content, keeping all other parameters constant. The changes in thermal conductivity and heat capacity between the two moisture contents minimally affect both propagation speed and peak temperature. Instead, the increase of (wet) bulk density is the main reason for the drop in propagation speed. In contrast, the increase in both wet bulk density and heat of reaction contribute to the drop in temperature. When increasing the wet fuel bulk density, more fuel needs to be dried by the smoldering front in a given volume, which decreases both temperature

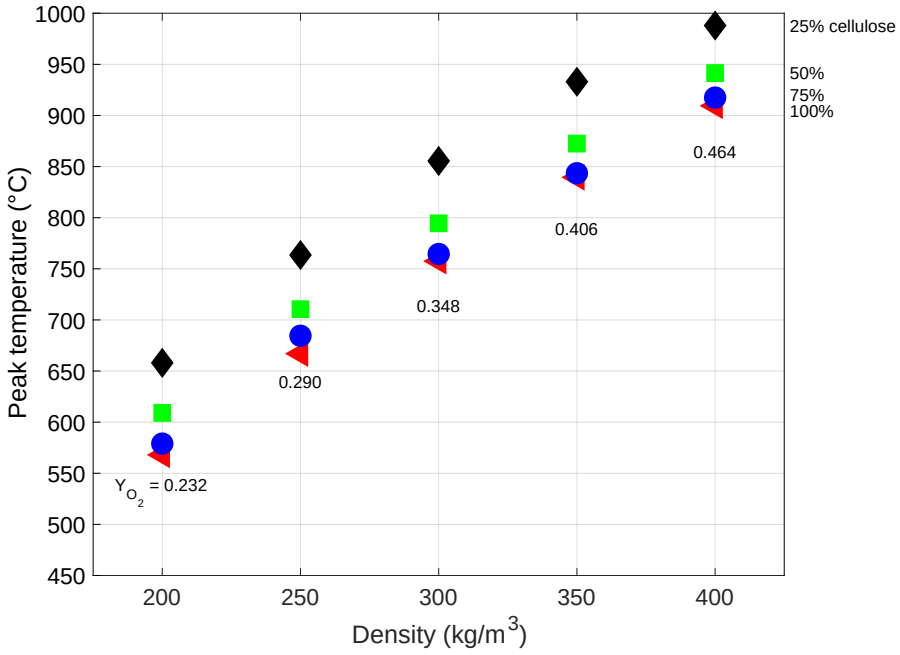

Figure 3.12: Peak temperatures when oxygen availability is linearly increased with density, where the value of Y_{O_2} indicates the value of mass fraction of oxygen used for the respective density.

and propagation speed. When the drying reaction becomes more endothermic, more heat is required to dry the fuel, which reduces the peak temperature attained.

When the fuel expands with water addition, the increase in speed could be due to either the expansion of the fuel, which reduces density, or the increase in thermal conductivity. By testing the effect of each parameter, we found that changing only the thermal conductivity of the fuel negligibly impacts the propagation speed and temperature, while expansion alone increases propagation speed. When a fuel expands the overall density of the fuel decreases, and as Fig. 3.8 shows when the density of the fuel drops the propagation speed increases. So, in this case, propagation speed is more influenced by the overall reduction in density than the increase in the wet mass of the fuel, which increases the propagation speed. This result further confirms the relationship Huang and Rein [38] first showed for peat. The temperature reduction in this case comes from the increasing mass of wet fuel and increasing endothermicity, similar to the case without expansion. The temperature trends are similar in both cases, since, as Eq. (3.29) shows,

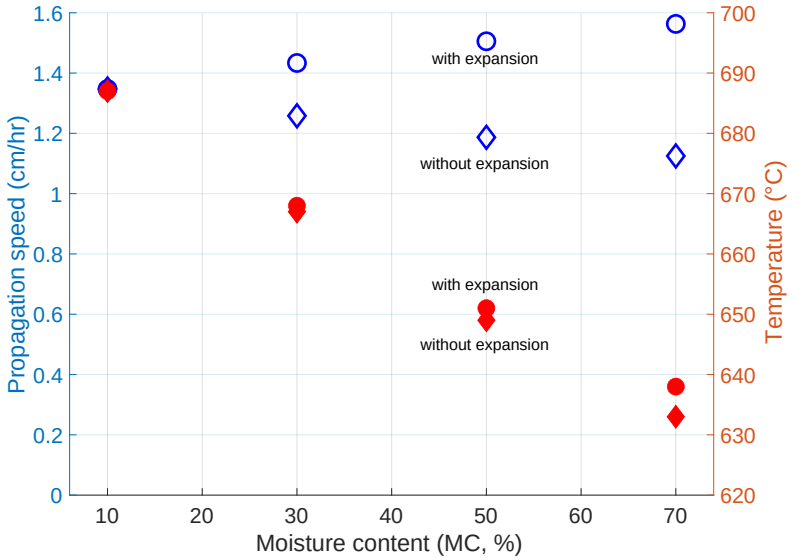

Figure 3.13: Effect of moisture content on propagation speed and peak temperature for 100% cellulose, with and without expansion, where the empty symbols indicate propagation speed and filled symbols indicate temperature.

temperature is comparatively less sensitive to density and thus expansion.

3.4.4 Effect of changing composition on critical moisture content

Critical moisture content of ignition is the moisture content above which a fuel will not ignite for a given boundary condition; critical moisture content of extinction is the moisture content above which an established smoldering front does not propagate for given upstream, downstream, and boundary conditions. In this section we examine whether the critical moisture contents change with fuel composition. For this study we held density of the fuel at $200\,\mathrm{kg/m^3}$ and applied heat flux of $25\,\mathrm{kW/m^2}$ for the first 20 min to ignite the sample. We ran simulations at compositions 100%, 75%, 50%, and 25% cellulose and increased the moisture content in intervals of 10%. To measure the critical moisture content of ignition, we set a uniform moisture content throughout the fuel sample. To measure the critical moisture content of extinction, we set the top 5 cm of the domain to have 10% moisture content to ensure a self-sustained smoldering front, followed by a wet layer of 2 cm whose moisture content was systematically increased to

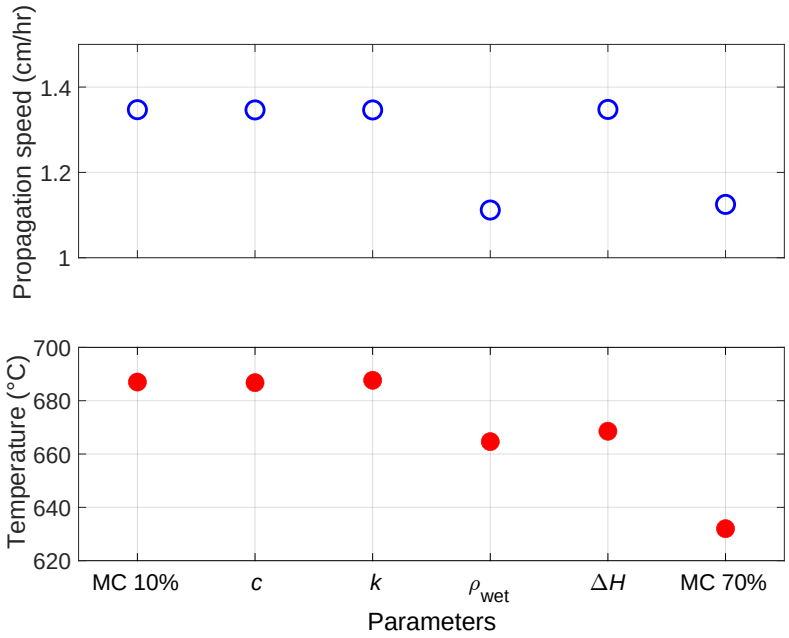

Figure 3.14: Parameter analysis for moisture content without expansion, showing impact of parameters on propagation speed (top) and peak temperature (bottom). Each parameter (c, k, ρ_{wet}, and ΔH) was changed to its value for 70% moisture content while holding all other properties to their values at 10%. These parameters increased by 55%, 48%, 58%, and 62%, respectively. The fully 10% and 70% MC cases are shown at the far left and right for comparison; note the axis scaling.

determine the critical moisture content of extinction, with the remaining 3 cm of the sample at 10% moisture content, as shown in Figure 3.15.

Table 3.3 shows how fuel composition affects the critical moisture contents of ignition and extinction. For all compositions, critical moisture content of ignition is always lower than critical moisture content of extinction. Neither critical moisture content is sensitive to fuel composition until the mixture contains 75% hemicellulose, when both critical moisture content of ignition and extinction increase by 10%. As previously shown in Fig. 3.4, adding hemicellulose to the fuel increases the mean peak temperature. At this composition, the fuel samples become hot enough to sustain smoldering combustion even at 10% higher moisture content.

Figure 3.16 shows the temperature profiles at different depths for fuel samples when the moisture content of the wet layer is 60% and 70%; for 60%, smoldering propagates through

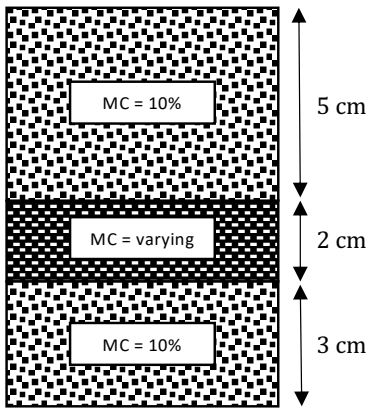

Figure 3.15: Schematic illustration of the one-dimensional computational domain with three layers of varying moisture content (MC).

Table 3.3: Critical moisture content (MC_c) of ignition and extinction for different fuel compositions.

% Cellulose	MC_c of ignition	MC_c of extinction
25	40	70
50	30	60
75	30	60
100	30	60

the wet layer, but at 70% smoldering combustion extinguishes. At 2 cm deep, the peak temperatures of the two cases match. However, as the smoldering fronts progress deeper, the difference in the moisture content downstream starts affecting the temperatures from 3 cm onward. At 4 cm deep the temperature of the 70% moisture content case drops below the point where smoldering cannot self-sustain and it extinguishes. On the other hand, the sample with 60% moisture content has a peak temperature just below 500 °C at 4 cm, which is high enough to sustain smoldering. The biggest drop in the peak temperature, for the case where there was self-sustained smoldering, is approximately 1 cm above the point where the wet layer begins and not at the point of wet layer. This is because, as observed in Fig. 3.9, the drying process starts before char oxidation reactions using

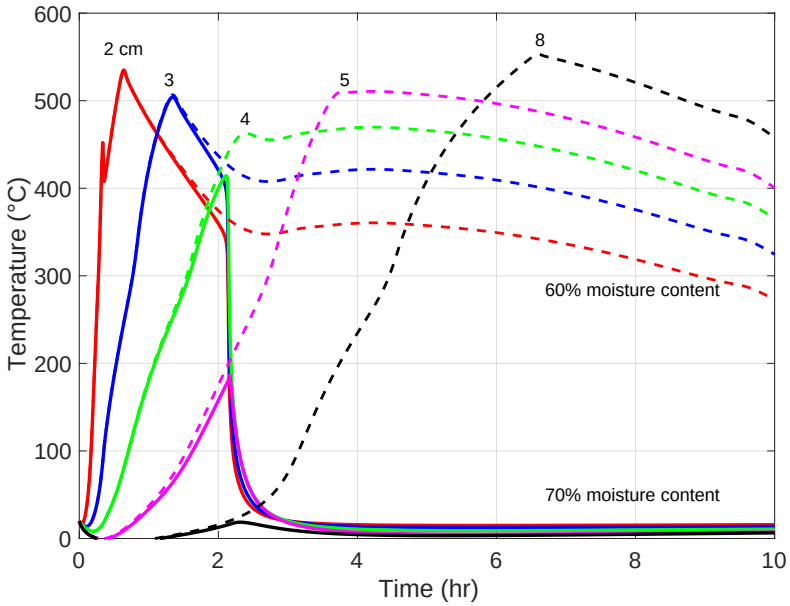

Figure 3.16: Temperature profiles of 100% cellulose with moisture content of wet layer 60% shown by dashed line and 70% shown by solid line at various depths.

the heat liberated from char oxidation reaction along the depth of the fuel. So in this particular case, the drying of the wet layer began when char oxidation reactions were occurring approximately 1 cm above the wet layer.

3.5 Conclusions

In this work, we updated a one-dimensional computational model for smoldering combustion of cellulose and hemicellulose mixtures using the open-source software Gpyro. The model successfully predicts results from experiments at four fuel densities and compositions. We used the model to examine the impact of changing fuel composition and density on smoldering propagation speed and peak temperature. We also examined the role of moisture content, and how fuel composition affects critical moisture content of ignition and extinction.

As the density of the fuel increases, the mean propagation speed drops. This is caused by the increase in the amount of fuel that needs to be converted to ash, which slows fuel shrinkage and thus access to oxygen. In contrast, propagation speed increases with

hemicellulose content in the fuel, due to the faster pyrolysis of hemicellulose compared with cellulose. Mean peak temperature also increases with additional hemicellulose content, caused by the formation of ash with lower radiation loss across pores. Mean peak temperature increases with increasing density, due to decreasing radiation losses across the pores of the fuel.

When moisture content is added and the fuel is allowed to expand, the propagation speed increases due to the reduction in density. If the fuel does not expand with the addition of water (i.e., moisture simply fills the pores), propagation speed drops primarily due to the increase in wet bulk density. Therefore, accurately modeling smoldering in a given fuel requires characterizing whether moisture content causes expansion. In both cases, additional moisture content reduces the mean peak temperature slightly. Fuel composition increases the critical moisture content of ignition and extinction only when hemicellulose becomes the major constituent, due to larger heat release.

Future studies should focus on generalizing the model to consider lignin, the third important component of biomass and woody fuels. In addition to validating a general fuel model with global outputs such as propagation speed and peak temperature, model outputs should be compared with experimental measurements of temperature profiles and mass to further-constrain the model. In addition, the impact of material and kinetic parameter uncertainty on quantities of interest should be studied. Based on the range of thermophysical parameter values (i.e., $\rho_{s,i}$, $k_{s,i}$, c_i) found in the literature [34, 38, 42, 99–102], initial estimations suggest an uncertainty of 5–8% in propagation speed and 3% in peak temperature, which warrants a more-complete uncertainty analysis.

Acknowledgements

We also thank David Blunck, Benjamin Smucker, and Daniel Cowan at Oregon State University for providing their experimental temperature measurements data for validation.

Funding

This research was funded by the Strategic Environmental Research and Development Program (SERDP) award RC-2651 under contract number W912HQ-16-C-0045.

The views, opinions, and/or findings contained in this report are those of the authors

and should not be construed as an official Department of Defense position of decision unless so designated by other official documentation.

Supplementary material

The supplementary material for this article contains the complete kinetic parameters used in the model, along with additional details about the experiments used to validate the model. In addition, all of the Gpyro input files, plotting scripts, and figures are available openly under the CC-BY license [103]. Gpyro itself is available openly [81].

Chapter 4: Smoldering combustion of cellulose, hemicellulose, and lignin: Investigating the roles of fuel composition, density, oxygen concentration and moisture content

W. Jayani Jayasuriya and Kyle E. Niemeyer

My contributions to this work included developing the computational model, running simulations, processing the output data, analyzing the results, and preparing the manuscript.

Proceedings of the 2019 Fall Technical Meeting of the Western States Section of the Combustion Institute
Albuquerque, NM, USA. October 2019.

4.1 Abstract

Smoldering combustion of biomass plays an important role in wildland fires because it can persist for long periods of time, transition to flaming combustion, and emit significant amounts of pollutants. Cellulose, hemicellulose, and lignin are the major constituents of biomass, in varying proportions based on the type of fuel. In this work, we developed a one-dimensional computational model using the open-source Gpyro software to simulate smoldering combustion, using mixtures of these three constituents to represent real fuels. First, we validated the model by comparing simulated propagation speeds with experimental measurements. Next, we studied how fuel composition, density, oxygen concentration, and moisture content affect smoldering behavior, including propagation speed and peak temperature. Notably, increasing lignin content decreases the propagation speed, while increasing hemicellulose content increases the propagation speed. Peak temperature rises with both increasing lignin and hemicellulose content. When the density of a mixture increases, propagation speed decreases and peak temperature rises. When the moisture content of a mixture increases, both propagation speed and peak temperature decrease. We also studied how oxygen concentration and moisture content affect smoldering ignition. We investigated in detail the reasons for these behaviors to better understand the smoldering behavior in real fuels.

4.2 Introduction

Smoldering combustion is one of the leading causes of wildland fires that contributes to destruction of vegetation, global greenhouse gas emissions, and other human/ecological hazards [5]. Smoldering can penetrate much deeper into the organic soil compared to flaming combustion, impacting the plant regrowth rate [5]. Even though the spread rate of smoldering is slower than with flames, it can burn for a longer periods of time, making it more difficult to suppress. Smoldering also emits more pollutants that flaming, due to incomplete and lower-temperature combustion [7, 8]. For these reasons, smoldering combustion has become a topic of interest in wildland fires.

The major organic constituents of biomass are cellulose, hemicellulose, and lignin. The composition of these constituents within a fuel varies significantly depending on the fuel source [21]. Each component has different characteristics when it comes to pyrolysis

and oxidation. Gani and Naruse [9] discussed pyrolysis and combustion characteristics of cellulose and lignin for several types of biomass. They identified two stages during burning: (1) cellulose decomposition and (2) lignin decomposition for pyrolysis and combustion of its char. They concluded that the amounts of cellulose and lignin in biomass play major roles in pyrolysis and char oxidation. Yang et al. [10], using a thermogravimetric analysis, identified that hemicellulose and cellulose pyrolysis happens earlier than lignin. In addition, lignin produces the highest solid residue during pyrolysis. Dorez et al. [11] found that natural fibers with a higher composition of lignin exhibit higher char yields, higher effective heat of combustion, and higher activation energy of combustion. These studies show that the three constituents have different and unique characteristics when it comes to pyrolysis and oxidation. Since smoldering combustion represents the combined effects of pyrolysis and oxidation reactions, there could be significant differences in smoldering behavior based on the fuel composition. Mulky and Niemeyer [1] performed a detailed study of smoldering behavior in terms of propagation speed and peak temperature of cellulose and hemicellulose mixtures. However, a computational study incorporating all three consituents has not yet been seen.

In addition to fuel composition, other major parameters that include the behavior of smoldering include density, moisture content, oxygen supply, and inorganic content [35–38]. Hartford [39] observed through experiments that the probability of sustained combustion drops with increases in the bulk density of organic soil. Chen, Rein, and Liu [36] studied the relationship between bulk density and critical moisture content, and observed a nearly linear decrease in critical moisture content with increases in organic bulk density of peat moss. Mulky and Niemeyer [1] numerically observed a decrease in propagation speed and an increase in peak temperature with density for cellulose and hemicellulose mixtures. Smucker et al. [40] experimentally saw similar trends for cellulose and hemicellulose mixtures. However, the importance of incorporating lignin in such mixtures is highlighted as it reflects the real composition of woody fuels.

Moisture content expressed as a percentage, defined in dry basis as mass of water in the fuel divided by mass of the dry fuel, is an important governing parameter for ignition and spread of smoldering, since porous media like woody fuels can hold moisture from 10% to as high as 300% [5, 41]. Huang and Rein [38] reported an increase in spread rate with moisture content for peat. Peat expands with addition of water, which they took into account, but most woody fuels do not undergo an expansion with moisture content,

so trends can change for biomass based on its origin. Another important parameter that needs attention is oxygen supply, as smoldering is limited by diffusion of oxygen from atmosphere into the fuel. For horizontal spread in peat smoldering fires, Yang et al. [104] found that increases in mass fraction of oxygen (Y_{O_2}) results in a transition from charring to surface glowing combustion in the upper surface of peat layer. For upward and downward smoldering, Huang and Rein [43] found the flow of water vapor and pyrolysis gases across the peat layer impact oxygen diffusion. Huang and Rein [23] identified an interdependency between oxygen concentration and fuel moisture in smoldering of peat fires. They observed that as moisture content increases, greater increases in oxygen concentration are needed to achieve ignition and prevent extinction. However, such study has not yet been conducted for more-general mixtures of cellulose, hemicellulose, and lignin.

It is evident that fuel composition, density, moisture content, and oxygen supply impact smoldering behavior, and thus understanding the parameters that control smoldering in woody fuels requires studying their effects. In this work, we developed a one-dimensional computational model to simulate smoldering of cellulose, hemicellulose, and lignin mixtures. We first validated the model using experimental data. Then, we used the validated model to analyze how fuel composition, density, and moisture content affect smoldering in terms of propagation speed and peak temperature. We also studied the interdependency between moisture content and oxygen concentration for ignition of a particular fuel composition that represents softwood.

4.3 Computational Model

We developed a one-dimensional transient numerical model to study downward propagation of smoldering of cellulose, hemicelloluse, and lignin mixtures using Gypro v0.8171 [105]. We used a cell size (Δz) of 1×10^{-4} m with an initial time step of 0.05 s. For the modeling effort we followed the approach of Mulky and Niemeyer [1], used to study mixtures of cellulose and hemicelloluse.

4.3.1 Governing equations and Boundary conditions

The model solves equations for both condensed and gas phases. The governing equations include: condensed-phase mass conservation (4.1), condensed-phase species conservation (4.2), gas-phase mass conservation (4.3), gas-phase species conservation (4.4), condensed-phase energy conservation (4.5), gas-phase momentum conservation (4.6), gas-phase energy conservation (4.7), and the ideal gas law equation of state (4.8):

$$\frac{\partial \overline{\rho}}{\partial t} = -\dot{\omega}'''_{fg} \ , \tag{4.1}$$

$$\frac{\partial (\overline{\rho} Y_i)}{\partial t} = \dot{\omega}'''_{fi} - \dot{\omega}'''_{di} \ , \tag{4.2}$$

$$\frac{\partial (\rho_g \overline{\psi})}{\partial t} + \frac{\partial \dot{m}''}{\partial z} = \dot{\omega}'''_{fg} \ , \tag{4.3}$$

$$\frac{\partial (\rho_g \overline{\psi} Y_j)}{\partial t} + \frac{\partial (\dot{m}'' Y_j)}{\partial z} = -\frac{\partial}{\partial z}(\overline{\psi} \rho_g D \frac{\partial Y_j}{\partial z}) + \dot{\omega}'''_{fj} - \dot{\omega}'''_{dj} \ , \tag{4.4}$$

$$\begin{aligned} \frac{\partial (\overline{\rho} \overline{h})}{\partial t} = {} & \frac{\partial}{\partial z}(\overline{k} \frac{\partial T}{\partial z}) - \dot{Q}'''_{s-g} + \sum_{k=1}^{K} \dot{Q}'''_{s,k} - \frac{\partial \dot{q}''_r}{\partial z} \\ & + \sum_{i=1}^{M} ((\dot{\omega}'''_{fi} - \dot{\omega}'''_{di}) h_i) \ , \end{aligned} \tag{4.5}$$

$$\dot{m}'' = -\frac{\overline{K}}{v} \frac{\partial P}{\partial z} \ , \tag{4.6}$$

$$\begin{aligned} \frac{\partial (\overline{\psi} \rho_g \overline{h_g})}{\partial t} + \frac{\partial (\dot{m}''_z \overline{h_g})}{\partial z} = {} & \frac{\partial}{\partial z}(\overline{\psi} \rho_g D \frac{\partial \overline{h_g}}{\partial z}) + h_{cv}(T - T_g) \\ & + \sum_{j=1}^{N} (\dot{\omega}'''_{s,fj} - \dot{\omega}'''_{s,dj}) h^*_{g,j} + \dot{Q}'''_{s-g} \ , \text{ and} \end{aligned} \tag{4.7}$$

$$P \overline{M} = \rho_g R T_g \ , \tag{4.8}$$

where ρ is the density; M is the number of condensed-phase species; X is the volume fraction; $\dot{\omega}'''$ is the reaction rate; T is the temperature; Y_j is the jth species mass fraction; ψ is the porosity; K is the permeability/number of reactions; h_{cv} is the volumetric heat transfer coefficient; $\overline{M}$ is the mean molecular mass obtained from local volume fractions of all gaseous species; $\dot{q}''_r$ is the radiative heat-flux; $\dot{Q}'''$ is the volumetric rate of heat release/absorption; R is the universal gas constant; D is the diffusion coefficient; h is the enthalpy; P is the pressure; subscripts f, d, i, j, k, s, and g represent formation,

destruction, condensed-phase species index, gas-phase species index, reaction index, solid, and gas; and * indicates that gas-phase species enthalpy is calculated at condensed phase temperature. The overbars over ρ, ψ, K, and k indicate an averaged value weighted by condensed-phase volume fraction, and the overbar over h indicates an averaged value weighted by condensed-phase mass fraction. Lautenberger and Fernandez-Pello [82] and Lautenberger [105] give detailed descriptions about the underlying model and solver.

At the top surface of the domain ($z = 0$) we set a convective heat transfer coefficient ($h_{c,0}$) of $10\,\mathrm{W/m^2K}$, simulating it as open to atmosphere with a mass-transfer coefficient ($h_{m,0}$) of $0.02\,\mathrm{kg/m^2s}$. The pressure and (ambient) temperature at the top surface were set as $1\,\mathrm{atm}$ and $300\,\mathrm{K}$, respectively. The bottom surface ($z = 10\,\mathrm{cm}$) was modeled as insulated to match the experimental setup used for validation [80]. To account for losses through the insulation we set a heat-transfer coefficient ($h_{c,L}$) of $3\,\mathrm{W/m^2K}$ and zero mass flux ($\dot{m}''$) at the bottom surface [35]. To ignite the sample we provided a heat flux ($\dot{q}''_e$) of $25\,\mathrm{kW/m^2}$ for $20\,\mathrm{min}$ at the top boundary to establish a self-sustained smoldering front. These boundary conditions were used for all simulations, except those where we analyzed the effects of moisture content on propagation speed (Section 4.4.3) where instead the heat flux was constant until the end of the simulation (to guarantee ignition).

4.3.2 Chemical kinetics

A heterogeneous reaction (k) involving condensed- and gas-phase species is described by

$$\mathrm{A}_k + \sum_{j=1}^{N} v'_{j,k}\,\mathrm{G}_j \longrightarrow v_{B,k}\,\mathrm{B}_k + \sum_{j=1}^{N} v''_{j,k}\,\mathrm{G}_j \;, \tag{4.9}$$

where $v'_{j,k}$ and $v''_{j,k}$ are the reactant and product stoichiometric coefficients for gas-phase species G_j in reaction k, $v_{B,k}$ is the stoichimetric coefficient for condensed-phase species B in reaction k, and N is the total number of gas-phase species. The destruction rate of species A in the above reaction is given by following Arrhenius equation:

$$\dot{\omega}'''_{dA_k} = Z_k \frac{(\overline{\rho} Y_{A_k} \Delta z)_{\sum}}{\Delta z} \left(\frac{\overline{\rho} Y_{A_k} \Delta z}{(\overline{\rho} Y_{A_k} \Delta z)_{\sum}} \right)^{n_k} \times \exp\left(-\frac{E_k}{RT}\right) g(Y_{\mathrm{O}_2}) \;, \tag{4.10}$$

where

$$(\overline{\rho} Y_{A_k} \Delta z)_{\sum} = \overline{\rho} Y_{A_k} \Delta z|_{t=0} + \int_0^t \dot{\omega}'''_{fi}(\tau) \Delta z(\tau) d\tau \ , \tag{4.11}$$

Z is the pre-exponential factor, E is the activation energy, n is the order of reaction, subscript dA stands for destruction of species A, and subscripts k, f, and i are reaction index, formation, and condensed-phase species index. Inert atmosphere is defined with $g(Y_{O_2}) = 1$ and oxidative atmosphere with $g(Y_{O_2}) = (1 + Y_{\mathrm{O_2}})^{n_{\mathrm{O_2},k}} - 1$ in Eq. (4.10) [82].

We used a chemical kinetic scheme with five reactions for each constituent (cellulose, hemicellulose, and lignin), which includes a drying step, pyrolysis step for the fuel, and three oxidation reactions of fuel, β-char, and α-char [23, 83]. The model includes 15 global reactions, with 15 condensed-phase species and 4 gas-phase species, where the following five reactions are repeated for cellulose, hemicellulose, and lignin (Fuel_k):

$$\mathrm{Fuel}_k \cdot v_{w,dr}\,\mathrm{H_2O} \longrightarrow \mathrm{Fuel}_k + v_{w,dr}\,\mathrm{H_2O\,(g)} \tag{R11}$$

$$\mathrm{Fuel}_k \longrightarrow v_{\alpha,cp}\,\alpha\text{-}\mathrm{Char_{f_k}} + v_{g,cp}\,\mathrm{Gas} \tag{R12}$$

$$\mathrm{Fuel}_k + v_{\mathrm{O_2},co}\,\mathrm{O_2} \longrightarrow v_{\beta,co}\,\beta\text{-}\mathrm{Char_{f_k}} + v_{g,co}\mathrm{Gas} \tag{R13}$$

$$\alpha\text{-}\mathrm{Char_{f_k}} + v_{\mathrm{O_2},c\alpha o}\,\mathrm{O_2} \longrightarrow v_{a,c\alpha o}\mathrm{Ash_{f_k}} + v_{g,c\alpha o}\mathrm{Gas} \tag{R14}$$

$$\beta\text{-}\mathrm{Char_{f_k}} + v_{\mathrm{O_2},c\beta o}\,\mathrm{O_2} \longrightarrow v_{a,c\beta o}\mathrm{Ash_{f_k}} + v_{g,c\beta o}\mathrm{Gas} \tag{R15}$$

where v is the stoichiometric coefficient; α and β indicate char produced from fuel pyrolysis and fuel oxidation reactions, respectively; and subscripts w, g, $\mathrm{O_2}$, a, f_k, dr, o, p, αo, βo are water, gas, oxygen, ash, fuel constitute, drying, oxidation, pyrolysis, α-char oxidation, and β-char oxidation, respectively. We obtained the chemical kinetic parameters (pre-exponential factor, activation energy, order of reaction, and heat of reaction) from Huang and Rein [23], stoichiometric coefficients for cellulose from Kashiwagi and Nambu [72] and for hemicellulose and lignin from Huang and Rein [34]. The consumption of oxygen is calculated using $v_{\mathrm{O_2},k} = \Delta H/(-13.1)$ MJ/kg [34, 85].

4.3.3 Physical properties

Table 4.1 lists the physical properties of condensed-phase species: solid density ($\rho_{s,i}$), thermal conductivity ($k_{s,i}$), and heat capacity (c_i). The bulk density of char is calculated using $\rho_{\mathrm{char}} \approx v_{\mathrm{char}} \times \rho_{\mathrm{fuel}}$ and the bulk density of ash using $\rho_{\mathrm{ash}} \approx \mathrm{AC}/100 \times 10 \times \rho_{\mathrm{fuel}}$,

where AC stands for ash content [1, 38]. The ash contents of cellulose, hemicellulose, and lignin are 0.3%, 1.2% and 1.4% respectively [1, 88]. We assumed that the physical properties of fuels do not depend on temperature [79].

Table 4.1: Thermophysical properties of condensed-phase species, taken from the literature for water, cellulose, hemicellulose, char, ash [1], and lignin [2–4].

Species	Solid density, $\rho_{s,i}$ (kg/m^3)	Thermal conductivity, $k_{s,i}$ ($W/(m\,K)$)	Heat capacity, c_i ($J/(kg\,K)$)
Water	1000	0.6	4186
Cellulose	1500	0.356	1674
Hemicellulose	1365	0.34	1200
Lignin	1305	0.39	1147
Char	1300	0.26	1260
Ash	2500	1.2	880

Porosity (ψ_i) and effective thermal conductivity (k_i) are calculated using $\psi_i = 1 - \rho_i/\rho_{s,i}$ and $k_i = k_{s,i}(1-\psi_i) + \gamma_i \sigma T^3$, where σ is the Stefan–Boltzmann constant and γ_i is an empirical parameter for radiation across pores. Pore size, γ_i, and permeability are calculated for each condensed-phase species using

$$d_{po,i} \approx d_{p,i} = \frac{1}{S_i \times \rho} \tag{4.12}$$

$$K_i = 1 \times 10^{-3} \times d_{p,i}^2 \tag{4.13}$$

$$\gamma_i = 3 \times d_{po,i}\ , \tag{4.14}$$

where ρ is the density of the fuel, S_i is the particle surface area for species i, $d_{p,i}$ is the particle size, K_i is the permeability, and $d_{po,i}$ is the pore size. For all simulations we set a 10% moisture content (MC), to represent the natural moisture present in fuels, except those where we explicitly varied the moisture content; the bulk density of moist fuel is calculated as $\rho_{\text{wet fuel}} = \rho_{\text{dry fuel}} \times (1 + \text{MC})$.

4.4 Results and Discussion

We determined the propagation speed and peak temperature to analyze smoldering behavior under different conditions. We calculated the propagation speed by the time

from when the temperature at 3 cm below the surface reached the ignition temperature to when that occurred at 6 cm below the surface. The ignition temperature is 300 °C for fuels with hemicellulose and 350 °C for fuels without hemicellulose. We followed the same approach as in experimental studies, since we validated our model results by comparing with the experimental results [80]. The peak temperature was calculated by taking the average of the peak temperatures every 1 cm.

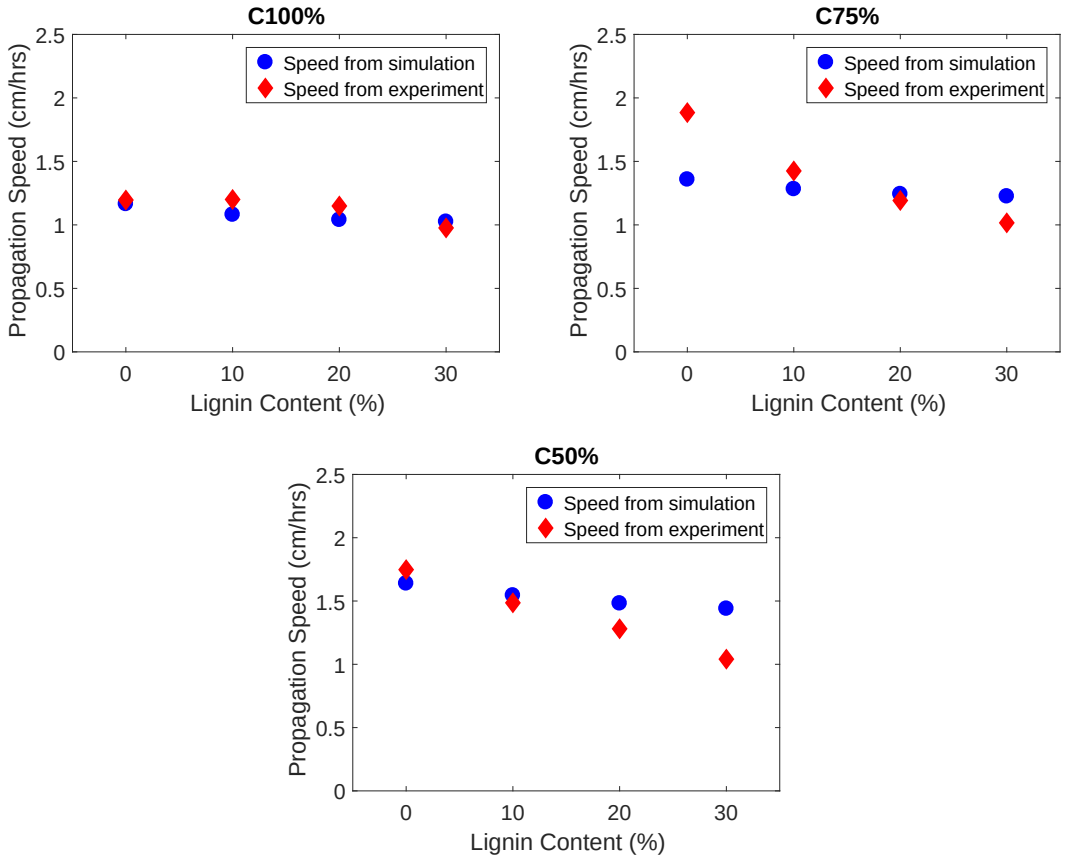

Figure 4.1: Comparison between numerical and experimental results for fuel mixtures with 100% cellulose (top left), 75% cellulose/25% hemicellulose (top right) and 50% cellulose/50% hemicellulose (bottom) combined with varying amounts of lignin.

4.4.1 Validation

We validated our model against the experimental data of Smucker and Blunck [80] considering the propagation speeds. Figure 4.1 shows the propagation speeds of different compositions at a density of 300 kg/m^3 where the lignin content varies from 0% to 30%. Two scenarios are considered: mixtures with 100% cellulose and varying amounts of lignin, and mixtures with 75% cellulose/25% hemicelloluse and varying amounts of lignin. For example, in the 100% cellulose cases, a lignin content of 10% means that the overall mixture has 10% lignin and 90% cellulose, while in the 75% cellulose cases, a lignin content of 10% means the overall mixture has 10% lignin, 67.5% cellulose, and 22.5% hemicellulose. Both the experimental and computational results exhibit similar trends, and the results match closely for the 100% cellulose cases. Simulation data for 50% cellulose case with no lignin content closely matches the experiments. However, for the 75% cellulose mixtures, the experimental results exhibit nearly 30% higher propagation speeds for no lignin content. This point could be an outlier, encouraging to investigate for experimental uncertainties. The propagation speeds of experiments drop more significantly with increasing lignin content for 75% and 50% cellulose mixtures than of simulations. This could be caused by the higher temperatures resulting from adding hemicellulose and lignin, which increase heat losses in the experiment that were not captured in the simulations.

4.4.2 Sensitivity to fuel composition and density

We investigated the effect of fuel composition on smoldering in terms of propagation speed and peak temperature. We varied the fuel composition in intervals of 10% for each constituent at a density of 300 kg/m^3, considering many possible combinations of cellulose, hemicellulose, and lignin. Figures 4.2 and 4.3 show the results for propagation speed and peak temperature, respectively.

Propagation speed decreases with increasing lignin content, while it rises with increasing hemicellulose content. However, if the hemicellulose content is kept constant, increasing lignin content decreases the speed (up to around 30% of that associated with lignin), and further increasing the lignin content slightly increases the propagation speed. We further investigated the reasons for why increasing lignin content decreases the prop-

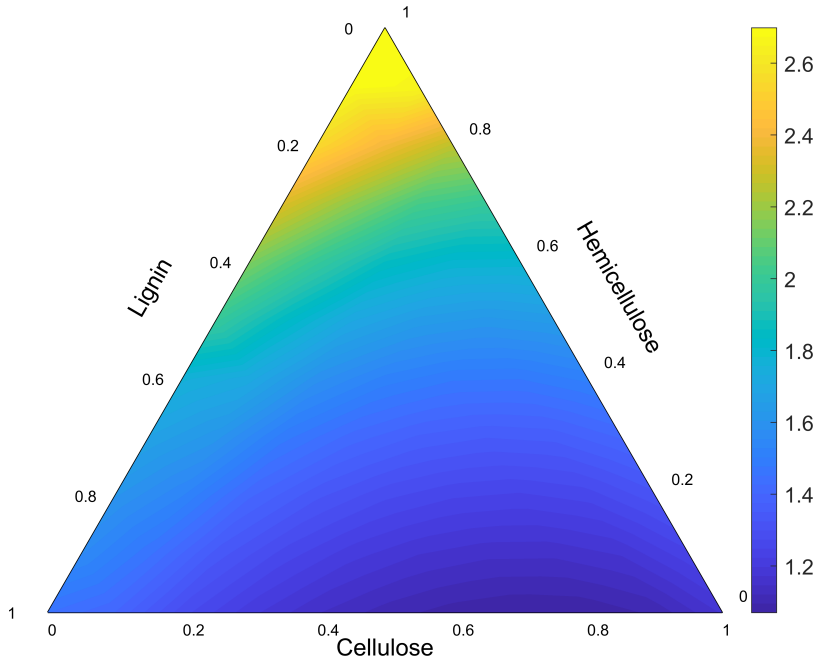

Figure 4.2: Propagation speeds (cm/h) for mixtures of cellulose, hemicelloluse, and lignin.

agation speed and increasing hemicellulose content increases the propagation speed.

Figure 4.4 shows reaction rates of the fuel components for a mixtuer with 45% cellulose, 45% hemicellulose and 10% lignin; hemicellulose undergoes pyrolysis first and lignin last. So, larger concentrations of hemicellulose lead to earlier mass loss, and the fuel shrinks faster, providing earlier access to oxygen and thus resulting in faster propagation. If the lignin content increases, the rate of pyrolysis drops, leading to decreases in speed. If the hemicellulose content is not changing for a particular composition, the changes in lignin and cellulose reactions need further attention.

Figure 4.3 shows that the peak temperature increases with both hemicellulose and lignin content. We investigated the reasons of this temperature behaviour, by individually varying the physical parameters of each constituent. Figure 4.5 shows the resulting temperature profiles along with temperature profiles of 67.5% cellulose with 10% lignin and 22.5% hemicellulose, and 90% cellulose with 10% lignin at a density of 300 $\mathrm{kg/m^3}$. The peak temperature of 67.5% cellulose with 10% lignin and 22.5% hemicellulose closely matches that of 90% cellulose with 10% lignin when γ associated with hemicellulose

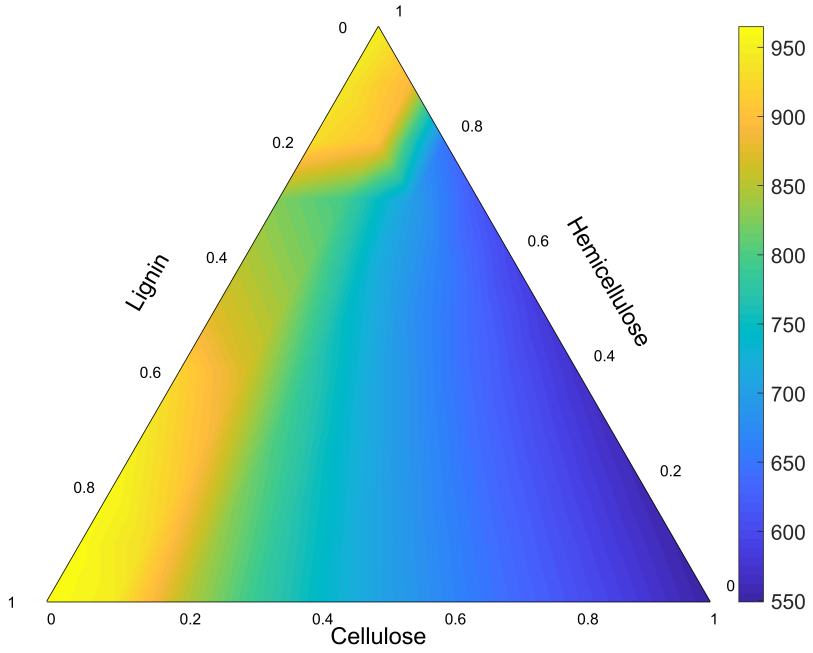

Figure 4.3: Peak temperatures (°C) for mixtures of cellulose, hemicelloluse, and lignin.

matches that of ash from pure cellulose.

Figure 4.6 shows the resulting temperature profiles along with temperature profiles of 70% cellulose with 30% lignin and 100% cellulose. The peak temperature of 70% cellulose with 30% lignin closely matches that of 100% cellulose when γ from lignin matches that of ash from pure cellulose. At 0–10% of cellulose, the temperature drops in the area where lignin content is in the range of 20–50% (remainder is hemicellulose), which needs further investigation.

Next, we investigated how density affects smoldering behavior. For this analysis we selected the compositions given in Table 4.2: the mean of softwood, the mean of hardwood, and paper [98]. Then, for the three compositions, we performed simulations with varying density. Figure 4.7 shows that propagation speed decreases with density and peak temperature increases with density. Hardwood has the highest propagation speeds, due to the fact that hardwood has the highest hemicellulose content. From hardwood to softwood the propagation speed decreases because lignin content increases. Softwood has higher peak temperature than hardwood. Paper has the lowest propagation

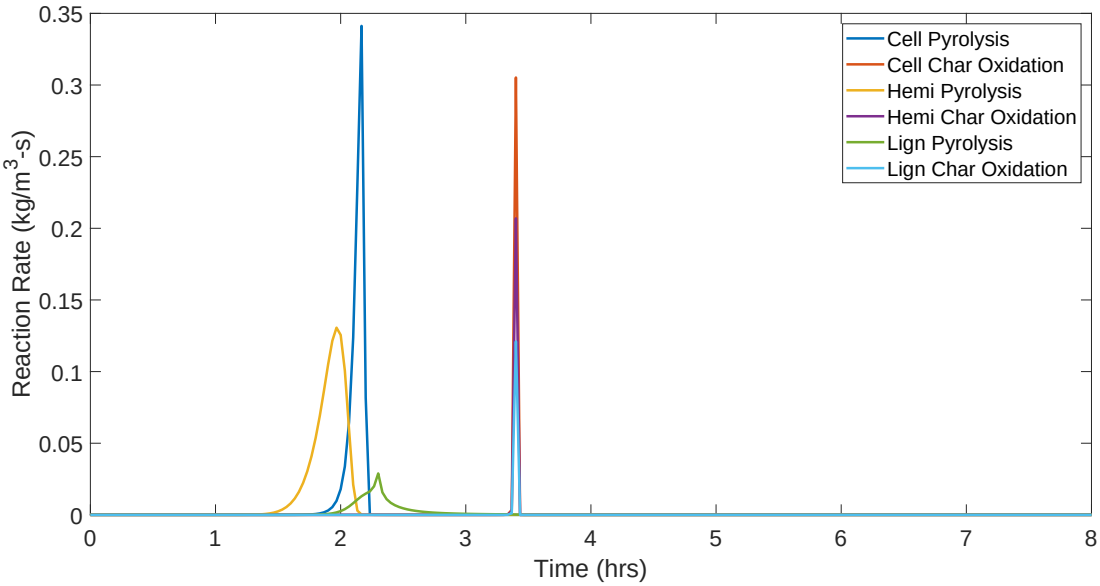

Figure 4.4: Reaction rates of cellulose, hemicellulose and lignin for pyrolysis and oxidation for 45% cellulose, 45% hemicellulose, and 10% lignin at density 300 kg/m^3.

speed and peak temperature, since paper is mostly comprised of cellulose. As the density increases, the effect of composition on propagation speeds decreases to the point where they nearly match for 400 kg/m^3; in contrast, composition plays an important role for peak temperature over the entire density range considered.

Table 4.2: Composition of softwood mean, hardwood mean, and paper [98]

Species	Cellulose content (%)	Hemicellulose content (%)	Lignin content (%)
Mean of softwood	47	24	29
Mean of hardwood	46	31	23
Paper	74	9	17

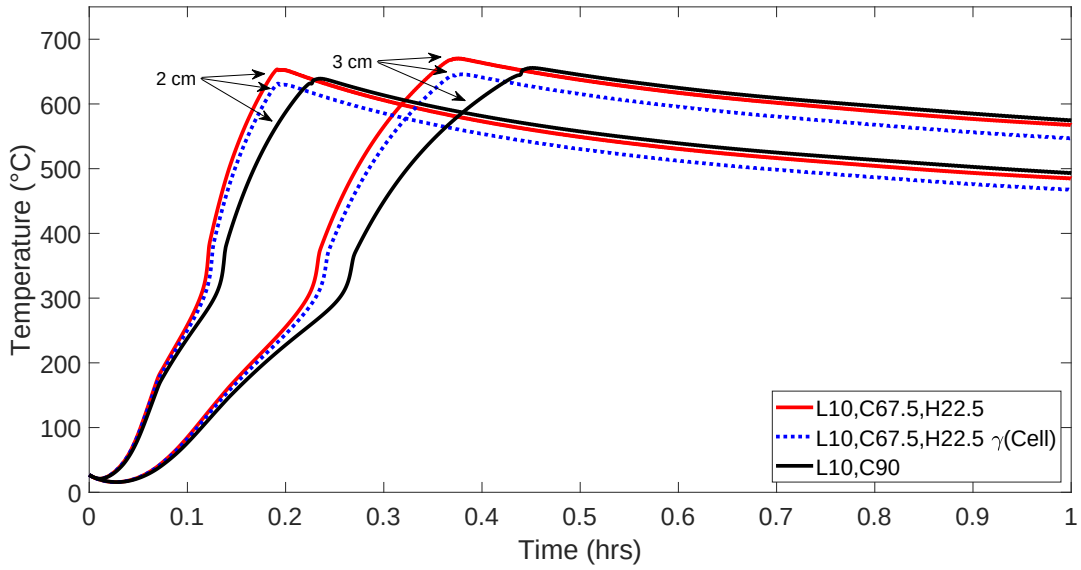

Figure 4.5: Temperature profiles at depths of 2 and 3 cm for fuels with density 300 kg/m^3 and composition of 67.5% cellulose, 90% cellulose, and 67.5% cellulose with the empirical parameter for radiation across pores of ash coming hemicellulose set equal to cellulose.

4.4.3 Effect of moisture content

Next, we analyzed how moisture content affects smoldering behavior for the three compositions given in Table 4.2. In this analysis we considered that the fuels do not expand with addition of water, since woody fuels do not have such reported expansion [38]. Figure 4.8 shows that both propagation speed and peak temperature decreases with increases in moisture content. Hardwood has the highest propagation speeds. Softwood and paper have very close propagation speeds, and the values become closer with increasing moisture content. The two fuels have matching propagation speeds at 70% moisture content. However, paper exhibits significantly lower peak temperatures, while softwood has the highest peak temperature. These results motivate further analysis into the reasons for these behaviors.

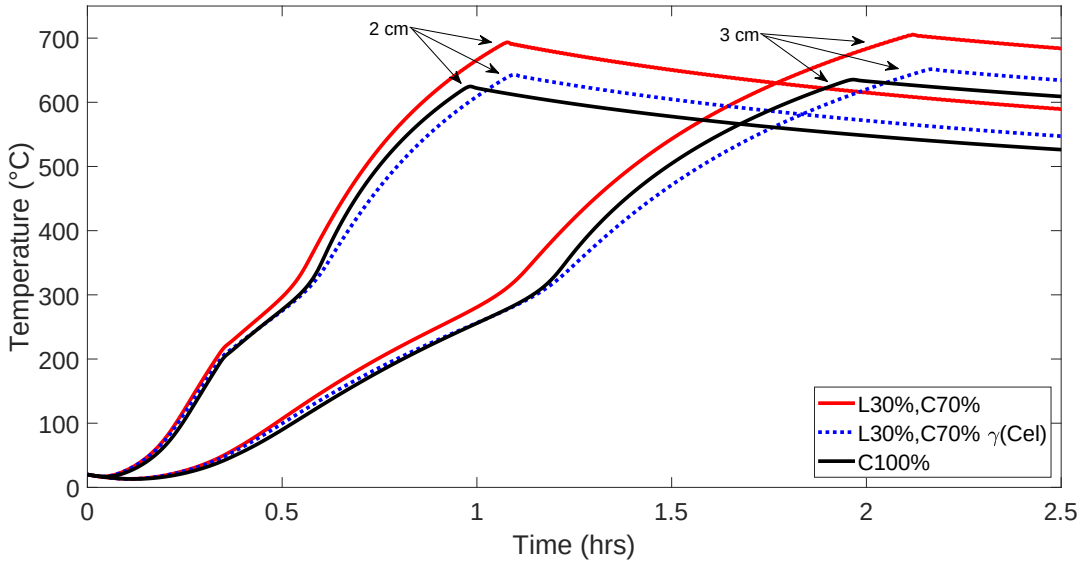

Figure 4.6: Temperature profiles at depth 2 and 3 cm for fuels with density 300 kg/m^3 and fuel composition of 70% cellulose, 100% cellulose, and 70% cellulose with the empirical parameter for radiation across pores of ash coming hemicellulose set equal to cellulose.

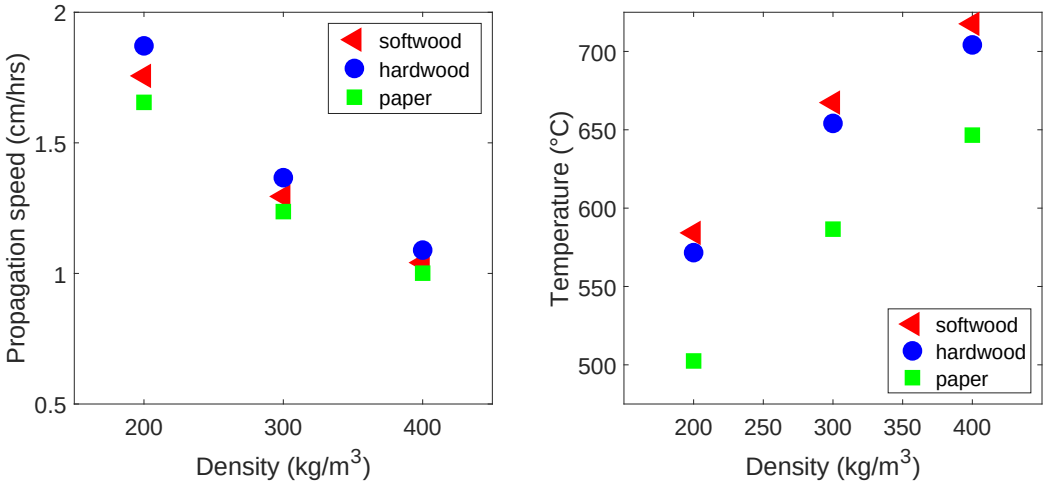

Figure 4.7: Effects of varying density on propagation speed (left) and peak temperature (right).

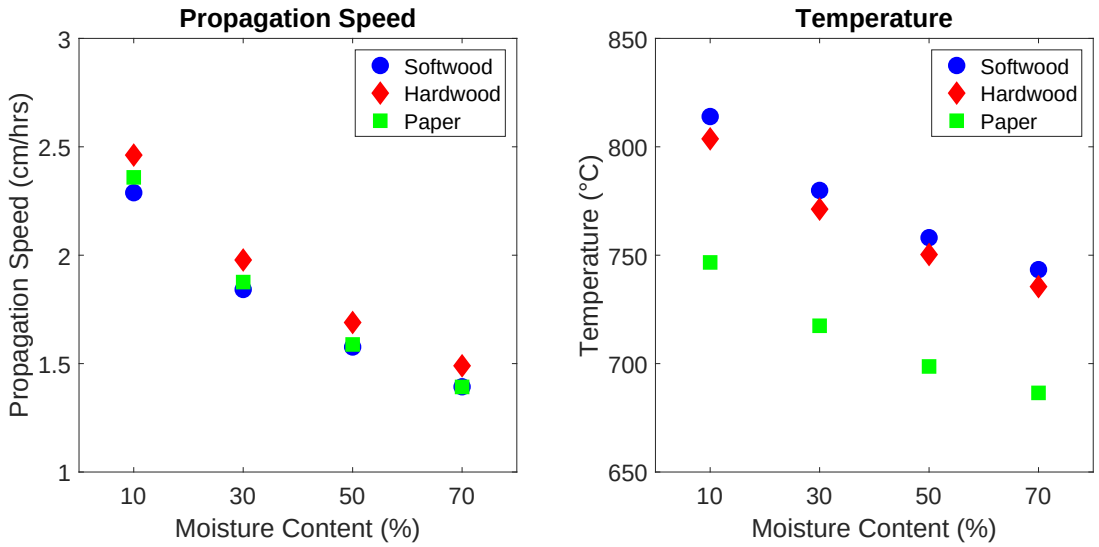

Figure 4.8: Effect of moisture content on propagation speed and peak temperature

4.4.4 Effect of oxygen concentration and moisture content on ignition

We also studied the interdependence between oxygen concentration and moisture content for a successful smoldering ignition, using softwood. We varied the moisture content from 10% to 110% in increments of 10%, and the oxygen concentration (Y_{O_2}) from 10% to 40% in increments of 5%. We used an increment of 1% near the boundary of the ignition and non-ignition zones to correctly identify the transition. Figure 4.9 shows the ignition and non-ignition zones considering different oxygen concentration and moisture content combinations. We find similar behavior as Huang and Rein [34] did for peat, where increases in moisture content require increases in oxygen concentration for successful ignition. This study helps to predict a relationship for critical moisture content and critical oxygen concentration for smoldering ignition of woody fuels.

4.5 Conclusions

In this work, we developed a one-dimensional computational model to study smoldering of cellulose, hemicellulose, and lignin mixtures. We validated the model by comparing the propagation speeds of different compositions of the three constituents with experimental

results. Then, we used the model to analyze how fuel composition, density, and moisture content affect propagation speed and peak temperature. We also examined the effect of moisture content and oxygen concentration on a successful smoldering ignition.

We found that increasing lignin content decreases the propagation speed, while increasing hemicellulose content raises the propagation speed due to slower pyrolysis of lignin and faster pyrolysis of hemicellulose, respectively. Peak temperature rises with both increasing lignin and hemicellulose content, caused by formation of ash that reduces the radiation loss across pores. We varied the density for three mixtures that represent softwood, hardwood, and paper, and showed that with increasing density, propagation speed decreases and peak temperature rises. When moisture content is increased, the propagation speed and peak temperature drop for the mixtures considered. We observed an interdependence between moisture content and oxygen concentration for ignition, where increasing moisture content needs matching increases in oxygen concentration to ignite. These findings help us to understand how fuel composition, density, moisture content, and oxygen concentration affect smoldering of woody fuels and encourage further investigation in this area.

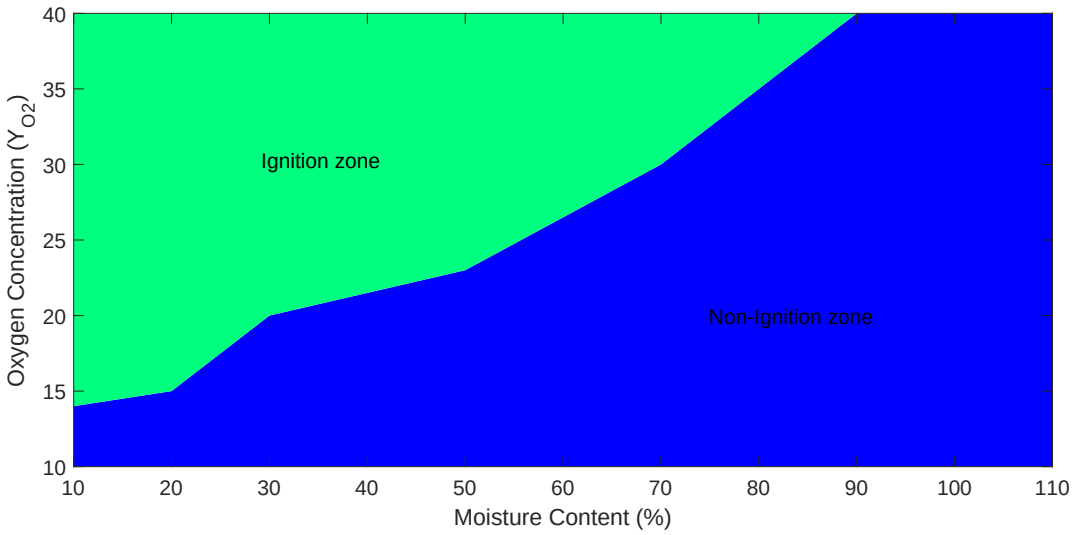

Figure 4.9: Effect of moisture content and oxygen concentration on ignition

4.6 Acknowledgements

The Strategic Environmental Research and Development Program (SERDP) funded this research, award RC-2651 under contract number W912HQ-16-C-0045. We thank David Blunck and Benjamin Smucker from Oregon State University for the experimental data provided for validation of our model.

The findings and views discussed in this paper are those of the authors and should not be interpreted as an official Department of Defense position of decision unless so designated by other official documentation.

Chapter 5: Uncertainty and sensitivity analysis for chemical kinetic parameters and thermophysical properties in smoldering combustion of wildland fuels

W. Jayani Jayasuriya and Kyle E. Niemeyer

My contributions to this work included developing the Monte Carlo model, running simulations, processing the output data, analyzing the results, and preparing the manuscript.

Initial study: Proceedings of the 2022 Spring Hybrid Meeting of the Western States Section of the Combustion Institute
Target Journal: Combustion Theory and Modelling (In Preparation)

5.1 Abstract

Smoldering combustion can be modeled using a kinetic scheme that involves kinetic parameters and thermophysical properties. These data can have different values depending on the source and the experimental setup used for measurements. Wildland fuels that under go smoldering can be modeled as a mixture of cellulose, hemicellulose and lignin. The composition can change depending on the species of origin, decomposition rate and fermentation method used to capture composition. Variations in input parameters can significantly impact the output calculations, but the impact of these variations have not been substantially studied previously. Here, we conducted three separate uncertainty analyses to investigate the effects of kinetic parameters, thermophysical properties and composition on smoldering behaviour. We used a Monte Carlo approach for our analysis, with propagation speed and mean peak temperature as global properties representing smoldering behaviour. The results indicate that uncertainties in physical properties result in higher computed uncertainty in both propagation speed and peak temperature, compared with kinetic parameters and composition. Next, we conducted a sensitivity analysis using One-at-a-time and Morris screening methods to identify which parameters have higher influence on output estimates. We saw that activation energy (E) has an exponentially increasing relationship with propagation speed and peak temperature. As second most important parameters, propagation speed is sensitive to heat capacity (C) and peak temperature to thermal conductivity (k). Hence, our work suggests that even though behavior of smoldering combustion is highly sensitive to kinetic properties, uncertainties associated with them are lower and even though physical properties have higher uncertainties associated, behavior of smoldering combustion in wildland fires is less sensitive to them.

5.2 Introduction

Smoldering combustion of wildland fuels can be computationally modeled using a chemical kinetic scheme [23]. The kinetic scheme that represents smoldering can vary depending on the complexity a numerical model can handle and the level of accuracy expected. Depending on the complexity of the kinetic scheme the parameters involved in computational modelling will also change. Thermophysical properties also play an important role

for accurate predictions of smoldering behaviour due to their impact on energy balances and chemical equilibrium [106]. These kinetic parameters and thermophysical property values can have different ranges depending on the source and the experiments used to determine them. With parameter ranges in input parameters, computed quantities such as propagation speed and peak temperature will also vary. Therefore, conducting uncertainty analysis is important to identify the effects of these parameters on smoldering behavior, and bound the uncertainty in computed results.

Anca-Couce [20] reviewed chemical kinetic schemes and multi-scale modeling of lignocellulosic biomass pyrolysis. Among other topics, they reviewed 10 chemical kinetic models, but did not consider the differing effects of these models/model parameters on outputs. Anca-Couce et al. [71] earlier studied kinetics and reaction heats of smouldering of pine wood, providing input parameters that are needed to model smoldering of pine wood. However, they did not examine the uncertainly associated with these parameters. Similarly, a number of studies [107, 108] focused on finding kinetic schemes and parameters that represent smoldering combustion, but to our knowledge none have focused on the uncertainties associated with these parameters and the impacts of these uncertainties. Thermochemical properties that are chosen for a particular kinetic scheme can vary depending on the source of information or experimental setup where these are measured [28–32]. With varying input parameters, the computed outputs are uncertain, and an analysis of this uncertainty can bound these.

Smoldering combustion can occur in surface and ground fuels within forest fuel beds. Forest fuel beds typically consist of three layers: the top (litter) layer, middle (fermentation) layer, and bottom (humus) layer. Barks of softwood and hardwood trees and twigs mostly comprise the litter layer, where smoldering can initiate. Larger smoldering fires occur in duff and peat fuels, which are present in the fermentation and humus layers [19]. The composition of these fuels can be expressed as a mixture of cellulose, hemicellulose, and lignin. The composition can change depending on the species of origin, decomposition rate, fermentation method used to capture composition and experimental setup. Anca-Couce and Obernberger [109] reported a composition of 44% cellulose, 34% hemicellulose, and 22% lignin for hardwood. Richter et al. [98] reported a range for composition of hardwood as 45±6% cellulose, 29±7% hemicellulose, and 23±5% lignin. Similarly, Anca-Couce and Obernberger [109] reported 44% cellulose, 26% hemicellulose, and 30% lignin for softwood. And Richter et al. [98] reported 47±6% cellulose, 21±7%

hemicellulose, and 29±5% lignin for softwood. Berg et al. [110] discussed the changes in composition of duff with time. A well decomposed duff layer has higher lignin content than a duff layer at an earlier stage of decomposition because lignin decomposes at the slowest rate compared to cellulose and hemicellulose. There are number of research done on smoldering of peat with different species of origins reported [23, 35, 38, 83]. The composition of twigs also differs mostly based on the species of origins [98, 107, 111]. These studies show that composition of forest fuels can differ, however they do not discuss on the uncertainties associated with composition when modeling smoldering of forest fuels. The effect of chemical composition on modeling charring of softwood and hardwood was studied by Richter et al. [98]. They have complied a database of over 600 compositions, and have studied across scales using a microscale and mesoscale model. They found that the variation in kinetics is negligible for predicting charring across scales. And they suggested that a kinetic model of charring derived for one wood species can be used for all wood species within softwood or hardwood. However, this study is limited for charring reactions and for softwood and hardwood.

It is evident that identifying uncertainties associated with kinetic parameters, thermophysical properties and composition is important when modeling smoldering combustion. It is also important to quantitatively analyze the influence of these different parameters to identify the level of the influence on output estimates using a sensitivity analysis. High priority should be given to the uncertainties of parameters that have significant effects on simulation results. For complex models its important to identify parameters with high significance because modellers can ignore uncertainties of low impact parameters to reduce their computational cost. There are two categories of sensitivity analyses, namely local and global. A local sensitivity analysis studies sensitivity relative to change of a single parameter value, while a global analysis examines sensitivity with regard to the entire parameter space. Sensitivity analyses conducted in modeling of smoldering combustion in wildland fuels have not been found. However, some related studies in the area of self-ignition of coal and smoldering of cellulose and hemicellulose mixtures are found. A computational model was developed by Yuan et al. [33] to simulate self-heating ignition for coal origins. They have conducted a local sensitivity analysis using one-at-a-time method to access the significance of kinetic and physical parameters on ignition temperature. They found that activation energy has the highest impact on ignition temperature and suggested that activation energy should be optimized when considering

measurement of uncertainty. Jayasuriya et al. [112] conducted a local sensitivity analysis to identify which parameters contribute most to reduce speed and temperature with moisture content in cellulose and hemicellulose mixtures. They identified that increase of wet bulk density is the main reason for the drop in propagation speed and increase in both wet bulk density and heat of reaction contribute to the drop in temperature.

In this work, we developed a one-dimensional computational model to simulate smoldering of cellulose, hemicellulose, and lignin mixtures. We modeled smoldering of mixtures that represent five different fuels that are most pron to under go smoldering in wildfires. Next, we conducted three separate uncertainty analyses, considering variations in kinetic parameters, thermophysical parameters and fuel composition using a Monte Carlo approach. We conducted another overall uncertainty analysis considering variations in all parameters together. Then, we conducted a sensitivity analysis using two methods to identify which parameters have higher significance on propagation speed and peak temperature. The first method was One-at-a-time analysis and second was Morris screening method. Finally, we investigated why some of the parameters are highly sensitive to our output estimates.

5.3 Methodology

Our one-dimensional transient numerical model simulates downward propagation of smoldering in cellulose, hemicelloluse, and lignin mixtures, using a set of heterogeneous reactions that involve complex kinetic schemes. On the other hand, we specify the physical properties of the condensed-phase species that are used in kinetic schemes. We used Gpyro v0.8171 [82] for our simulations. For our uncertainty analysis, we considered mixtures of cellulose, hemicelloluse, and lignin that represents the composition of five different fuels (listed in Table 5.3) at a density of 300 $\mathrm{kg/m^3}$. For our sensitivity analysis, we considered a mixture of cellulose, hemicelloluse, and lignin that represents the composition of one-year decomposed duff from Scots pines at a density of 300 kg/m3.

5.3.1 Chemical kinetics

A heterogeneous reaction (k) involving condensed- and gas-phase species is described by

$$\mathrm{A}_k + \sum_{j=1}^{N} v'_{j,k}\,\mathrm{G}_j \longrightarrow v_{B,k}\,\mathrm{B}_k + \sum_{j=1}^{N} v''_{j,k}\,\mathrm{G}_j \ , \tag{5.1}$$

where $v'_{j,k}$ and $v''_{j,k}$ are the reactant and product stoichiometric coefficients for gas-phase species G_j in reaction k, $v_{B,k}$ is the stoichimetric coefficient for condensed-phase species B in reaction k, and N is the total number of gas-phase species. The destruction rate of species A in the above reaction is given by following Arrhenius equation:

$$\dot{\omega}'''_{dA_k} = Z_k \frac{(\overline{\rho} Y_{A_k} \Delta z)_{\sum}}{\Delta z} \left(\frac{\overline{\rho} Y_{A_k} \Delta z}{(\overline{\rho} Y_{A_k} \Delta z)_{\sum}} \right)^{n_k} \times \exp\left(-\frac{E_k}{RT}\right) g(Y_{\mathrm{O}_2}) \ , \tag{5.2}$$

where

$$(\overline{\rho} Y_{A_k} \Delta z)_{\sum} = \overline{\rho} Y_{A_k} \Delta z|_{t=0} + \int_0^t \dot{\omega}'''_{fi}(\tau) \Delta z(\tau) d\tau \ , \tag{5.3}$$

Z is the pre-exponential factor, E is the activation energy, n is the order of reaction, subscript dA stands for destruction of species A, and subscripts k, f, and i are reaction index, formation, and condensed-phase species index. Inert atmosphere is defined with $g(Y_{O_2}) = 1$ and oxidative atmosphere with $g(Y_{O_2}) = (1 + Y_{\mathrm{O}_2})^{n_{\mathrm{O}_2,k}} - 1$ in Eq. (5.2) [82].

We used a chemical-kinetic scheme with five reactions for each constituent (cellulose, hemicellulose, and lignin), which includes a drying step, pyrolysis step for the fuel, and three oxidation reactions of fuel, β-char, and α-char [23, 83]. The model includes 15 global reactions, with 15 condensed-phase species and 4 gas-phase species, where the following five reactions are repeated for cellulose, hemicellulose, and lignin (Fuel_i, $i = 1, 2, 3$):

$$\mathrm{Fuel}_i \cdot \nu_{w,dr}\,\mathrm{H_2O} \longrightarrow \mathrm{Fuel}_i + \nu_{w,dr}\,\mathrm{H_2O(g)} \tag{R16}$$

$$\mathrm{Fuel}_i \longrightarrow \nu_{\alpha,ip}\,\alpha\text{-}\mathrm{Char}_{\mathrm{f_i}} + \nu_{g,ip}\,\mathrm{Gas} \tag{R17}$$

$$\mathrm{Fuel}_i + \nu_{\mathrm{O}_2,io}\,\mathrm{O_2} \longrightarrow \nu_{\beta,io}\,\beta\text{-}\mathrm{Char}_{\mathrm{f_k}} + \nu_{g,io}\mathrm{Gas} \tag{R18}$$

$$\alpha\text{-}\mathrm{Char}_{\mathrm{f_i}} + \nu_{\mathrm{O}_2,i\alpha o}\,\mathrm{O_2} \longrightarrow \nu_{a,i\alpha o}\mathrm{Ash}_{\mathrm{f_i}} + \nu_{g,i\alpha o}\mathrm{Gas} \tag{R19}$$

$$\beta\text{-}\mathrm{Char}_{\mathrm{f_i}} + \nu_{\mathrm{O}_2,i\beta o}\,\mathrm{O_2} \longrightarrow \nu_{a,i\beta o}\,\mathrm{Ash}_{\mathrm{f_i}} + \nu_{g,i\beta o}\mathrm{Gas} \tag{R20}$$

where ν is the stoichiometric coefficient; α and β indicate char produced from fuel pyrolysis and fuel oxidation reactions, respectively; and subscripts w, g, O_2, a, f_i, dr, o, p, αo, and βo are water, gas, oxygen, ash, fuel constituent, drying, oxidation, pyrolysis, α-char oxidation, and β-char oxidation, respectively.

We obtained all the chemical kinetic parameters from Huang and Rein [23]. They have specified a range for these chemical kinetic parameters while giving the choice of one value for each parameter out of that range. Table 5.1 shows the range for each parameter. We conducted an uncertainty analysis considering that all the chemical kinetic parameters can be any value inside each range, using random sampling.

5.3.2 Physical properties

Table 5.2 lists the data ranges for physical properties of condensed-phase species: solid density ($\rho_{s,i}$), thermal conductivity ($k_{s,i}$), and heat capacity (c_i). The bulk density of char is calculated using $\rho_{\text{char}} \approx$ stoichiometric coefficient of char $\times \rho_{\text{fuel}}$ and the bulk density of ash using $\rho_{\text{ash}} \approx \text{AC}/100 \times 10 \times \rho_{\text{fuel}}$, where AC stands for ash content [1, 38]. The ash contents of cellulose, hemicellulose, and lignin are 0.3%, 1.2% and 1.4% respectively [1, 88]. We have conducted another uncertainty analysis for physical property inputs to analyse the impacts on smoldering behaviour.

5.3.3 Fuel composition

The five different fuels that we selected for the uncertainty analysis are commonly subjected to smoldering in wildfires. The composition of these fuels can change depending on the source and experimental setup. Table 5.3 gives the composition of each fuel based on the mass fraction of cellulose, hemicellulose, and lignin. So we conducted a separate uncertainty analysis to investigate the effects of composition on our output estimates.

5.3.4 Calculation of global quantities

The two main parameters that we used as estimates for uncertainty and sensitivity analyses are mean propagation speed of smoldering and mean peak temperature. We calculated propagation speed using the time between when the temperature at 3 cm below

Table 5.1: Kinetic parameter ranges for cellulose, hemicellulose, and lignin models.

Reaction	$\log Z$ $\log \mathrm{s}^{-1}$	E kJ/mol	ΔH MJ/kg	n –	n_{O_2} –
		Cellulose			
Drying	[6.62, 7.35]	[56.9, 61.5]	2.26	[2.25, 2.53]	–
Pyrolysis	[9.43, 12.9]	[131, 168]	0.5	[0.88, 1.13]	–
Oxidation	[20.4, 25.4]	[236, 297]	-28.2	[1.00, 1.97]	[0.72, 0.91]
β-char oxidation	[6.89, 8.2]	[110, 127]	-28.8	[1.08, 1.45]	[0.74, 0.95]
α-char oxidation	[10.6, 12.8]	[159, 186]	-27.8	[0.75, 0.99]	[0.50, 0.64]
		Hemicellulose			
Reaction	$\log Z$ $\log \mathrm{s}^{-1}$	E kJ/mol	ΔH MJ/kg	n –	n_{O_2} –
Drying	[6.62, 7.35]	[56.9, 61.5]	2.26	[2.25, 2.53]	–
Pyrolysis	[5.29, 7.20]	[78.5, 96.5]	0.5	[0.74, 1.00]	–
Oxidation	[15.0, 20.2]	[228, 295]	-20.9	[0.40, 1.60]	[0.10, 0.13]
β-char oxidation	[6.89, 8.2]	[110, 127]	-28.8	[1.08, 1.45]	[0.74, 0.95]
α-char oxidation	[10.6, 12.8]	[159, 186]	-27.8	[0.75, 0.99]	[0.50, 0.64]
		Lignin			
Reaction	$\log Z$ $\log \mathrm{s}^{-1}$	E kJ/mol	ΔH MJ/kg	n –	n_{O_2} –
Drying	[6.62, 7.35]	[56.9, 61.5]	2.26	[2.25, 2.53]	–
Pyrolysis	[10.1, 12.5]	[135, 158]	0.5	[6.20, 8.10]	–
Oxidation	[20.6, 24.5]	[254, 299]	-9.7	[2.79, 4.16]	[0.91, 1.08]
β-char oxidation	[6.89, 8.2]	[110, 127]	-28.8	[1.08, 1.45]	[0.74, 0.95]
α-char oxidation	[10.6, 12.8]	[159, 186]	-27.8	[0.75, 0.99]	[0.50, 0.64]

Table 5.2: Thermophysical properties of condensed-phase species

Species	Solid density, $\rho_{s,i}$ $(\mathrm{kg/m^3})$	Thermal conductivity, $k_{s,i}$ $(\mathrm{W/(m\,K)})$	Heat capacity, c_i $(\mathrm{J/(kg\,K)})$
Cellulose	[1500, 1600]	[0.26, 0.356]	[1209, 1674]
Hemicellulose	[1365, 1400]	[0.2, 0.34]	[1200, 1305]
Lignin	[1305, 1400]	[0.2, 0.39]	[1140, 1200]
Char	[1300, 2333]	[0.117, 0.26]	[1100, 1260]
Ash	[2400, 2500]	[0.8, 1.2]	[880, 1380]

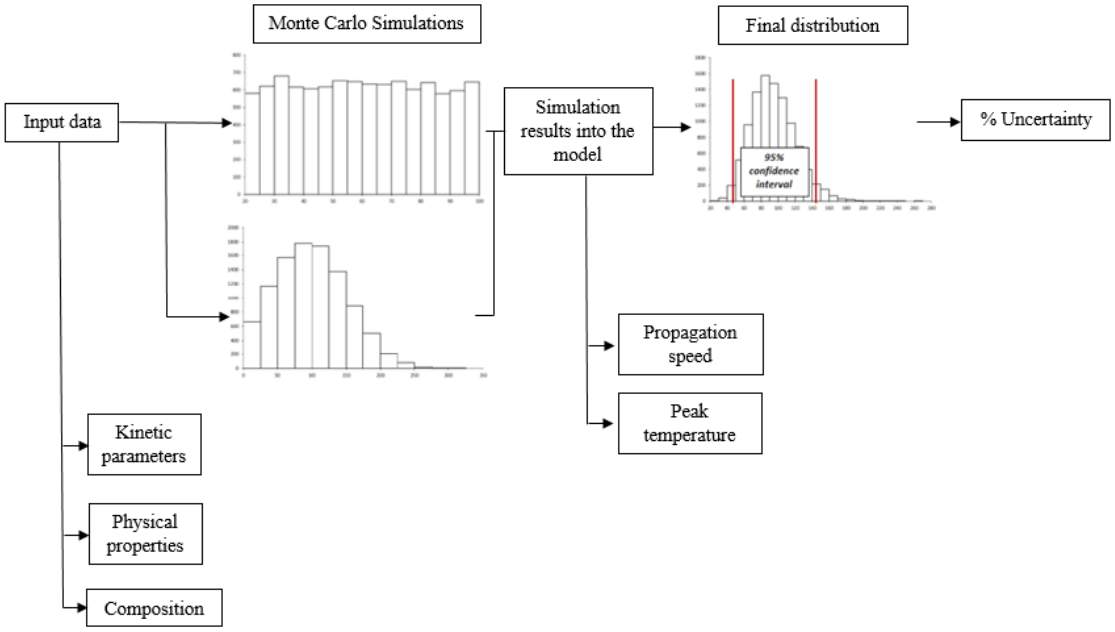

Figure 5.1: Illustration of the approach.

the surface reaches the ignition temperature and when that occurs at 6 cm below the surface. The ignition temperature is 300 °C. We calculated mean peak temperature by averaging the peak temperatures at every 1 cm depth intervals.

5.3.5 Monte Carlo simulation approach for uncertainty analysis

The Monte Carlo approach involves repeated simulation of samples within the probability density functions (PDF) of the input data. We assumed that the input data is following a uniform distribution for physical properties and composition, and a normal distribution for kinetic properties. The Monte Carlo simulations are run using algorithms which generate stochastic (i.e., random) values based on the PDF of the data. The objective of these repeated simulations is to produce distributions that represent the likelihood of different estimates. The estimates that we used to analyse smoldering behavior are propagation speed and mean peak temperature. To calculate the uncertainty, the confidence interval can then be identified for the final distributions of propagation speed and mean peak temperature. Figure 5.1 shows a summary of our approach. We estimated the uncertainty

Table 5.3: Composition of the fuels [98, 109, 110, 113]

Species	Cellulose (%)	Hemicellulose (%)	Lignin (%)
Duff	[30, 35]	[20, 25]	[40, 50]
Peat	[25, 30]	[10, 15]	[55, 65]
Softwood	[40, 45]	[20, 30]	[30, 35]
Hardwood	[40, 45]	[30, 40]	[20, 25]
Twigs	[10, 20]	[50, 55]	[30, 35]

of variations in kinetic parameters, physical properties and composition separately as three different analyses because we wanted to find out which of those has the higher impact on smoldering behaviour. Then we conducted another uncertainty analysis considering variation in kinetic parameters, physical properties and composition simultaneously to see the overall uncertainty of the estimates.

We calculated the confidence interval of the two estimates using

$$\bar{x} \pm z \times \frac{\sigma}{\sqrt{n}} \,, \tag{5.4}$$

where $\bar{x}$ is the sample mean of the distribution, z is z-value for a given confidence level (95%), σ is standard deviation of the mean and n is number of simulations. Table 5.4 shows the number of simulations conducted. Then, we calculated the uncertainty as a percentage using

$$\% \text{ uncertainty} = \frac{\frac{1}{2} \times (\text{confidence interval width})}{(\text{median of the final distribution})} \times 100 \,. \tag{5.5}$$

5.3.6 Sensitivity analysis

In our uncertainty analysis we saw that physical properties and kinetic parameters have bigger impacts on the overall uncertainty of our estimates. It is necessary to quantitatively analyze the influence of these different parameters to identify the level of the influence on estimates. For the parameters that have significant effects on simulation results, their uncertainties should be given higher priority. We conducted two sensitivity analysis

Table 5.4: Number of simulations for each uncertainty analysis

Species	Kinetic	Physical	Composition	Overall
Duff	480	280	120	100
Peat	120	120	120	120
Softwood	150	150	150	150
Hardwood	100	100	100	100
Twigs	150	150	150	150

approaches considering physical properties and kinetic parameters to identify and quantify the significance of the impacts on each estimate, namely propagation speed and mean peak temperature separately for duff.

5.3.6.1 One-at-a-time analysis

One-at-a-time analysis (OAT) is a local sensitivity analysis technique that quantifies the sensitivity levels of different parameters using a sensitivity coefficient. Sensitivity coefficient derived as the derivative of output (y) with respect to the parameter of interest (X). We used a dimensionless sensitivity coefficient ($\bar{s}$) because the parameters compared have different units. It can be calculated using [114]:

$$\bar{s} = \frac{y(X_i + \Delta X_i) - y(X_i)}{\Delta X_i} \times \frac{X_i}{y(X_i)} \ . \tag{5.6}$$

We used propagation speed and mean peak temperature as y estimates and all the other kinetic and physical properties listed in Table 5.1 and Table 5.2 as X_i input parameters of interest. We chose Δ as 50%.

5.3.6.2 Morris screening analysis

The Morris screening method is based on the repetition of a set of randomized OAT analyses. The Morris method overcomes the limitation of the local sensitivity analysis by performing partial derivative calculations in different locations of the input variable domain of variation. The method is global because the input variables can vary over their entire domain of definition [115]. Morris screening calculates the mean (μ) and standard

deviation (σ) of sensitivity of parameter X using

$$d_i^j = \frac{y(X_i^j + \Delta X_i^j) - y(X_i^j)}{\Delta X_i^j} \times \frac{X_i^j}{y(X_i^j)} \,, \tag{5.7}$$

$$\mu_i = \frac{1}{N} \sum_{j=1}^{N} |d_i^j| \,, \tag{5.8}$$

$$\sigma_i = \sqrt{\frac{1}{N-1} \sum_{j=1}^{N} (d_i^j - \mu_i)^2} \,, \tag{5.9}$$

where d_i^j is the OAT sensitivity matrix of parameter X_i^j, X_i^j indicates each ith input parameter at each jth random pick and N is number of parameter samples. We used propagation speed and mean peak temperature as y estimates and all the other kinetic and physical properties listed in Table 5.1 and Table 5.2 as X_i input parameters of interest. We used Δ as 50% and a sample size (N) of 10.

5.4 Results and Discussion

5.4.1 Uncertainty analysis

We used five fuel mixtures that commonly undergo smoldering combustion is wildfires in our uncertainty analysis. We conducted four uncertainty analyses to identify the effects of kinetic parameters, physical properties, fuel composition and an overall uncertainty. Our output estimates are propagation speed and peak temperature. For all the five fuels we saw normal distributions in computed output estimates. In this paper we included output distributions for the fuel duff as an example. Figure 5.2 shows the normal distribution of computed outputs with varying kinetic parameters for duff. As Figure 5.3 shows, the calculations with varying physical properties also follows an expected normal distribution, and similarly a normal distribution for variations in composition as per Figure 5.4 Since the output data followed normal distributions as expected, we carried out our uncertainty analysis using the approach discussed in Section 5.3.5.

Figure 5.5 shows the outcomes of our uncertainty analysis for propagation speed of the five fuels. Figure 5.6 shows uncertainty analysis for peak temperature of the five fuels. Table 5.5 shows the percent uncertainties calculated using Eq. 5.5. Kinetic and physical

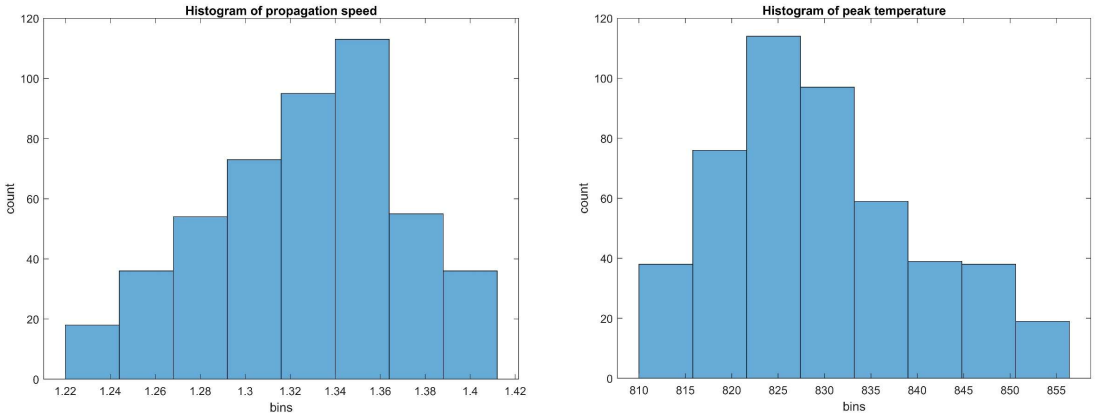

Figure 5.2: Histograms of propagation speed and peak temperature considering kinetic parameter variations for duff

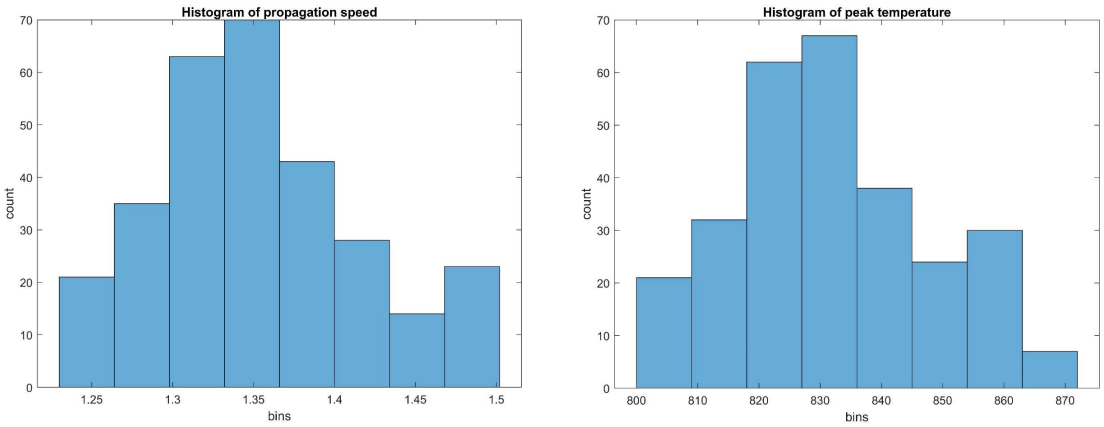

Figure 5.3: Histograms of propagation speed and peak temperature considering physical property variations for duff

parameters may cause percent uncertainties in Table 5.5 to spread beyond the ranges stated because input parameter values in Table 5.1 and Table 5.2 can have their own uncertainties. Variations in physical properties result in a higher uncertainty for both propagation speed and peak temperature than of the variations in kinetic parameters and composition for all the five fuels. Composition of the fuel cause lower uncertainties in both propagation speed and peak temperature for all the fuels. Therefore, the accuracy of input data of physical properties should be focused more than the kinetics and composition

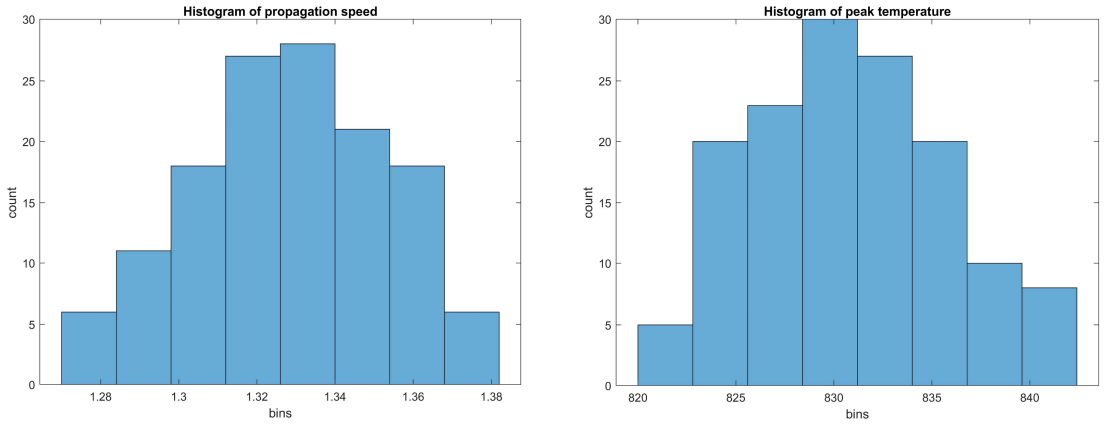

Figure 5.4: Histograms of propagation speed and peak temperature considering composition variations for duff

of species when modeling smoldering combustion. When we compare the results of the five fuels against each other, we saw that peat and duff overall have higher uncertainties. According to Table 5.3, both of these fuels have higher lignin contents (55-65% for peat and 40-50% for duff). This indicates that properties of lignin have higher uncertainties associated compared to properties of cellulose and hemicellulose.

Table 5.5: Percentage uncertainty values for five fuels

Parameter set	Estimate	% uncertainty				
		Duff	Peat	Softwood	Hardwood	Twigs
Kinetic	Speed	2.33%	3.11%	1.44%	1.50%	0.87%
	Temperature	0.76%	1.07%	0.71%	1.14%	1.00%
Physical	Speed	3.96%	5.08%	2.60%	2.09%	2.21%
	Temperature	2.70%	2.79%	2.63%	2.28%	1.62%
Composition	Speed	2.43%	3.24%	0.84%	1.07%	0.96%
	Temperature	0.62%	0.70%	0.84%	0.99%	0.78%
All	Speed	4.26%	5.30%	2.62%	2.13%	2.46%
	Temperature	3.06%	3.06%	3.04%	2.83%	2.01%

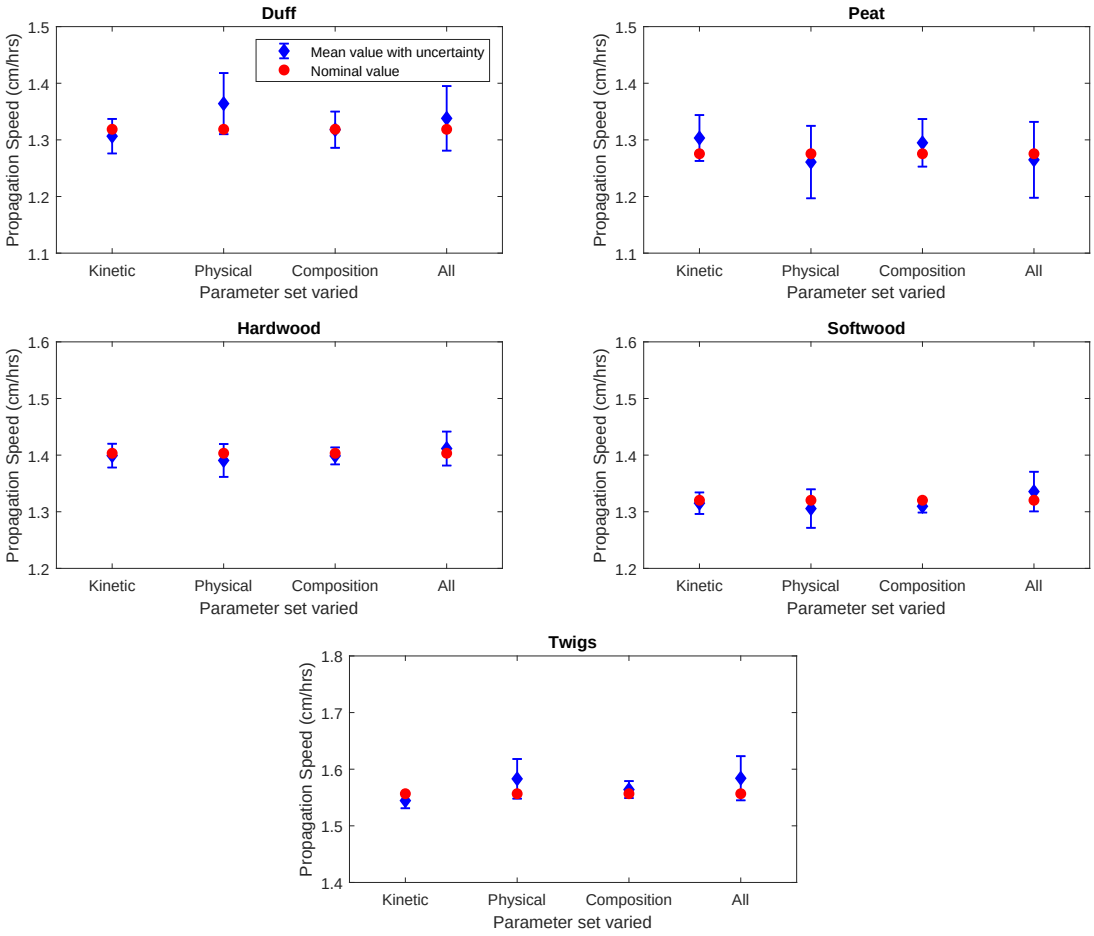

Figure 5.5: Propagation speed with model uncertainties for five fuels

5.4.2 Sensitivity analysis

Next, we conducted a sensitivity analysis to quantitatively analyze the influence of these different parameters. For the parameters that have significant effects on simulation results, their uncertainties should be given higher priority in computational models. We conducted two different sensitivity analysis approaches considering physical properties and kinetic parameters for duff as discuss in Section 5.4.2. The constituents of duff we selected are 35% of cellulose, 22% of hemicellulose and 43% of lignin which represent one-year decomposed duff from Scots pine [110].

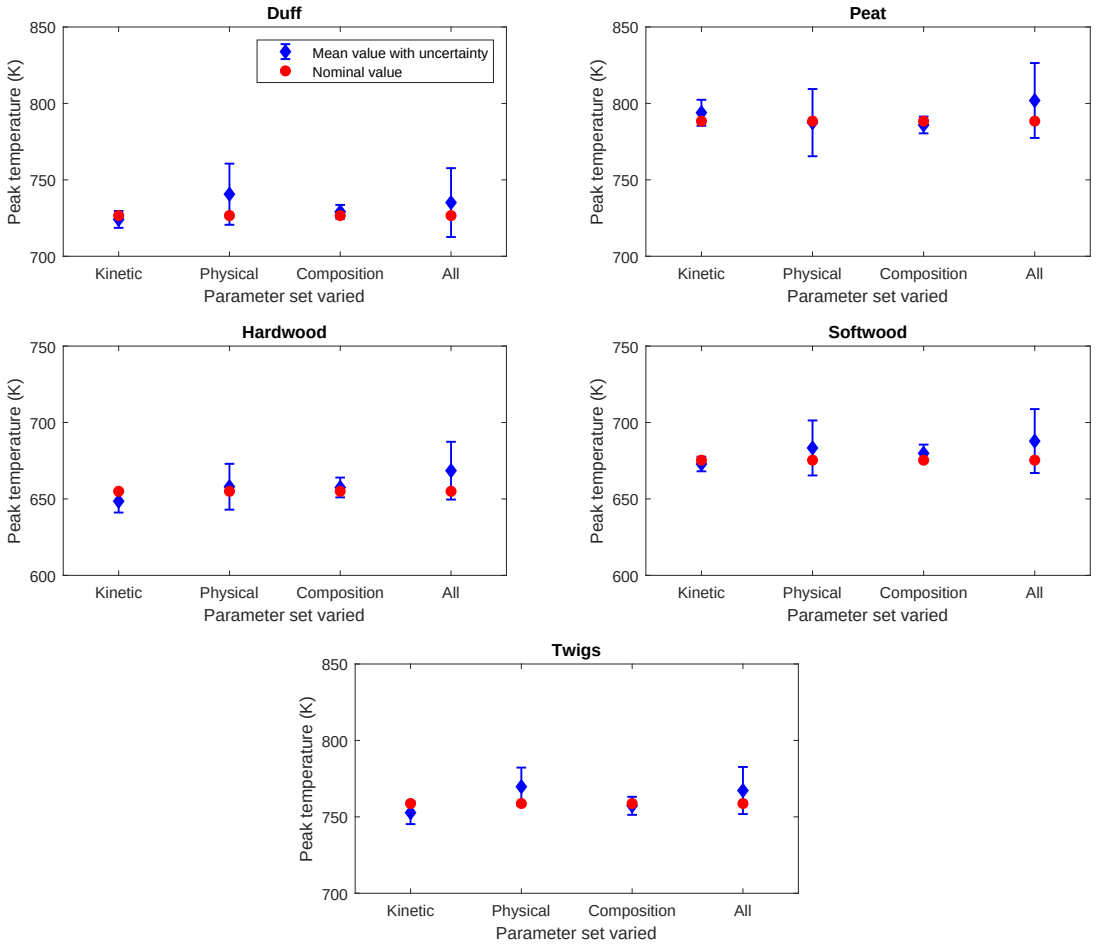

Figure 5.6: Peak temperature with model uncertainties for five fuels

5.4.2.1 One-at-a-time analysis

We calculated absolute value of sensitivity coefficients ($|\bar{s}|$) for kinetic parameters and physical properties of a cellulose, hemicellulose and lignin mixture that represent duff using Eq. 5.6. We estimated the sensitivity of these parameters on propagation speed and peak temperature. The results are summarized in Figure 5.7. We saw that activation energy (E) is the determining parameter with very high sensitivity coefficients for all three constituents of duff for both propagation speed and peak temperature. The second most important parameter is heat capacity (C) of all three constituents for propagation

speed, and for peak temperature, it is thermal conductivity (k).

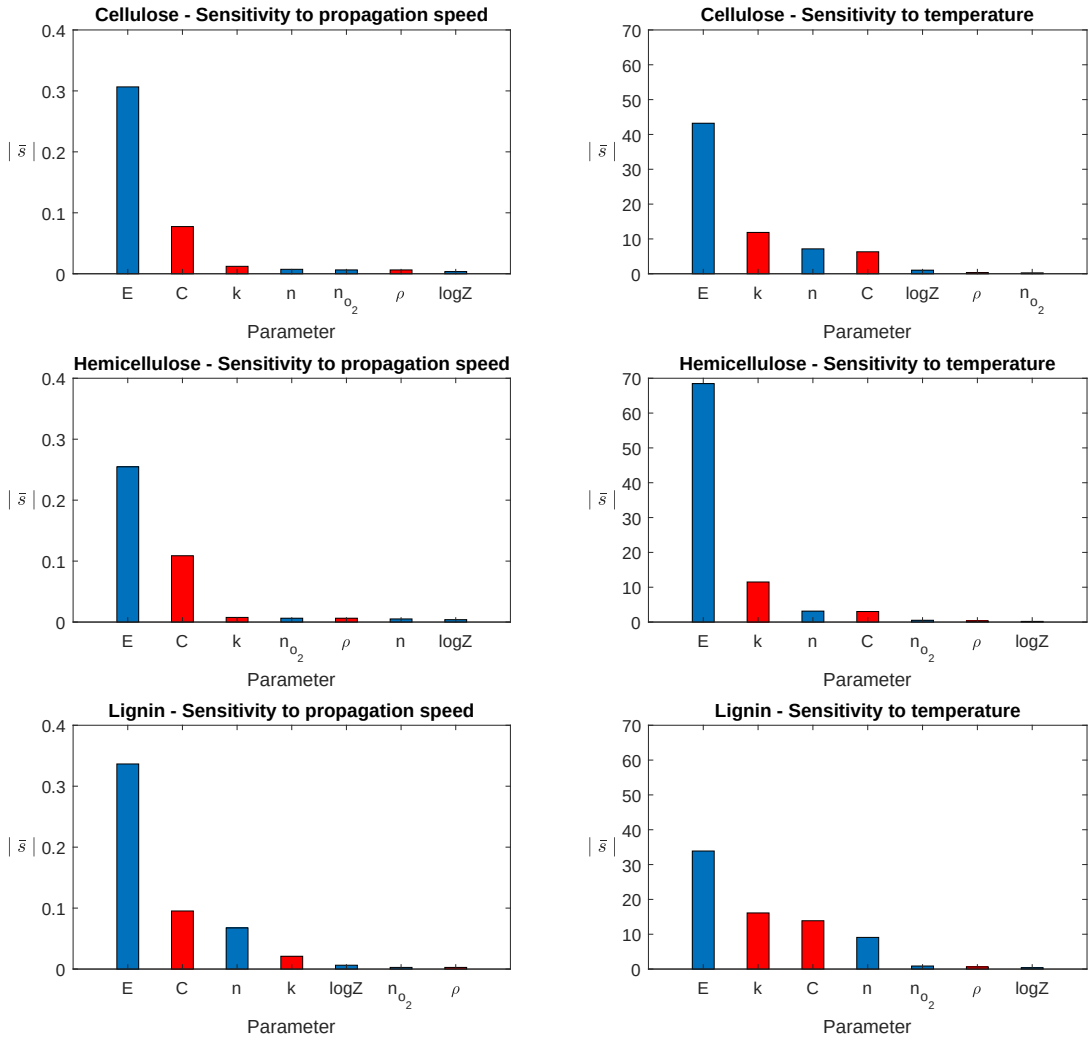

Figure 5.7: OAT analysis results for a mixture of cellulose, hemicellulose and lignin that represent duff. Blue columns represent kinetic properties and red columns represent physical parameters. $|\bar{s}|$ is the absolute value of sensitivity coefficient.

5.4.2.2 Morris screening analysis

We conducted a Morris screening analysis where we calculated mean (μ) and standard deviation (σ) of sensitivity for kinetic parameters and physical properties of a cellulose, hemicellulose and lignin mixture that represent duff using Eq. 5.8 and Eq. 5.9. Figure 5.8 shows sensitivity to propagation speed. Activation energy (E) resulted higher mean and higher standard deviation, while heat capacity (C) showed higher mean values with lower standard deviation. All the other parameters (k, n, n_o2, ρ, $logZ$) resulted lower mean values with lower standard deviation. Therefore, results suggest that E has a non-linear influence on propagation speed and/or it has interactions with other parameters. It also suggests that C has a linear positive influence and additive effect with propagation speed. And the sensitivity of all other parameters to propagation speed is negligible. Figure 5.9 shows the results of sensitivity to peak temperature. Activation energy (E) showed higher mean and higher standard deviation, while thermal conductivity (k) showed higher mean values with lower standard deviation. All the other parameters (C, n, n_o2, ρ, $logZ$) resulted lower mean values with lower standard deviation. Therefore, E has a non-linear influence on peak temperature and/or it has interactions with other parameters and, k has a linear positive influence and additive effect with peak temperature. The sensitivity of all other parameters to peak temperature is negligible.

We further investigated why activation energy (E) has higher mean and high standard deviation for both propagation speed and peak temperature to identify whether its non-linear effect or whether it has interactions with other parameters. An intuitive explanation can be given based on heat release rate. The total heat release rate for species A can be given by the following equation using the previously defined destruction rate ($\dot{\omega}'''$) in Section 5.3.1 by Eq. 5.2 and change in enthalpy (ΔH).

$$\dot{Q}_A = \Delta H \times \dot{\omega}'''_{dA} = \Delta H \times Z \frac{(\bar{\rho} Y_A \Delta z)_{\sum}}{\Delta z} \left(\frac{\bar{\rho} Y_A \Delta z}{(\bar{\rho} Y_A \Delta z)_{\sum}} \right)^n \times \exp\left(-\frac{E}{RT} \right) g(Y_{O_2}) \quad (5.10)$$

Propagation speed and peak temperature increase with increases in heat release. Eq. 5.10 shows that slight change in activation energy (E) would exponentially change heat generation and hence largely influence propagation speed and peak temperature. Therefore, the effect of E is much larger than the other parameters and has a non-linear

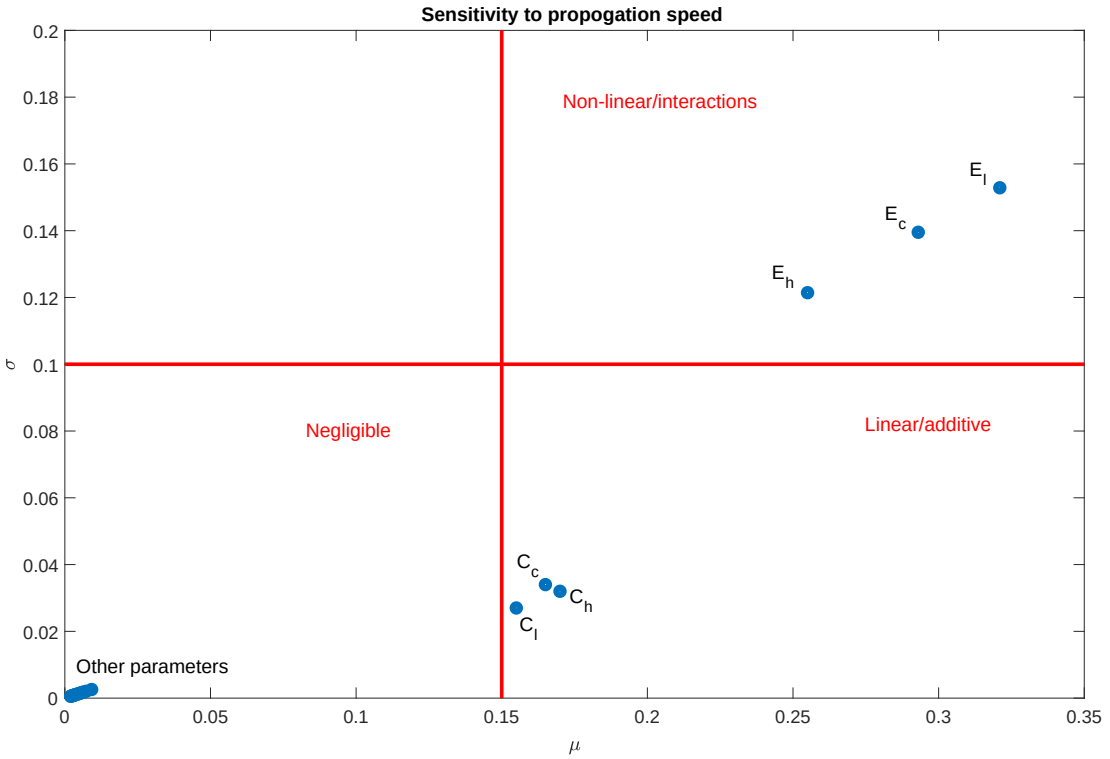

Figure 5.8: Morris screening analysis results for a mixture of cellulose, hemicellulose and lignin that represent duff. E is activation energy and C is heat capacity. Subscripts c, h, and l stand for cellulose, hemicellulose, and lignin, respectively.

relationship, confirming what is fundamentally expected.

Our sensitivity study suggests that our estimates are most sensitive to activation energy (E), which is a kinetic property. This implies the need to improve the measurement accuracy of E and uncertainties must be captured more precisely. Second most important parameters are heat capacity (C) and thermal conductivity (k), which are physical properties. However, our uncertainty analysis indicates that kinetic parameters have lower uncertainties and physical properties have higher uncertainties. So our work suggests that even though behavior of smoldering combustion is highly sensitive to kinetic properties, uncertainties associated with them are lower and even though physical properties have higher uncertainties associated, smoldering behavior is less sensitive to those properties.

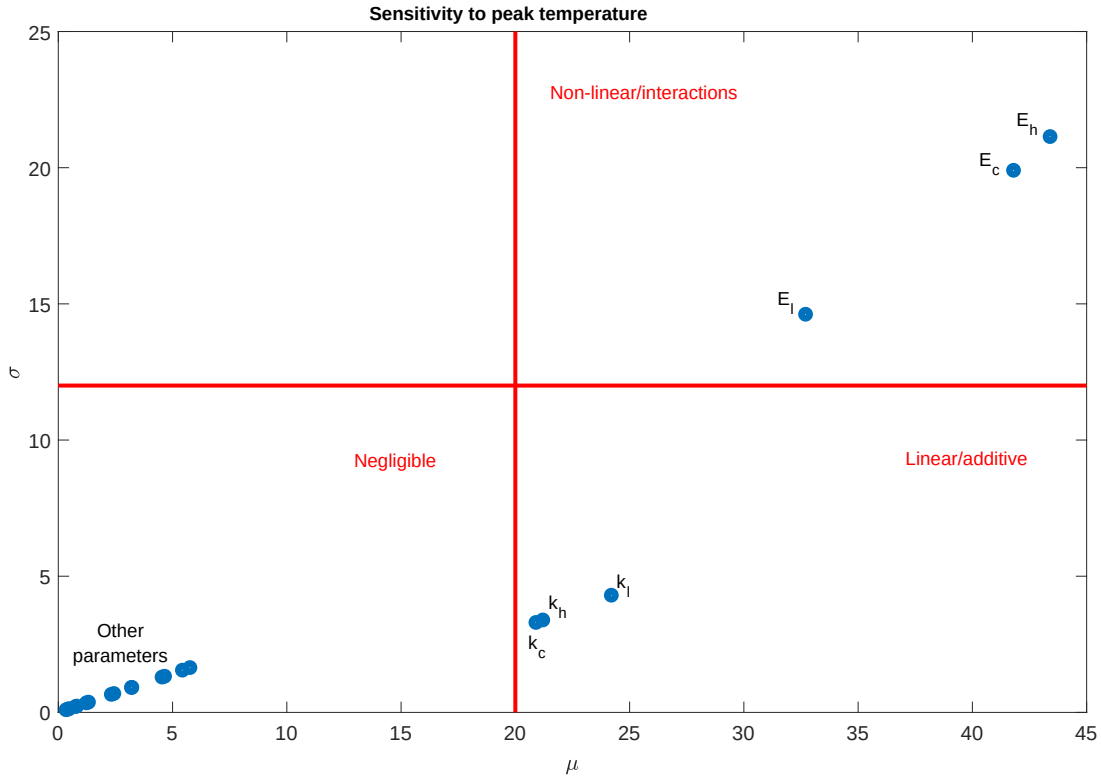

Figure 5.9: Morris screening analysis results for a mixture of cellulose, hemicellulose and lignin that represent duff. E is activation energy and k is thermal conductivity. Subscripts c, h, and l stand for cellulose, hemicellulose, and lignin, respectively.

5.5 Summary and Conclusions

In this work, we used a one-dimensional computational model that studies smoldering of cellulose, hemicellulose, and lignin mixtures, to estimate uncertainties associated with input parameters and to identify which parameters are highly sensitive to input parameters. We conducted the analysis for five different mixtures that represent fuels that commonly under go smoldering in wild fires. We considered three categories of input parameters: kinetic parameters, thermophysical properties and fuel composition. We conducted three separate uncertainty analyses because we wanted to investigate the effects of kinetic parameters, thermophysical properties and composition separately and, compare the outcomes. We used a Monte Carlo approach for our analysis, where we

assumed kinetic parameters follows a normal distribution and physical parameters and variations in composition follow uniform distributions, and simulated all the generated cases using our computational model. We conducted another analysis to capture overall uncertainty by varying all the parameters together. We used propagation speed and mean peak temperature as our estimates to analyse smoldering behaviour. All output data follow normal distributions. Variations in physical properties result a higher uncertainty for both propagation speed and peak temperature than of the variations in kinetic parameters and composition. Composition of the fuel cause lower uncertainties in both propagation speed and peak temperature. Therefore, the accuracy of input data of physical properties is important than the kinetics and composition of species when modeling smoldering combustion. Comparison between the results for five fuels indicated that fuels with high lignin content (50-65%) have higher uncertainties. This indicates that properties of lignin have higher uncertainties associated compared to properties of cellulose and hemicellulose. The sensitivity study suggests that output estimates are most sensitive to activation energy (E) with a non-linear relationship. This implies the need to improve the measurement accuracy of E and uncertainties must be captured more precisely. As the second most important parameter, heat capacity (C) is sensitive to propagation speed and thermal conductivity (k) to peak temperature. This concludes that even though some kinetic properties are highly sensitive to behavior of smoldering combustion uncertainties associated with them are lower and even though physical properties have higher uncertainties associated, they are less sensitive to behavior of smoldering combustion in wildland fires.

Funding

This research was funded by the Strategic Environmental Research and Development Program (SERDP) award RC-2651 under contract number W912HQ-16-C-0045.

Chapter 6: A computational investigation into the ignition of smoldering combustion

W. Jayani Jayasuriya and Kyle E. Niemeyer

My contributions to this work included developing the computational model including the ignition model, running simulations, processing the output data, analyzing the results, and preparing the manuscript.

Target Journal: International Journal of Wildland Fire (In Preparation)

6.1 Abstract

Smoldering ignition of natural fuels by radiative heat sources and hot metal particles can initiate smoldering combustion in wildfires resulting destruction of wildlands, emission of pollutants, and transition to flaming combustion. In this work, we studied how fuel composition and moisture content affect smoldering ignition via radiation and conduction using fuels with varying composition. First, we developed a one-dimensional computational model to simulate the ignition of smoldering combustion, using mixtures of cellulose, hemicellulose, and lignin to represent real fuels. We validated the model by comparing simulated propagation speeds with experimental measurements. Next, we simulated smoldering ignition via radiation for fuel mixtures. We identified a minimum heat flux required to initiative smoldering for these fuels. The minimum heat flux for smoldering ignition decreases with cellulose content and increases with hemicellulose content. In addition, increasing the external heat flux decreases the exposure time required for ignition, but this relationship depends on fuel composition. Moisture content in the fuel raises the required exposure time for ignition for a given heat flux. In the context of smoldering ignition via conduction, we modelled a hot metal layer in contact with the fuel bed to study hot particle ignition. Ignition temperature decreases non-linearly with increasing thickness of the metal for all the fuel types considered. The overall thermal conductivity of the fuel mixture plays a major role in igniting the sample. Fuels with higher lignin content ignite at lower temperatures due to their higher overall thermal conductivity, while fuels with higher cellulose and hemicellulose contents ignite at higher temperatures. We also investigated on the effect of the material of the metal layer by repeating the simulations with steel. Smaller aluminum metal particles ignite the fuel at a lower temperature than steel. When particle size increases, the difference in ignition temperatures decreases.

6.2 Introduction

Smoldering combustion is one of the leading causes of wildland fires that contributes to destruction of vegetation, global greenhouse gas emissions, and other human/ecological hazards [5]. Smoldering can penetrate much deeper into the organic soil compared to flaming combustion, impacting plant regrowth rates [6]. Even though the spread rate

of smoldering is slower than that of flames, it can burn for a longer periods of time, making it more difficult to suppress. It can be initiated with weaker ignition sources and can transition to flaming combustion. Smoldering also emits more pollutants than flaming, due to incomplete and lower-temperature combustion [7, 8]. For these reasons, smoldering combustion has become a topic of interest in wildland fires.

It is important to investigate on smoldering ignition since it is the pathway to fires associated with smoldering combustion. Smoldering ignition can be directly initiated by a radiant heat source, hot metal particle, firebrand or by self-heating. Compared to flaming combustion smoldering can ignite at lower radiation heat fluxes: Smoldering ignites in polyurethane foam at $7\,\mathrm{kW/m^2}$, while for flaming combustion ignites at $30\,\mathrm{kW/m^2}$ [44]. Jones et al. [45] developed a method to evaluate the risk of smoldering ignition based on the activation energy for pyrolysis and a characteristic temperature from thermogravimetric analysis for different biomass types. However, they did not discuss the minimum ignition heat fluxes or exposure times of different heat fluxes, two parameters that drive smoldering ignition. For polyurethane foam, a few studies have examined the minimum ignition heat fluxes and exposure times of different heat fluxes. Anderson, Sleight, and Torero [46] observed a self-sustained smolder with a heat flux of 6.1–$6.8\,\mathrm{kW/m^2}$ while Hadden et al. [44] reported a minimum heat flux of $7\,\mathrm{kW/m^2}$ for polyurethane foam, indicating the sample size also can change the heat flux [44, 46]. Gratkowski, Dembsey, and Beyler conducted a similar study for plywood and found a minimum ignition flux of $7.5\,\mathrm{kW/m^2}$ for an 18 mm thick maple plywood block [47]. However, most of these studies focused on materials not relevant to wildland fires.

Smoldering combustion can occur in surface and ground fuels within forest fuel beds. Forest fuel beds typically consist of three layers: the top (litter) layer, middle (fermentation) layer, and bottom (humus) layer. Twigs and leaves mostly comprise the litter layer, where smoldering can initiate. Larger smoldering fires occur in duff and peat fuels, which are present in the fermentation and humus layers [19]. Thus, understanding ignition of smoldering in wildland fires requires focusing on these fuels.

Spot ignition by firebrands and metal particles is another common and important ignition pathway. Firebrand or ember ignition can cause a secondary fire or spread an existing fire more intensely [14]. Some well-known fires that started off by firebrand spot ignition include the 1998 Florida wildfires, 2007 Witch Creek fire, and 2015 Butte fire [14, 48]. Hot metal particles generated from power lines, mechanical cutting, bullets, and

friction in railroads can cause local ignitions which may grow into large fires. Recently this has been identified as the cause for a large number of wildland fires all around the world. Examples of fires started by particles produced by powerlines or rebar cutting/welding include the 2007 Witch Creek and Guejito fires [12], the 2011 Bastrop County Complex wildfire in Texas [49] and the Taylor Bridge fire in Washington [13]. Globally New Zealand and Australia have many cases reported with the cause of hot particle spot ignition in recent history [50, 51].

Various groups have experimentally studied spot ignition of flaming combustion in natural fuels; only a small number forced in ignition of smoldering. [52–57]. A validated numerical model can simulate number of scenarios by changing the natural fuel, material of the ignition source, fuel density, and fuel moisture content which will be helpful in estimating spot ignition risks. Wang et al. studied smoldering, flaming ignition, and smoldering-to-flaming transition of pine needles for various moisture contents, from ignition by hot large stainless steel particles [48]. They developed an empirical correlation for ignition temperature, moisture content, and particle diameter. Urban et al. experimentally studied smoldering ignition of a grass blend powder by hot steel and aluminum particles accompanied by a simplified numerical study [58]. They found that smaller particles require higher temperatures to ignite, and the latent heat of fusion allows aluminum particles to ignite at lower temperatures. However, this study only considered one grass blend fuel. Non of these studies looked into the effects of fuel composition on smoldering ignition. A validated numerical model that can simulate both radiant and conductive smoldering ignition considering number of scenarios by changing the natural fuel, material of the ignition source, fuel density, and fuel moisture content will help in estimating risks associated with smoldering ignition.

The major organic constituents of biomass fuels are cellulose, hemicellulose, and lignin, in varying proportions depending on the fuel and its source [21]. Each component has different pyrolysis and oxidation characteristics, which can impact smoldering ignition and behavior. Gani and Naruse discussed pyrolysis and combustion characteristics of cellulose and lignin for several types of biomass [9]. They identified two stages of burning: (1) cellulose decomposition and (2) lignin decomposition for pyrolysis and oxidation of its char. They concluded that the relative amounts of cellulose and lignin in biomass play major roles in pyrolysis and char oxidation. Yang, using thermogravimetric analysis, showed that hemicellulose and cellulose pyrolize earlier than lignin, while lignin produces

the highest solid residue during pyrolysis [22]. Dorez et al. found that natural fibers with a higher composition of lignin exhibit higher char yields and higher effective heats of combustion [11]. These studies show that the three biomass constituents exhibit different characteristics during pyrolysis and oxidation. Since smoldering combustion represents the combined effects of pyrolysis and oxidation, fuel composition may lead to differences in ignition of smoldering.

In this work, we developed a one-dimensional computational model to simulate smoldering of cellulose, hemicellulose, and lignin mixtures. We first validated the model using experimental data. Then, we simulated ignition via radiant heat source. We determined the minimum heat flux required for smoldering to ignite, and the exposure time needed to ignite for different heat fluxes. We considered eight fuels, including both common fuels and those most important for wildland fires. Then, we investigated the driving forces of the minimum heat flux and exposure time for ignition in terms of smoldering kinetics and properties. We also analyzed how fuel composition and moisture content modify ignition characteristics. Finally, we extended the computational model to simulate smoldering ignition by hot metal particles, examining the same eight fuels and considering steel and aluminum for the metal particles. We investigated how fuel composition and metal properties affect smoldering ignition.

6.3 Computational model

We developed a one-dimensional transient numerical model to study downward propagation of smoldering of cellulose, hemicelloluse, and lignin mixtures using Gypro v0.8171 [105]. For the modeling effort we followed the approach Mulky and Niemeyer used to study mixtures of cellulose and hemicelloluse [1]. For all cases, we used a cell size (Δz) of 1×10^{-4} m with an initial time step of 0.05 s. The computation domain is $10 \times 10 \times 10$ cm. This domain size was chosen to match that of the experiment against which we validated our model.

6.3.1 Governing equations and boundary conditions

Gpyro solves equations for both condensed and gas phases. The governing equations include: condensed-phase mass conservation (6.1), condensed-phase species conserva-

tion (6.2), gas-phase mass conservation (6.3), gas-phase species conservation (6.4), condensed-phase energy conservation (6.4), gas-phase momentum conservation (6.5), gas-phase energy conservation (6.6), and the ideal gas equation of state (6.6):

$$\frac{\partial \overline{\rho}}{\partial t} = -\dot{\omega}'''_{fg} \,, \tag{6.1}$$

$$\frac{\partial (\overline{\rho} Y_i)}{\partial t} = \dot{\omega}'''_{fi} - \dot{\omega}'''_{di} \,, \tag{6.2}$$

$$\frac{\partial (\rho_g \overline{\psi})}{\partial t} + \frac{\partial \dot{m}''}{\partial z} = \dot{\omega}'''_{fg} \,, \tag{6.3}$$

$$\begin{aligned} \frac{\partial (\rho_g \overline{\psi} Y_j)}{\partial t} + \frac{\partial (\dot{m}'' Y_j)}{\partial z} &= -\frac{\partial}{\partial z}\left(\overline{\psi} \rho_g D \frac{\partial Y_j}{\partial z}\right) + \dot{\omega}'''_{fj} - \dot{\omega}'''_{dj} \,, \\ \frac{\partial (\overline{\rho}\overline{h})}{\partial t} &= \frac{\partial}{\partial z}\left(\overline{k}\frac{\partial T}{\partial z}\right) - \dot{Q}'''_{s-g} + \sum_{k=1}^{K} \dot{Q}'''_{s,k} \\ &\quad - \frac{\partial \dot{q}''_r}{\partial z} + \sum_{i=1}^{M} \left(\dot{\omega}'''_{fi} - \dot{\omega}'''_{di}\right) h_i \,, \end{aligned} \tag{6.4}$$

$$\dot{m}'' = -\frac{\overline{K}}{v}\frac{\partial P}{\partial z} \,, \tag{6.5}$$

$$\begin{aligned} \frac{\partial (\overline{\psi} \rho_g \overline{h_g})}{\partial t} + \frac{\partial (\dot{m}''_z \overline{h_g})}{\partial z} &= \frac{\partial}{\partial z}\left(\overline{\psi} \rho_g D \frac{\partial \overline{h_g}}{\partial z}\right) + h_{cv}(T - T_g) \\ &\quad + \sum_{j=1}^{N} (\dot{\omega}'''_{s,fj} - \dot{\omega}'''_{s,dj}) h^*_{g,j} + \dot{Q}'''_{s-g} \,, \text{ and} \\ P\overline{M} &= \rho_g R T_g \,, \end{aligned} \tag{6.6}$$

where ρ is the density; M is the number of condensed-phase species; X is the volume fraction; $\dot{\omega}'''$ is the reaction rate; T is the temperature; Y_j is the jth species mass fraction; ψ is the porosity; K is the permeability/number of reactions; N is the number of gas-phase species; h_{cv} is the volumetric heat transfer coefficient; $\overline{M}$ is the mean molecular mass obtained from local volume fractions of all gaseous species; $\dot{q}''_r$ is the radiative heat-flux; $\dot{Q}'''$ is the volumetric rate of heat release/absorption; R is the universal gas constant; D is the diffusion coefficient; h is the enthalpy; P is the pressure; subscripts f, d, i, j, k, s, and g represent formation, destruction, condensed-phase species index, gas-phase species index, reaction index, solid, and gas; and * indicates that gas-phase species enthalpy is calculated at condensed-phase temperature. The overbars over ρ, ψ, K, and k indicate an averaged value weighted by condensed-phase volume fraction, and the overbar over h

indicates an averaged value weighted by condensed-phase mass fraction. Lautenberger and Fernandez-Pello give detailed descriptions of the underlying model and solver [82, 105].

At the top surface of the domain ($z = 0$) we set a convective heat-transfer coefficient ($h_{c,0}$) of $10\,\mathrm{W/m^2K}$, simulating it as open to atmosphere with a mass-transfer coefficient ($h_{m,0}$) of $0.02\,\mathrm{kg/m^2s}$. The pressure and (ambient) temperature at the top surface were 1 atm and 300 K, respectively. We modeled the bottom surface ($z = 10\,\mathrm{cm}$) as insulated to match the experimental setup used for validation. To account for losses through the insulation, we set a heat-transfer coefficient ($h_{c,L}$) of $3\,\mathrm{W/m^2K}$ and zero mass flux ($\dot{m}''$) at the bottom surface [79]. First to validate the model we simulated few smoldering fires by igniting the mixtures using a heat flux on the top surface of $25\,\mathrm{kW/m^2}$ for 20 minutes. The results are discussed in Section 6.4.1.1.

The model was further modified to simulate radiant smoldering. The first objective was to identify a minimum heat flux required for ignition. To determine this, we set an external heat flux on the upper boundary and applied it for the full simulation time of 15 hours. We varied the magnitude of this external heat flux using increments of $0.1\,\mathrm{kW/m^2}$. Next, to develop relationships between heat flux and exposure time for ignition we varied the external heat flux and found a corresponding minimum exposure time required for ignition. We defined the required exposure time as the minimum time required to achieve self-sustained smoldering ignition for a given applied heat flux. The results from these simulations are found in Section 6.4.2.

Finally, we extended the model to investigate smoldering ignition via hot metal particles. We geometrically created a layer of the metal on top of the sample in the one-dimensional domain. Figure 6.1 shows the geometry of the model. We specified a particular initial temperature to the metal layer. Surface 1 is created to be exposed to the open atmosphere by giving the boundary conditions same as our previous simulations, and surface 2 allows heat transfer at the bottom just as our previous simulations.

Then we varied the thickness of the metal from 1 mm to 10 mm. The corresponding ignition temperatures for each thickness values are captured by changing the temperature with a step size of 10 °C. For the initial study we used Aluminum 1100 as the metal, then to analyze the affect of the type of the metal we repeated the simulations for steel 302/304. The properties of the two metals are presented in Table 6.1. The results from these simulations are discussed in Section 6.4.3.

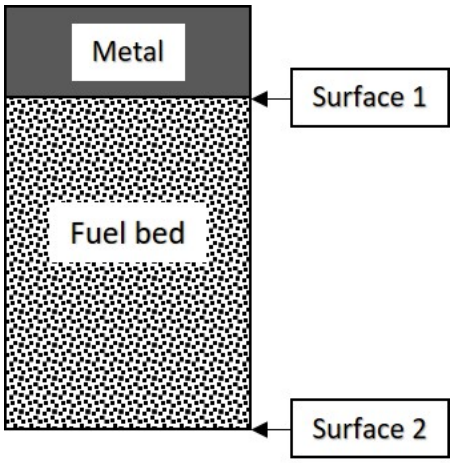

Figure 6.1: Schematic of fuel bed and metal layer.

Table 6.1: Properties of the two metals. Molten properties are in parentheses [58]

Metal	Aluminum 1100	Steel 302/304
Density [kg/m^3]	2710 (2375)	7860
Specific heat [J/(kg K)]	900 (1141)	500
Thermal conductivity [W/(m K)]	220 (90.7)	21.5
Melting temperature [K]	933	1693

6.3.2 Chemical kinetics

A heterogeneous reaction (k) involving condensed- and gas-phase species is described by

$$\mathrm{A}_k + \sum_{j=1}^{N} v'_{j,k}\,\mathrm{G}_j \longrightarrow v_{B,k}\,\mathrm{B}_k + \sum_{j=1}^{N} v''_{j,k}\,\mathrm{G}_j\ , \tag{6.7}$$

where $v'_{j,k}$ and $v''_{j,k}$ are the reactant and product stoichiometric coefficients for gas-phase species G_j in reaction k, and $v_{B,k}$ is the stoichiometric coefficient for condensed-phase species B in reaction k. The destruction rate of species A in reaction k is given by the

Arrhenius law:

$$\dot{\omega}'''_{dA_k} = \frac{(\overline{\rho}Y_{A_k}\Delta z)_\Sigma}{\Delta z} Z_k e^{\frac{-E_k}{RT}} \left[\frac{\overline{\rho}Y_{A_k}\Delta z}{(\overline{\rho}Y_{A_k}\Delta z)_\Sigma}\right]^{n_k} g(Y_{O_2}) \,, \tag{6.8}$$

$$(\overline{\rho}Y_{A_k}\Delta z)_\Sigma = \overline{\rho}Y_{A_k}\Delta z|_{t=0} + \int_0^t \dot{\omega}'''_{fi}(\tau)\Delta z(\tau)d\tau \,, \tag{6.9}$$

$$g(Y_{O_2}) = (1 + Y_{O_2})^{n_{O_2,k}} - 1 \,, \tag{6.10}$$

where Z is the pre-exponential factor, E is the activation energy, n is the order of reaction, subscript dA stands for destruction of species A, and subscripts f and i represent formation and the condensed-phase species index.

We used a chemical-kinetic scheme with five reactions for each constituent (cellulose, hemicellulose, and lignin), which includes a drying step, pyrolysis step for the fuel, and three oxidation reactions of fuel, β-char, and α-char [23, 83]. The model includes 15 global reactions, with 15 condensed-phase species and 4 gas-phase species, where the following five reactions are repeated for cellulose, hemicellulose, and lignin (Fuel_i, $i = 1, 2, 3$):

$$\text{Fuel}_i \cdot \nu_{w,dr}\,\text{H}_2\text{O} \longrightarrow \text{Fuel}_i + \nu_{w,dr}\,\text{H}_2\text{O(g)} \tag{R21}$$

$$\text{Fuel}_i \longrightarrow \nu_{\alpha,ip}\,\alpha\text{-Char}_{\text{f}_\text{i}} + \nu_{g,ip}\,\text{Gas} \tag{R22}$$

$$\text{Fuel}_i + \nu_{\text{O}_2,io}\,\text{O}_2 \longrightarrow \nu_{\beta,io}\,\beta\text{-Char}_{\text{f}_\text{k}} + \nu_{g,io}\text{Gas} \tag{R23}$$

$$\alpha\text{-Char}_{\text{f}_\text{i}} + \nu_{\text{O}_2,i\alpha o}\,\text{O}_2 \longrightarrow \nu_{a,i\alpha o}\text{Ash}_{\text{f}_\text{i}} + \nu_{g,i\alpha o}\text{Gas} \tag{R24}$$

$$\beta\text{-Char}_{\text{f}_\text{i}} + \nu_{\text{O}_2,i\beta o}\,\text{O}_2 \longrightarrow \nu_{a,i\beta o}\,\text{Ash}_{\text{f}_\text{i}} + \nu_{g,i\beta o}\text{Gas} \tag{R25}$$

where ν is the stoichiometric coefficient; α and β indicate char produced from fuel pyrolysis and fuel oxidation reactions, respectively; and subscripts w, g, O_2, a, f_i, dr, o, p, αo, and βo are water, gas, oxygen, ash, fuel constituent, drying, oxidation, pyrolysis, α-char oxidation, and β-char oxidation, respectively. We obtained the chemical kinetic parameters (pre-exponential factor, activation energy, order of reaction, and heat of reaction) from Huang and Rein, stoichiometric coefficients for cellulose from Kashiwagi and Nambu and for hemicellulose and lignin from Huang and Rein [23, 72]. The consumption of oxygen is calculated using $\nu_{\text{O}_2,i} = \Delta H/(-13.1)$ MJ/kg [34, 85].

6.3.3 Physical properties

Table 6.2 lists the physical properties of condensed-phase species (i): solid density ($\rho_{s,i}$), thermal conductivity ($k_{s,i}$), and heat capacity (c_i). We calculated the bulk density of char using $\rho_{\text{char}} = \nu_{\text{char}} \times \rho_{\text{fuel}}$ and the bulk density of ash using $\rho_{\text{ash}} = \text{AC}/100 \times 10 \times \rho_{\text{fuel}}$, where AC stands for ash content [1, 38]. The ash contents of cellulose, hemicellulose, and lignin are 0.3%, 1.2%, and 1.4%, respectively [1, 88]. We assumed that the physical properties of fuels do not depend on temperature [79].

Table 6.2: Thermophysical properties of condensed-phase species, taken from the literature for water, cellulose, hemicellulose, char, ash [1], and lignin [2–4].

Species (i)	$\rho_{s,i}$ (kg/m^3)	$k_{s,i}$ (W/(m K))	c_i (J/(kg K))
Cellulose	1500	0.356	1674
Hemicellulose	1365	0.34	1200
Lignin	1305	0.39	1147
Char	1300	0.26	1260
Ash	2500	1.2	880
Water	1000	0.6	4186

Porosity (ψ_i) and effective thermal conductivity (k_i) are calculated using $\psi_i = 1 - \rho_i/\rho_{s,i}$ and $k_i = k_{s,i}(1-\psi_i) + \gamma_i \sigma T^3$, where σ is the Stefan–Boltzmann constant and γ_i is an empirical parameter for radiation across pores. Pore size ($d_{po,i}$), permeability (K_i), and γ_i are calculated for each condensed-phase species using

$$d_{po,i} \approx d_{p,i} = \frac{1}{S_i \times \rho} , \tag{6.11}$$

$$K_i = 1 \times 10^{-3} \times d_{p,i}^2 , \tag{6.12}$$

$$\gamma_i = 3 \times d_{po,i} , \tag{6.13}$$

where ρ is the density of the fuel, S_i is the particle surface area for species i, and $d_{p,i}$ is the particle size. For all simulations we set a 10% moisture content (MC), to represent the natural moisture present in fuels, except those where we explicitly varied the moisture content; the bulk density of moist fuel is calculated as $\rho_{\text{wet fuel}} = \rho_{\text{dry fuel}} \times (1 + \text{MC})$. The dry fuel density was considered to be 300 kg/m^3 for this study, unless otherwise mentioned

in the relevant section. We selected this density value as the baseline density because the experiments are conducted using fuel samples at this density by our collaborators.

6.4 Results and discussion

First, we validated our model against our experimental results and data from literature. Then, we selected eight fuels to study the effect of fuel composition on smoldering ignition. We analysed smoldering ignition via radiation and conduction for those fuels. Table 6.3 gives the composition of each fuel based on the mass fraction of cellulose, hemicellulose, and lignin. In cases where we found multiple values for composition in the literature, we chose the mostly widely used. For duff, we considered the composition of one-year decomposed duff from Scots pines [110]. Around 10% of extractives are present in dead fuels [98], we assumed that to be zero.

Table 6.3: Composition of the fuels [98, 109, 110, 113, 116]

Species	Cellulose (%)	Hemicellulose (%)	Lignin (%)
Duff	35	22	43
Peat	28	10	62
Softwood	44	26	30
Hardwood	44	34	22
Twigs	18	52	30
Paper	75	15	10
Pine needle	41	28	31
Grass blend	42	30	28

Duff and peat are the major fuels that undergo smoldering combustion in forest fires, and lignin is the primary constituent in both. Duff is present mostly in the middle fermentation layer in forest beds, characterized by partially decomposed litter. Well-decomposed duff will be in the bottom humus layer. Peat is mostly considered to be in bottom humus layer of well-decomposed organic matter [19]. Lignin decomposes slower than cellulose and hemicellulose [110], so the lignin component is higher in duff and peat. Twigs are in the top litter layer of forest beds, and they are undecomposed and dead litter, so the hemicellulose content is higher in these fuels. Smoldering can be initiated in

this top litter layer in forest beds, so understanding its behavior is also important. Pine needles can be also present in top litter layer to middle fermentation layer depending on the level of decomposition. We adopted the composition of a more decomposed pine needle [113]. We also considered a mixture of grass blend to compare our results of smoldering spot ignition with the study by Urban et al. [58]. In contrast, cellulose makes up around 50% of softwood and hardwood, and paper mostly consists of cellulose.

6.4.1 Validation

First we validated the model against our experiments (personal comm. from B. Smucker and D. Blunck). In the experimental setup the fuel samples were held in a rector box with the dimensions of $10 \times 10 \times 10\,\text{cm}$. The reactor box was made from ceramic fiberboard. The top surface was open to the atmosphere. The cellulose used in the experiments was α-cellulose purchased from Sigma-Aldrich (CAS no : 9004-34-6), hemicellulose used in the experiments was glucomannon purchased from Nutricost, and the lignin was an organosolv lignin dericed from yellow pine (Attis Industries). The fuel was ignited using a 20W cartridge heater with a diameter of 64mm. The cartridge heater was placed at the center of the reactor box. Type-K thermocouples were placed at 1cm apart from 1 to 8cm below the top surface.

Then we compared our results against literature data for peat. Huang and Rein conducted their experiments to analyse downward spread of smouldering peat fire at different densities and moisture contents [38]. We simulated smoldering fires for peat at their conditions and compared the results against the extracted data from their experiments.

6.4.1.1 Validation against experimental data

We validated our model against the experimental measurements of propagation speeds with varying composition. We calculated propagation speed using the time between when the temperature at 3 cm below the surface reaches the ignition temperature and when that occurs at 6 cm below the surface. The ignition temperature is 300 °C for fuels with hemicellulose and 350 °C for fuels without hemicellulose. The ignition temperatures were based on when the fuels started to release heat during differential scanning calorimetry testing.

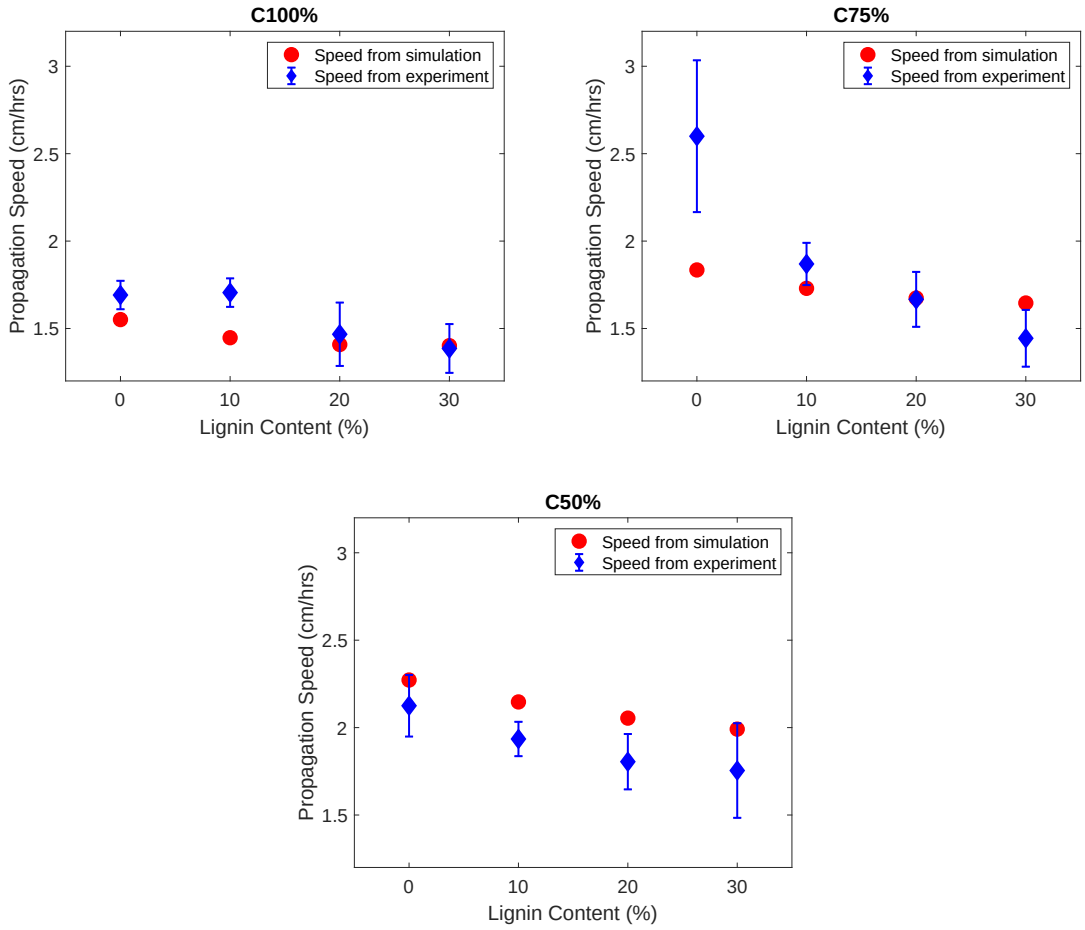

Figure 6.2: Comparison between numerical and experimental results for fuel mixtures with 100% cellulose (left), and 50% cellulose/50% hemicellulose (right) combined with varying amounts of lignin.

Figure 6.2 shows the propagation speeds of different compositions at a density of $200\,\mathrm{kg/m^3}$, where the lignin content varies from 0% to 30%. Three scenarios are considered: mixtures with 100% cellulose and varying amounts of lignin, mixtures with 50% cellulose/50% hemicellulose and mixtures with 75% cellulose/25% hemicellulose and varying amounts of lignin. For example, in the 100% cellulose cases, a lignin content of 10% means that the overall mixture has 10% lignin and 90% cellulose, while in the 50% cellulose cases, a lignin content of 10% means the overall mixture has 10% lignin, 45%

cellulose, and 45% hemicellulose. The experimental and computational results exhibit similar trends, where with increases in lignin content the propagation speed decreases. This is due to slower pyrolysis reaction rate of lignin compared to other two constituents. The results match closely for the 100% cellulose cases. For the 50% cellulose case with small amounts of lignin, predictions match experimental measurements closely. However, the experiments show that propagation speeds drop more significantly with increasing lignin content than predicted. The reasons for this discrepancy are not clear, but it could be caused by the higher temperatures resulting from adding hemicellulose and lignin, which increase heat losses in the experiment not captured in the simulations precisely. Another limitation of this model is, it being a one-dimensional model, so this can contribute to unclear discrepancies. This work is build on the model that was validated with propagation speeds and the ignition trends have not themselves been validated.

6.4.1.2 Validation against literature

Huang and Rein conducted their experiments and simulations using a fuel sample of peat of cross section of $10 \times 10\,\mathrm{cm}$ and a height of $30\,\mathrm{cm}$ [38]. We extracted the experimental results for propagation speed of following three cases; a) moisture content of 10% with density of $135\,\mathrm{kg/m^3}$, b) moisture content of 35% with density of $150\,\mathrm{kg/m^3}$, and c) moisture content of 70% with density of $160\,\mathrm{kg/m^3}$. We simulated the same cases using a fuel mixture that represent peat composition and using the same geometric and boundary conditions.

Figure 6.3 shows the comparison of propagation speed at different depths between the data from literature and our simulations. Here the propagation speed is calculated by taking the derivative of depth with respect to time at the depth where the peak temperature at a particular time. At higher depths simulated results are very close to experimental data and at lower depths the differences increase. We found good agreement with the experimental data: around 20% of maximum over-prediction of their experimental data, but following the same trends.

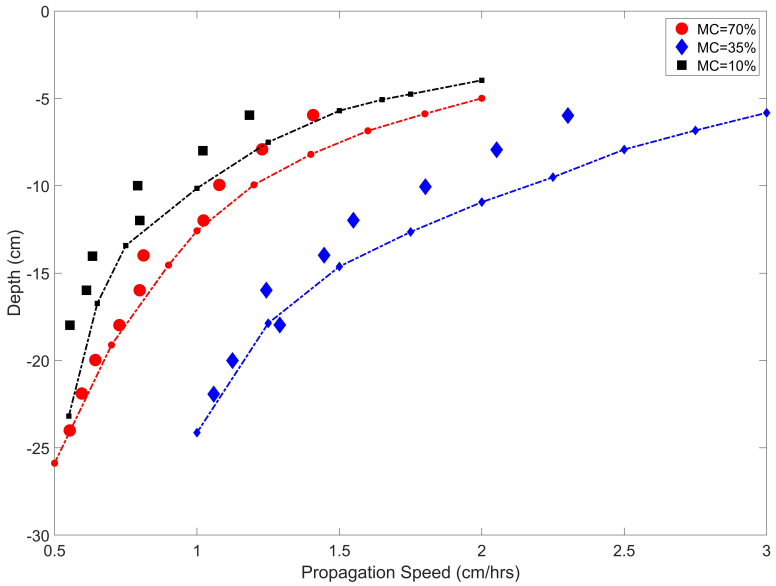

Figure 6.3: Comparison of propagation speed between experimental results from literature and simulations. Symbols show experimental measurements and lines show simulations.

6.4.2 Radiant smoldering ignition

6.4.2.1 Minimum heat flux for ignition

The objective of this part of the study was to identify the minimum heat flux required for ignition. To determine this, we set an external heat flux on the upper boundary and applied it for the full simulation time of 15 hours. We varied the magnitude of this external heat flux using increments of $0.1\,\mathrm{kW/m^2}$. For this study we considered the selected eight fuel types, and found the minimum heat flux for ignition ranging over 7–$8.8\,\mathrm{kW/m^2}$, as shown in Table 6.4. In other words, these values are the minimum heat flux required for ignition for any exposure time.

Paper, comprised mostly of cellulose, ignites with the lowest heat flux, while twigs, comprised of over 50% hemicellulose, require the highest heat flux to ignite. Of the fuels considered, peat and duff have the most lignin, and ignite with moderate heat fluxes.

Thus, it appears that composition correlates to minimum heat flux required for ignition. We posit that activation energy for oxidation of the fuel (E_f) drives this

Table 6.4: Minimum heat flux ($Q_{\min}$) for ignition

Fuel	$Q_{\min}$ (kW/m^2)
Paper	7
Softwood	7.6
Hardwood	7.8
Pine needles	7.8
Grass blend	7.8
Peat	7.9
Duff	7.9
Twigs	8.8

minimum heat flux to be different for each fuel. If applied heat flux is lower than the minimum heat flux for ignition (Q_{min}), the fuel does not ignite because the heat input is insufficient to initiate oxidation reactions. The activation energy for oxidation is 278 kJ/mol for cellulose, 289 kJ/mol for lignin, and 294 kJ/mol for hemicellulose. Since cellulose has lowest activation energy, it will ignite at lower heat fluxes, while hemicellulose needs higher heat fluxes to overcome its higher activation energy.

6.4.2.2 Heat flux and exposure time for ignition

Next, we varied the external heat flux and found the corresponding minimum exposure time required for ignition. We define the required exposure time as the minimum time required to achieve self-sustained smoldering ignition for a given applied heat flux. Figure 6.4 shows the exposure times required for varying heat flux for the eight fuels. As the external heat flux increases, the required exposure time for ignition decreases, though in a nonlinear fashion. Initially, increases in heat flux past the minimum value lead to sharp drops in the required exposure time, but the exposure time levels off with further increases in heat flux past approximately 12 kW/m^2.

Figure 6.4 shows the relationship between minimum heat flux and exposure time changes for different fuels, showing that fuel composition plays a role in smoldering ignition. To model how exposure time and heat flux quantitatively scale with the fuel composition, we performed a linear regression of the data shown in Figure 6.4 using

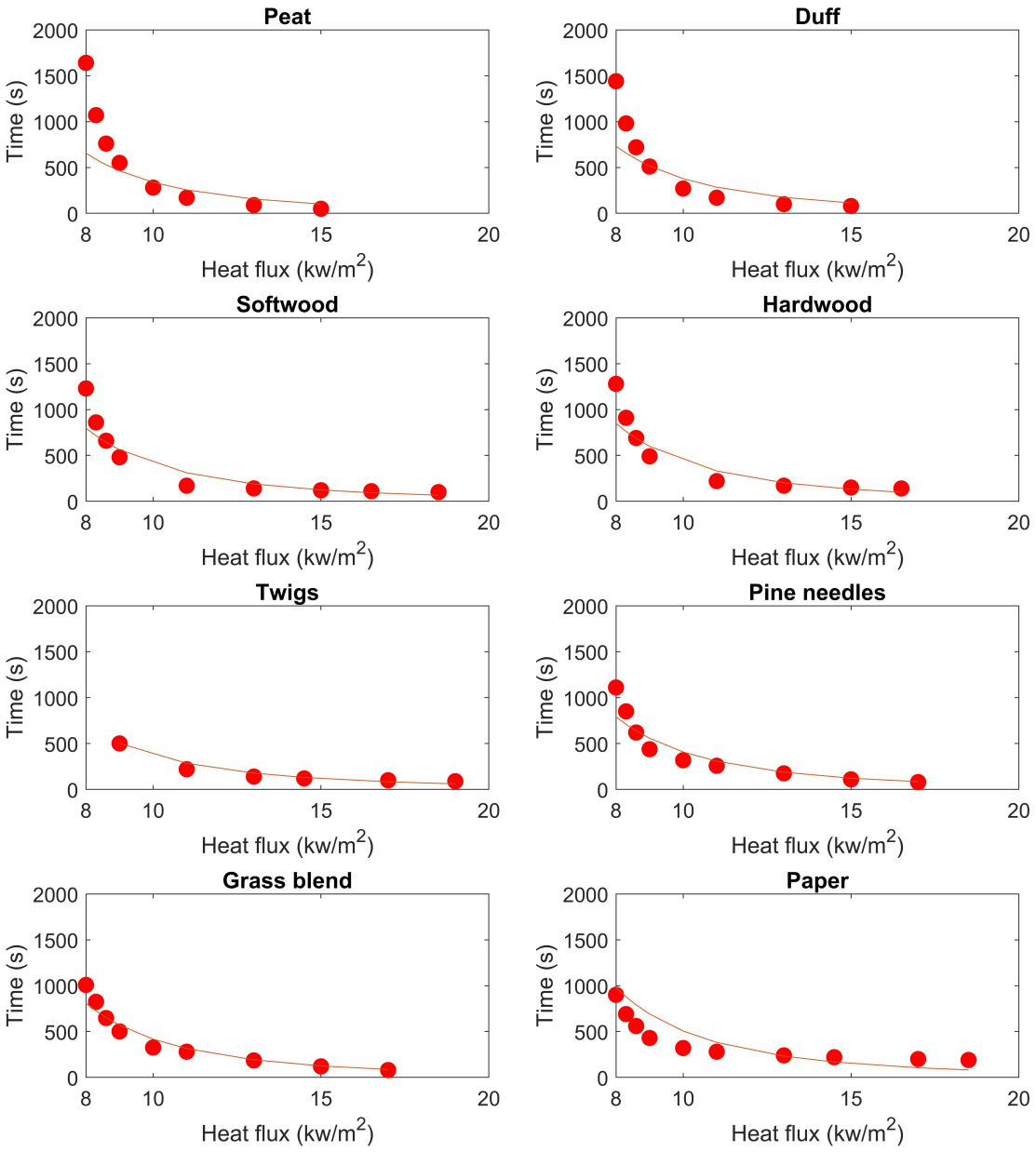

Figure 6.4: Minimum exposure time for ignition with varying heat flux for the six fuels considered. Note that the horizontal axes (abscissa) do not start at zero.

the Matlab function `regress()`, where the independent variables are mass fraction of cellulose ($Y_{\text{cellulose}}$), mass fraction of hemicellulose ($Y_{\text{hemicellulose}}$), mass fraction of lignin (Y_{lignin}), and radiant heat flux (Q, in kW/m^2) and the dependent variable is exposure time (t, in s). The resulting relationship is

$$t = 2.05 \times 10^5 \frac{Y_{\text{cellulose}}^{0.0904} \times Y_{\text{hemicellulose}}^{0.0530}}{Y_{\text{lignin}}^{0.1914} \times Q^{3.0846}} \ , \tag{6.14}$$

with a goodness of fit (R^2) value of 0.8302, indicating reasonable agreement. We simulated five more cases with different compositions for this regression model to get a better fit. Figure 6.4 also shows the fit for each fuel, based on the associated composition. There is a strong inverse relationship between heat flux and exposure time. The dependence on composition is weaker, but with a relatively larger (inverse) dependence on lignin, because lignin has a higher char yield that releases more heat.

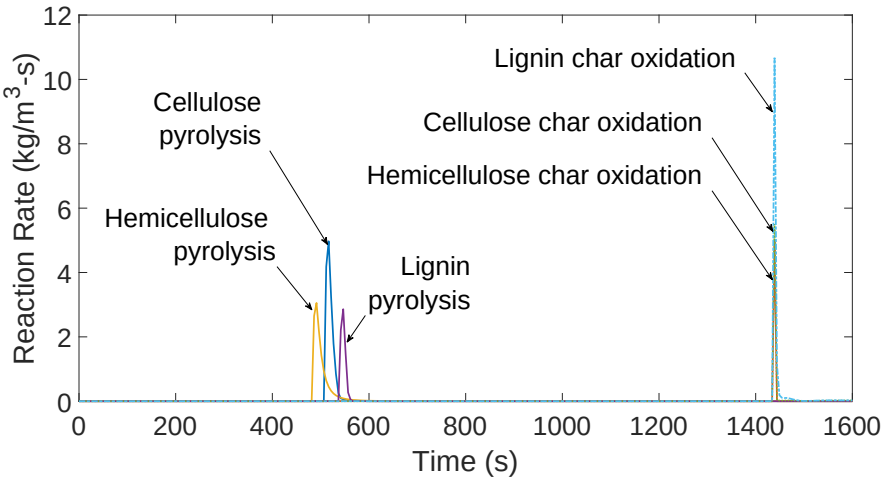

Figure 6.5: Reaction rates of cellulose, hemicellulose, and lignin for pyrolysis and oxidation for duff at the surface.

Next, we investigated what drives the variations in exposure time. Figure 6.5 shows the reaction rates for duff smoldering with a heat flux of 8 kW/m^2. At the surface, the oxidation reactions begin at 1440 s, which coincides with the minimum exposure time necessary to ignite. Thus, the heat-flux exposure time is also the ignition time of the fuel and char. The heat produced from oxidation overcomes the heat required

for the endothermic processes (heat losses, pyrolysis, and drying) and smoldering front to propagate without an external heat flux. The total heat produced by oxidation is 10.65 MJ, while the combined convective and radiative losses together with the heat required for pyrolysis and drying are just 1.86 MJ. Thus, the heat produced from oxidation reactions overcomes the heat required for endothermic processes and enables smoldering propagation.

6.4.2.3 Effect of moisture content

Next we investigated the effect of moisture content on ignition, because the moisture content in fuel beds may vary due to weather conditions and the changing climate. Figure 6.6 shows that when moisture content increases from 10% to 30% for duff and hardwood, the minimum exposure time for ignition for a given heat flux increases. However, the two fuels respond differently for the same increase in moisture content; for example, at higher heat fluxes (13–15 kW/m^2) the exposure time increases by 104% for duff and by 153% for hardwood. This coupling between moisture content and composition warrants further investigation.

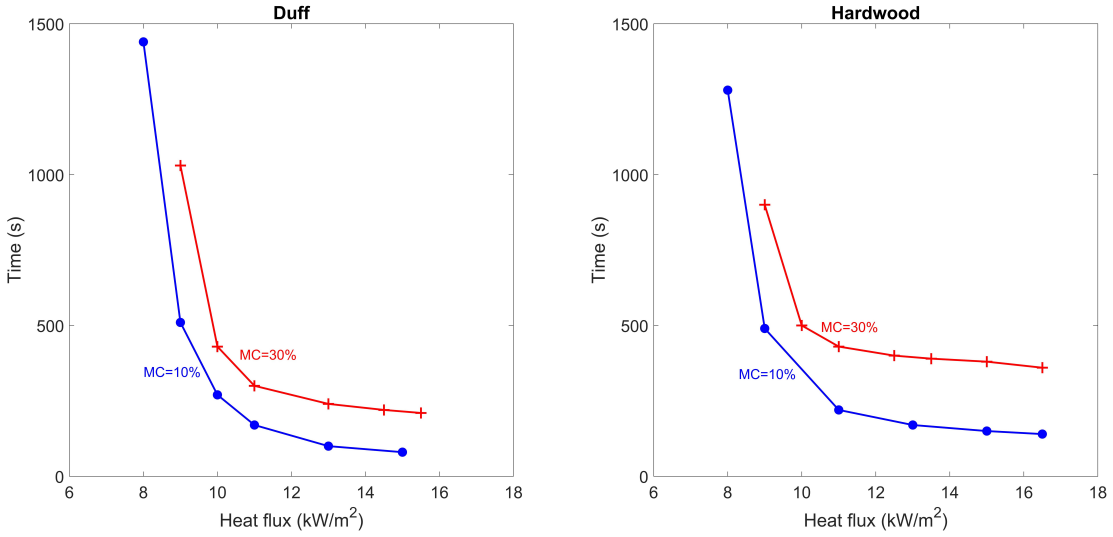

Figure 6.6: Minimum exposure time for ignition with varying applied heat flux for duff and hardwood at Moisture Contents (MC) of 10% and 30%.

6.4.3 Conductive smoldering ignition

Finally, we investigated how a hot metal particle ignites smoldering when it comes into contact with the surface of the fuel bed at a particular temperature. This analysis focuses on the affect of fuel composition on smoldering ignition and an investigation for reasons behind it. We identified a particular smoldering ignition temperature for a particular thickness of the metal layer. So we further searched for a relationship between the thickness of the metal and the ignition temperature. Also, we saw that these ignition temperatures change with the type of the fuel. So we repeated the simulations for the same eight different fuel types. For the initial study we used Aluminum 1100 as the metal, then to analyze the affect of the type of the metal we repeated the study for steel 302/304.

6.4.3.1 Smoldering ignition results for the eight fuels

To investigate the relationship between ignition temperature and the thickness of the metal layer, we varied the thickness of the aluminum layer at the top of the fuel bed from 1 mm to 10 mm for the eight different fuel beds. For each type of the fuel, the ignition temperature decreases nonlinearly with varying thickness of the metal. Figure 6.7 shows how ignition temperature varies with metal thickness for the eight fuels. Urban et al. [58] showed similar trends in ignition temperature with varying particle diameter in their experimental study of grass blends. Assuming that the particle diameter is proportional to the thickness of metal layer in one-dimensional domain, the results are in similar range in terms of temperatures. However, their experiments were done under a wind velocity of 0.5 m/s, and they did not mention the species composition of the grass blend, so the fuel may not be the same composition we have used, which may explain the observed differences of around 10% in temperatures.

Next, we investigated the causes of variations in ignition temperatures for different fuels. Our results show that the overall thermal conductivity of the fuel mixture plays a major role in igniting the sample. The thermal conductivity of cellulose, hemicellulose, and lignin are 0.356, 0.34, and 0.39 W/(m K) respectively. Table 6.5 shows the overall thermal conductivity of each fuel, determined based on the fuel mixture composition, with ignition temperature at 1 mm metal thickness. Ignition temperature increases with

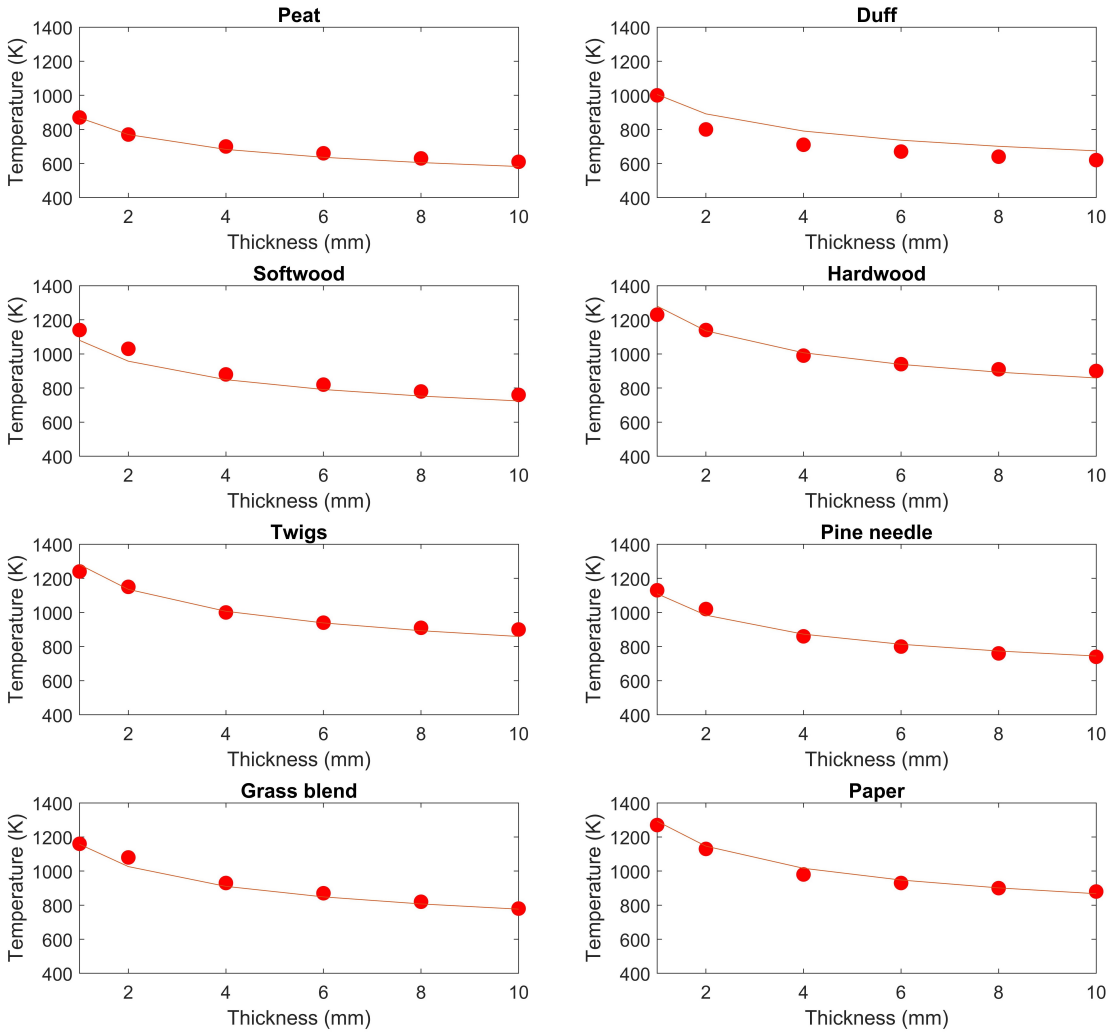

Figure 6.7: Ignition temperatures at different metal layer thicknesses for the eight fuel bed types. Points show simulation results and curves show the trend lines from curve fitting.

decreases in the overall thermal conductivity.

We further investigated the effect of thermal conductivity by artificially creating a fuel mixture with the composition of paper but which has the overall thermal conductivity of duff, holding constant all other physical and kinetic parameter. Figure 6.8 shows that the ignition temperatures of paper drop and approach the behavior of duff. This confirms

that overall thermal conductivity of the fuel mixture is the driving factor of fuel samples igniting at different temperatures.

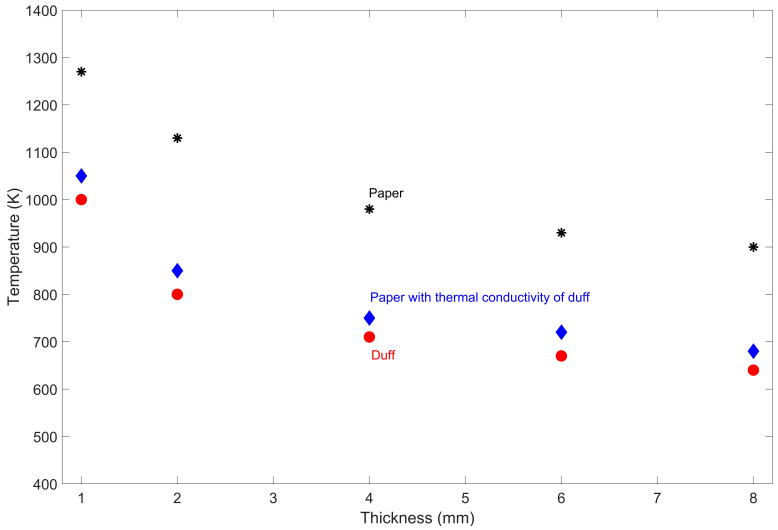

Figure 6.8: Ignition temperature with varying metal layer thickness, comparing paper, modified paper (with the thermal conductivity of duff), and duff.

These results show that thermal conductivity controls smoldering ignition via conduction, while in contrast activation energy drives ignition via radiation (discussed in Section 6.4.2.1) This implies that chemical kinetics drive the ignition via radiation, while physical properties drive ignition from conduction. Thus, fuels with varying physical and chemical characteristics will behave differently under different ignition sources.

Figure 6.7 shows the relationship between ignition temperature and thickness of the metal layer changes for different fuels, showing that fuel composition plays a role in smoldering ignition together with the metal layer thickness. To model how ignition temperature and thickness of the metal layer quantitatively scale with the fuel composition, we performed a linear regression of the data shown in Figure 6.7 using the Matlab function `regress()`, where the independent variables are mass fraction of cellulose ($Y_{\text{cellulose}}$), mass fraction of hemicellulose ($Y_{\text{hemicellulose}}$), mass fraction of lignin (Y_{lignin}), and thickness of the metal layer (Δh, in mm) and the dependent variable is ignition temperature (T_{ig}, in

Table 6.5: Thermal conductivity of each fuel and ignition temperature

Fuel	Thermal conductivity (W/(m K))	Ignition temperature at 1 mm thick metal layer (K)
Peat	0.3755	870
Duff	0.3671	1000
Pine needle	0.3621	1130
Softwood	0.3620	1140
Grass blend	0.3607	1160
Hardwood	0.3580	1230
Twigs	0.3579	1240
Paper	0.3570	1270

K). The resulting relationship is

$$T_{\text{ig}} = 489.9 \frac{Y_{\text{hemicellulose}}^{0.1116}}{Y_{\text{cellulose}}^{0.4809} \times Y_{\text{lignin}}^{0.4530} \times \Delta h^{0.1732}} \ , \tag{6.15}$$

with a goodness of fit (R^2) value of 0.9493, indicating a good agreement. Figure 6.7 also shows the fit as curves in each plot for each fuel, based on the associated composition. Ignition temperature shows a weak inverse relationship with thickness of the metal, relatively strong inverse relationships with cellulose and lignin, and weak direct relationship with hemicellulose because cellulose and lignin have higher thermal conductivity relative to hemicellulose.

6.4.3.2 Effect of the type of the metal layer

To analyze the effect of the type of the metal layer on top of the fuel bed, we repeated the simulations for steel 302/304. In practical scenarios the hot metal particles that drop onto forest beds can be different materials. Figure 6.9 shows the plots of ignition temperatures at different metal layer thicknesses for aluminum and steel for the eight fuel types. In the repeated simulations for steel, we changed the temperatures with a step size of 5 K to capture variations. The ignition temperatures of steel are higher than of aluminum for all fuels except peat. At smaller thicknesses, aluminum shows a slightly lower ignition temperature for all the fuels. At 1 mm, the ignition temperatures for aluminum to steel

differ by around 60 and 40K for all fuels. Urban et al. saw similar results in their experimental studies where grass fuel beds ignited at lower ignition temperatures with hot aluminum particles [58].

There can be two reasons for aluminum to show lower ignition temperatures: higher thermal conductivity and changes in physical properties due to melting. We can see that the changes in physical properties due to melting has the higher impact by investigating the trends of peat. For peat we do not find a significant drop in temperatures for aluminum as for the other fuels. The ignition temperatures of peat are lower that aluminum melting temperature. Then the temperature increment decreases and at 8 mm the increment is around 25 and 20K. When the particle is bigger, ignition temperatures drop below the melting temperature of aluminum for all the metals, so only the effect of higher thermal conductivity causes the differences.

6.5 Summary and Conclusions

In this work, we developed a one-dimensional computational model to study smoldering ignition of cellulose, hemicellulose, and lignin mixtures. We validated the model by comparing the propagation speeds of different compositions of the three constituents with experimental results and by comparing the the propagation speeds of a peat mixture with data from literature. Then, we used the model to study the ignition of smoldering via radiation and conduction for different fuel types with varying compositions.

Under radiant ignition we studied minimum heat flux required for ignition, relationship between heat flux and exposure time, and effect of moisture content on ignition. For each fuel, a minimum external heat flux is required to ignite smoldering. This minimum heat flux decreases with cellulose content and increases with hemicellulose content, due to variations in activation energy for oxidation of the fuels. For all fuels, increasing the heat flux decreases the exposure time required for ignition. This exposure time corresponds with the ignition time of fuel and char for oxidation, since the heat produced from oxidation can overcome required heat for endothermic processes. Next, we investigated the effects of moisture content on smoldering ignition for two fuels, and found that increasing moisture content increases the required exposure time but by a composition-dependent amount.

Finally we studied conductive smoldering ignition by modelling a hot metal layer

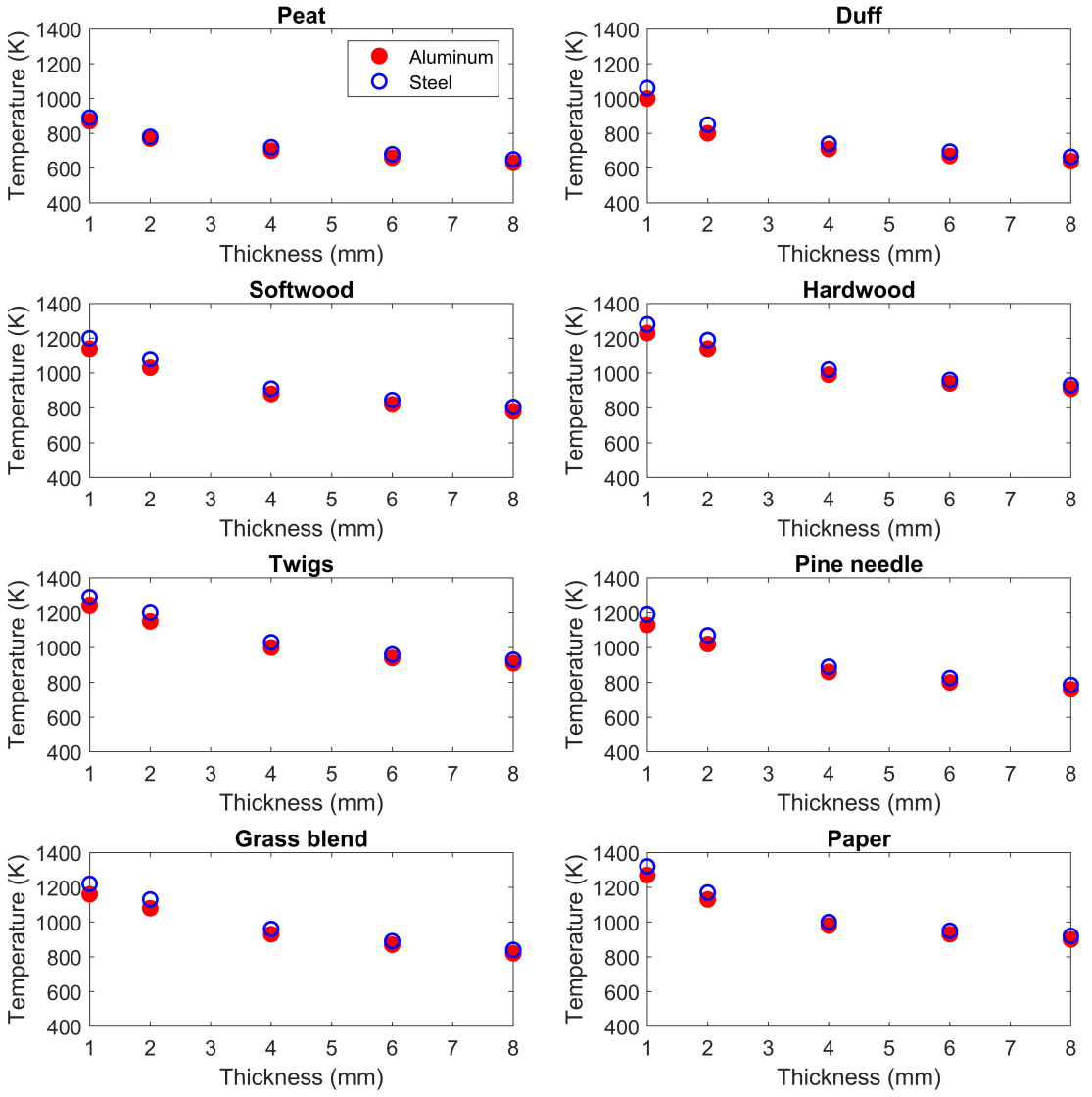

Figure 6.9: Ignition temperatures at different metal layer thicknesses for the eight fuel bed types for aluminum and steel.

(aluminum) in contact with eight different types of fuels. Ignition temperature decreases non-linearly with increasing thickness of the metal for all the fuels. We investigated what drives the variations in ignition temperatures for different fuels. The overall thermal conductivity of the fuel mixture plays the predominate role when it comes to igniting

the sample. Lignin has the highest thermal conductivity and hemicellulose has the lowest. Fuels with higher lignin content ignite at lower temperatures while fuels with higher cellulose and hemicellulose contents ignite at higher temperatures. This trend is opposite to that observed in radiant ignition, where decreases in cellulose content decrease minimum ignition heat flux. We also investigated on the effect of the material of the metal layer by repeating the simulations with Steel. With smaller aluminum metal particles fuel ignites at a lower temperature than steel due to changes in physical properties by melting. When particle size increases only the effect of higher thermal conductivity impacts the behaviour.

Acknowledgments

This research was funded by the Strategic Environmental Research and Development Program (SERDP) award RC-2651 under contract number W912HQ-16-C-0045. We also thank Benjamin Smucker and David Blunck from Oregon State University for providing their experimental temperature measurements.

Chapter 7: Conclusions

This chapter presents findings from the studies and the implications of the results as they pertain to each specific objective and the overall objective of this dissertation. The specific research questions are restated below:

1. How does smoldering combustion occur in real forest fuels?
2. How do chemical kinetic parameters and thermophysical properties affect smoldering combustion?
3. How do physical and environmental conditions affect smoldering behavior?
4. How does smoldering combustion initiate?

7.1 Smoldering combustion in cellulose and hemicellulose mixtures: Examining the roles of density, fuel composition, oxygen concentration, and moisture content

In this study, I developed a one-dimensional computational model for smoldering combustion of cellulose and hemicellulose mixtures, and used the model simulations to make below conclusions hence support first and third research question.

1. Smoldering propagation speed decreases with increasing fuel density. This is caused by the increase in the amount of fuel that needs to be converted to ash, which slows fuel shrinkage and thus access to oxygen. The propagation speed increases with hemicellulose content in the fuel, due to the faster pyrolysis of hemicellulose compared with cellulose.
2. Mean peak temperature of a smoldering fire increases with increasing density, due to decreasing radiation losses across the pores of the fuel. Mean peak temperature increases with additional hemicellulose content. This is caused by the formation of

ash with lower radiation loss across pores. The physical parameters of condensed-phase species control the observed variations in peak temperature, both as density and fuel composition change.

3. Fuels that expand with the addition of water show increases in propagation speed with moisture content due to the reduction in density. If the fuel does not expand and moisture simply fills the pores, propagation speed drops with moisture content due to the increase in wet bulk density. Therefore, accurately predicting smoldering in a given fuel requires distinguishing whether moisture content causes expansion. In both expanding and non-expanding fuel mixtures, the mean peak temperature slightly drops with additional moisture content. Fuel mixtures dominated by hemicellulose have 10% higher critical moisture content of ignition and extinction due to larger heat release.

7.2 Smoldering combustion of cellulose, hemicellulose, and lignin: Investigating the roles of fuel composition, density, oxygen concentration and moisture content

I developed a computational model that simulates real fuels as mixtures of cellulose, hemicellulose and lignin, which helped to answer the first research question. Then I analysed the smoldering behaviour of real forest fuel mixtures using the model. The following conclusions further fulfill the third question.

1. Increasing lignin content reduce the propagation speed, while increasing hemicellulose content raises the propagation speed due to the slower pyrolysis of lignin and faster pyrolysis of hemicellulose, respectively.

2. Peak temperature rises with both increasing lignin and hemicellulose content, caused by formation of ash that reduces the radiation loss across pores.

3. This work defines a new oxygen concentration threshold for forest fires (14%), which is lower than previously considered threshold in earth sciences (16%).

7.3 Uncertainty and sensitivity analysis for chemical kinetic parameters and thermophysical properties in smoldering combustion of wildland fuels

This section addresses the second research question. I used the computational model to estimate uncertainties associated with input parameters and to identify which parameters are highly sensitive. I conducted the analysis for five different mixtures that represent fuels that commonly under go smoldering in wild fires and considered three categories of input parameters: kinetic parameters, thermophysical properties and fuel composition.

1. Variations in physical properties result a higher uncertainty for both propagation speed and peak temperature than of the variations in kinetic parameters and composition. Uncertainly in composition of the fuel cause lower uncertainties in both propagation speed and peak temperature. Therefore, the accuracy of input data of physical properties is important than the kinetics and composition of species.

2. Comparing the results for five fuels indicated that fuels with high lignin content (50-65%) have higher uncertainties. This indicates that properties of lignin have higher uncertainties associated compared to properties of cellulose and hemicellulose.

3. The sensitivity study suggests that output estimates are most sensitive to activation energy (E) with a non-linear relationship. This implies the need to improve the measurement accuracy of E and uncertainties must be captured more precisely.

4. This study concludes that even though some kinetic properties are highly sensitive to behavior of smoldering combustion uncertainties associated with them are lower and even though physical properties have higher uncertainties associated, they are less sensitive to behavior of smoldering combustion in wildland fires.

7.4 A computational investigation into the ignition of smoldering combustion

I used the model to study the ignition of smoldering via radiation and conduction for different fuel types with varying compositions, hence address the fourth research objective.

1. A minimum external heat flux is required for radiant smoldering ignition. This minimum heat flux decreases with cellulose content and increases with hemicellulose content, due to variations in activation energy for oxidation of the fuels.

2. Increasing the radiant heat flux decreases the exposure time required for ignition. This exposure time corresponds with the ignition time of fuel and char for oxidation, since the heat produced from oxidation can overcome required heat for endothermic processes.

3. Ignition temperature decreases non-linearly with increasing thickness of the metal for conductive smoldering ignition. The overall thermal conductivity of the fuel mixture plays the predominate role in conductive ignition. The fuels with higher lignin content ignites at lower temperatures while fuels with higher cellulose and hemicellulose contents ignite at higher temperatures. Fuel ignites at a lower temperature with aluminum metal particles than steel due to changes in physical properties by melting.

4. Chemical kinetics drive the ignition via radiation, while physical properties drive ignition from conduction. Thus, fuels with varying physical and chemical characteristics will behave differently under different ignition sources.

7.5 Overall conclusions

This dissertation answers the stated research questions as below:

1. How does smoldering combustion occur in real forest fuels? The composition of the forest fuels change depending on the species of origin and decomposition rate, effecting propagation speed and peak temperatures to change over a wide range.

2. How do chemical kinetic parameters and thermophysical properties affect smoldering combustion? Behavior of smoldering combustion is highly sensitive to kinetic properties and uncertainties associated with them are lower. Thermophysical properties have higher uncertainties associated, but behavior of smoldering combustion is less sensitive to them.

3. How do physical and environmental conditions affect smoldering behavior? Density, moisture content, and oxygen concentration of the fuel affect smoldering behavior in terms of propagation speed and peak temperature. Table 7.1 summarizes the trends in smoldering behavior.

Table 7.1: Trends in smoldering behavior

Increased property	Propagation speed	Peak temperature
Density	Decrease	Increase
Moisture content (Expanding fuels)	Increase	Decrease
Moisture content (Non-expanding fuels)	Decrease	Decrease
Lignin content	Decrease	Increase
Hemicellulose content	Increase	Increase

4. How does smoldering combustion initiate? Smoldering combustion can be initiated via radiant and conductive heat sources. Chemical kinetics drive the ignition via radiation, while physical properties drive ignition from conduction. Hence, fuels with varying physical and chemical characteristics will react differently depending on the ignition sources that they are exposed.

7.6 Impacts of the dissertation

Following are the main outcomes of this dissertation:

1. The developed model uses mixtures of cellulose, hemicellulose, and lignin as surrogates of natural fuels, hence has the flexibility to simulate any forest fuel.

2. This work provide an understanding on how fuel composition, density, moisture content and oxygen concentration affect smoldering behavior and ignition.

3. The model can act as a framework to predict about a particular smoldering wildfire and can be integrated to large-scale forest fire management models helping land managers to make critical decisions.

Chapter 8: Future Work

Specific developments that could be implemented as extensions to my current work are,

1. Smoldering behaviour - Forest fuels that smolder can have some percentage (2–10 dry weight.% in wood) of inorganic content and extractives (i.e. nonstructural components). My model has not considered this. Incorporating this into the model can better represent smoldering behaviour of the fuels. Wind can have a significant impact on smoldering behavior, which I have not studied. This can be an interesting study to further look into effect of wind on smoldering behaviour.

2. Uncertainties associated with kinetic parameters and thermophysical properties - Kinetic parameters and thermophysical properties of cellulose, hemicellulose, and lignin vary over a wide variety in literature. My work has identified potential parameters that need improved measurements to reduce overall uncertainty. A study that involves precise measurements of these parameters will be a strong outcome.

I have identified two useful research areas in modeling of smoldering combustion that would be beneficial,

1. Smouldering emissions are a health concern for two reasons, generating large volumes of smoke and smoke toxicity [16]. Developing a standalone computational model that can accurately capture emissions from smoldering combustion is challenging. Hence a multidisciplinary research together with experimental and theoretical study would be beneficial to serve this purpose.

2. The transition from smoldering to flaming is a potential of serious fire hazard. This is a quick initiation of homogeneous gas-phase ignition preceded by smouldering combustion. Considering the high complexity of this phenomena, most studied materials are synthetic polymers [117, 118]. Hence, a computational model with multiphase formulations to simulate smoldering and spontaneous transition to flaming of wildland fuels would be very useful.

Bibliography

[1] TC Mulky and KE Niemeyer, "Computational study of the effects of density, fuel content, and moisture content on smoldering propagation of cellulose and hemicellulose mixtures", Proceedings of the Combustion Institute **37**, 4091–4098 (2019) 10.1016/j.proci.2018.06.164.

[2] J Eitelberger and K Hofstetter, "Prediction of transport properties of wood below the fiber saturation point - A multiscale homogenization approach and its experimental validation. Part I: Thermal conductivity", Composites Science and Technology **71**, 134–144 (2011) 10.1016/j.compscitech.2010.11.007.

[3] OV Voitkevich, GJ Kabo, AV Blokhin, YU Paulechka, and MV Shishonok, "Thermodynamic properties of plant biomass components. heat capacity, combustion energy, and gasification equilibria of lignin", Journal of Chemical & Engineering Data **57**, 1903–1909 (2012) https://doi.org/10.1021/je2012814.

[4] R Aseeva, B Serkov, and A Sivenkov, *Fire behavior and fire protection in timber buildings*, Springer Series in Wood Science (Springer, Dordrecht, 2014), 10.1007/978-94-007-7460-5.

[5] G Rein, "Smouldering fires and natural fuels", in *Fire phenomena and the earth system* (Wiley-Blackwell, 2013) Chap. 2, pp. 15–33, 10.1002/9781118529539.ch2.

[6] G Rein, "Smouldering combustion phenomena in science and technology", International Review of Chemical Engineering **1**, 3–18 (2009).

[7] T Lee, AP Sullivan, L Mack, JL Jimenez, SM Kreidenweis, TB Onasch, DR Worsnop, W Malm, CE Wold, WM Hao, et al., "Chemical smoke marker emissions during flaming and smoldering phases of laboratory open burning of wildland fuels", Aerosol Science and Technology **44**, i–v (2010) 10.1080/02786826.2010.499884.

[8] LM McKenzie, WM Hao, GN Richards, and DE Ward, "Measurement and modeling of air toxins from smoldering combustion of biomass", Environmental Science & Technology **29**, 2047–2054 (1995) https://doi.org/10.1021/es00008a025.

[9] A Gani and I Naruse, "Effect of cellulose and lignin content on pyrolysis and combustion characteristics for several types of biomass", Renewable Energy **32**, 649–661 (2007) 10.1016/j.renene.2006.02.017.

[10] H Yang, R Yan, H Chen, DH Lee, and C Zheng, "Characteristics of hemicellulose, cellulose and lignin pyrolysis", Fuel **86**, 1781–1788 (2007) https://doi.org/10.1016/j.fuel.2006.12.013.

[11] G Dorez, L Ferry, R Sonnier, A Taguet, and JM Lopez-Cuesta, "Effect of cellulose, hemicellulose and lignin contents on pyrolysis and combustion of natural fibers", Journal of Analytical and Applied Pyrolysis **107**, 323–331 (2014) https://doi.org/10.1016/j.jaap.2014.03.017.

[12] A Maranghides and W Mell, "A case study of a community affected by the witch and guejito wildland fires", Fire technology **47**, 379–420 (2011) 10.1007/s10694-010-0164-y.

[13] JP Prestemon, TJ Hawbaker, M Bowden, J Carpenter, MT Brooks, KL Abt, R Sutphen, and S Scranton, "Wildfire ignitions: a review of the science and recommendations for empirical modeling", Gen. Tech. Rep. SRS-GTR-171. Asheville, NC: USDA-Forest Service, Southern Research Station. 20 p. **171**, 1–20 (2013) https://doi.org/10.2737/SRS-GTR-171.

[14] JL Urban, J Song, S Santamaria, and C Fernandez-Pello, "Ignition of a spot smolder in a moist fuel bed by a firebrand", Fire safety journal **108**, 102833 (2019) 10.1016/j.firesaf.2019.102833.

[15] G Rein, "Smoldering combustion", in *Sfpe handbook of fire protection engineering*, edited by MJ Hurley, D Gottuk, JR Hall, K Harada, E Kuligowski, M Puchovsky, J Torero, JM Watts, and C Wieczorek (Springer New York, New York, NY, 2016), pp. 581–603, 10.1007/978-1-4939-2565-0_19.

[16] G Rein and X Huang, "Smouldering wildfires in peatlands, forests and the arctic: challenges and perspectives", Current Opinion in Environmental Science & Health **24**, 100296 (2021) 10.1016/j.coesh.2021.100296.

[17] SE Page, F Siegert, JO Rieley, HDV Boehm, A Jaya, and S Limin, "The amount of carbon released from peat and forest fires in indonesia during 1997", Nature **420**, 61–65 (2002) 10.1038/nature01131.

[18] AG Merschel, PA Beedlow, DC Shaw, DR Woodruff, EH Lee, SP Cline, RL Comeleo, RK Hagmann, and MJ Reilly, "An ecological perspective on living with fire in ponderosa pine forests of oregon and washington: resistance, gone but not forgotten", Trees, Forests and People **4**, 100074 (2021) https://doi.org/10.1016/j.tfp.2021.100074.

[19] K Miyanshi, "Duff Composition", in *Forest Fires: Behavior and Ecological Effects*, edited by EA Johnson and K Miyanishi (Academic Press, 2001), pp. 435–475, 10.1016/B978-012386660-8/50015-5.

[20] A Anca-Couce, "Reaction mechanisms and multi-scale modelling of lignocellulosic biomass pyrolysis", Progress in Energy and Combustion Science **53**, 41–79 (2016) 10.1016/j.pecs.2015.10.002.

[21] SA WAKSMAN, "Humus origin, chemical composition, and importance in nature", Soil Science **41**, 10.1097/00010694-193605000-00010 (1936) 10.1097/00010694-193605000-00010.

[22] H Yang, "Characteristics of hemicellulose, cellulose and lignin pyrolysis", Fuel **86**, 1781–1788 (2007) 10.1016/j.fuel.2006.12.013.

[23] X Huang and G Rein, "Thermochemical conversion of biomass in smouldering combustion across scales: the roles of heterogeneous kinetics, oxygen and transport phenomena", Bioresource Technology **207**, 409–421 (2016) https://doi.org/10.1016/j.biortech.2016.01.027.

[24] Fv Lehn, L Cai, and H Pitsch, "Sensitivity analysis, uncertainty quantification, and optimization for thermochemical properties in chemical kinetic combustion models", Proceedings of the Combustion Institute **37**, 771–779 (2019) https://doi.org/10.1016/j.proci.2018.06.188.

[25] A Anca-Couce, N Zobel, A Berger, and F Behrendt, "Smouldering of pine wood: Kinetics and reaction heats", Combustion and Flame **159**, 1708–1719 (2012) 10.1016/j.combustflame.2011.11.015.

[26] KY Li, X Huang, C Fleischmann, G Rein, and J Ji, "Pyrolysis of medium-density fiberboard: optimized search for kinetics scheme and parameters via a genetic algorithm driven by kissinger's method", Energy & Fuels **28**, 6130–6139 (2014) 10.1021/ef501380c.

[27] A Anca-Couce, A Berger, and N Zobel, "How to determine consistent biomass pyrolysis kinetics in a parallel reaction scheme", Fuel **123**, 230–240 (2014) https://doi.org/10.1016/j.fuel.2014.01.014.

[28] J Yang, N Liu, H Chen, and W Gao, "Smoldering and spontaneous transition to flaming over horizontal cellulosic insulation", Proceedings of the Combustion Institute **37**, 4073–4081 (2019) 10.1016/j.proci.2018.05.054.

[29] R Wooley and V Putsche, *Development of an ASPEN PLUS physical property database for biofuels components*, tech. rep. NREL/TP–425-20685, 257362 (Apr. 1996), NREL/TP–425–20685, 257362, 10.2172/257362.

[30] C Qi, S Hou, J Lu, W Xue, and K Sun, "Thermal characteristics of birch and its cellulose and hemicelluloses isolated by alkaline solution", Holzforschung **74**, 1099–1112 (2020) 10.1515/hf-2019-0285.

[31] WC Park, A Atreya, and HR Baum, "Experimental and theoretical investigation of heat and mass transfer processes during wood pyrolysis", Combustion and Flame **157**, 481–494 (2010) 10.1016/j.combustflame.2009.10.006.

[32] R Miller and J Bellan, "A Generalized Biomass Pyrolysis Model Based on Superimposed Cellulose, Hemicelluloseand Liqnin Kinetics", Combustion Science and Technology **126**, 97–137 (1997) 10.1080/00102209708935670.

[33] H Yuan, F Restuccia, F Richter, and G Rein, "A computational model to simulate self-heating ignition across scales, configurations, and coal origins", Fuel **236**, 1100–1109 (2019) 10.1016/j.fuel.2018.09.065.

[34] X Huang and G Rein, "Interactions of earth's atmospheric oxygen and fuel moisture in smouldering wildfires", Science of the Total Environment **572**, 1440–1446 (2016) https://doi.org/10.1016/j.scitotenv.2016.02.201.

[35] X Huang, G Rein, and H Chen, "Computational smoldering combustion: predicting the roles of moisture and inert contents in peat wildfires", Proceedings of the Combustion Institute **35**, 2673–2681 (2015) 10.1016/j.proci.2014.05.048.

[36] H Chen, G Rein, and N Liu, "Numerical investigation of downward smoldering combustion in an organic soil column", International Journal of Heat and Mass Transfer **84**, 253–261 (2015) https://doi.org/10.1016/j.ijheatmasstransfer.2015.01.016.

[37] J Yang and H Chen, "Natural downward smouldering of peat: effects of inorganic content and piled bed height", Fire Technology **54**, 1219–1247 (2018) 10.1007/s10694-018-0737-8.

[38] X Huang and G Rein, "Downward spread of smouldering peat fire: the role of moisture, density and oxygen supply", International Journal of Wildland Fire **26**, 907–918 (2017) 10.1071/WF16198.

[39] RA Hartford, "Smoldering combustion limits in peat as influenced by moisture, mineral content, and organic bulk density", in Proceedings of the 10th conference on fire and forest whitewood, edited by DC Maiver, H Auld, and R Whitewood (Apr. 1989).

[40] BD Smucker, TC Mulky, DA Cowan, KE Niemeyer, and DL Blunck, "Effects of fuel content and density on the smoldering characteristics of cellulose and hemicellulose", Proceedings of the Combustion Institute **37**, 4107–4116 (2019) 10.1016/j.proci.2018.07.047.

[41] B Benscoter, D Thompson, J Waddington, M Flannigan, B Wotton, W De Groot, and M Turetsky, "Interactive effects of vegetation, soil moisture and bulk density on depth of burning of thick organic soils", International Journal of Wildland Fire **20**, 418–429 (2011) 10.1071/WF08183.

[42] H Yan and O Fujita, "Experimental investigation on the smoldering limit of scraps of paper initiated by a cylindrical rod heater", Proceedings of the Combustion Institute **37**, 4099–4106 (2019) 10.1016/j.proci.2018.07.049.

[43] X Huang and G Rein, "Upward-and-downward spread of smoldering peat fire", Proceedings of the Combustion Institute **37**, 4025–4033 (2019) https://doi.org/10.1016/j.proci.2018.05.125.

[44] R Hadden, A Alkatib, G Rein, and JL Torero, "Radiant ignition of polyurethane foam: the effect of sample size", Fire Technology **50**, 673–691 (2014) https://doi.org/10.1007/s10694-012-0257-x.

[45] JM Jones, A Saddawi, B Dooley, EJS Mitchell, J Werner, DJ Waldron, S Weatherstone, and A Williams, "Low temperature ignition of biomass", Fuel Processing Technology **134**, 372–377 (2015) 10.1016/j.fuproc.2015.02.019.

[46] MK Anderson, RT Sleight, and JL Torero, "Ignition signatures of a downward smolder reaction", Experimental Thermal and Fluid Science **21**, 33–40 (2000) 10.1016/S0894-1777(99)00051-5.

[47] MT Gratkowski, N Dembsey, and CL Beyler, "Radiant smoldering ignition of plywood", Fire safety journal **41**, 427–443 (2006) 10.1016/j.firesaf.2006.03.006.

[48] S Wang, X Huang, H Chen, and N Liu, "Interaction between flaming and smouldering in hot-particle ignition of forest fuels and effects of moisture and wind", International Journal of Wildland Fire **26**, 71–81 (2017) https://doi.org/10.1071/WF16096.

[49] S Rissel and K Ridenour, "Ember production during the bastrop complex fire", Fire management today **72**, 7–13 (2013).

[50] C Farbotko, "Tuvalu and climate change: constructions of environmental displacement in the sydney morning herald", Geografiska Annaler: Series B, Human Geography **87**, 279–293 (2005) 10.1111/j.0435-3684.2005.00199.x.

[51] PJ Jakes and EL Langer, "The adaptive capacity of new zealand communities to wildfire", International Journal of Wildland Fire **21**, 764–772 (2012) https://doi.org/10.1071/WF11086.

[52] JL Urban, CD Zak, and C Fernandez-Pello, "Spot fire ignition of natural fuels by hot aluminum particles", Fire technology **54**, 797–808 (2018) 10.1007/s10694-018-0712-4.

[53] JL Urban, CD Zak, and C Fernandez-Pello, "Cellulose spot fire ignition by hot metal particles", Proceedings of the Combustion Institute **35**, 2707–2714 (2015) 10.1016/j.proci.2014.05.081.

[54] CD Zak, JL Urban, and C Fernandez-Pello, "Characterizing the flaming ignition of cellulose fuel beds by hot steel spheres", Combustion Science and Technology **186**, 1618–1631 (2014) 10.1080/00102202.2014.935612.

[55] C Zak, J Urban, V Tran, and A Fernandez-Pello, "Flaming ignition behavior of hot steel and aluminum spheres landing in cellulose fuel beds", Fire Safety Science **11**, 1368–1378 (2014) 10.3801/IAFSS.FSS.11-1368.

[56] MA Finney, SS McAllister, TB Maynard, and IJ Grob, "A study of wildfire ignition by rifle bullets", Fire technology **52**, 931–954 (2016) 10.1007/s10694-015-0518-6.

[57] RM Hadden, S Scott, C Lautenberger, and AC Fernandez-Pello, "Ignition of combustible fuel beds by hot particles: an experimental and theoretical study", Fire Technology **47**, 341–355 (2011) 10.1007/s10694-010-0181-x.

[58] JL Urban, CD Zak, J Song, and C Fernandez-Pello, "Smoldering spot ignition of natural fuels by a hot metal particle", Proceedings of the Combustion Institute **36**, 3211–3218 (2017) 10.1016/j.proci.2016.09.014.

[59] G Rein, S Cohen, and A Simeoni, "Carbon emissions from smouldering peat in shallow and strong fronts", Proceedings of the Combustion Institute **32**, 2489–2496 (2009) 10.1016/j.proci.2008.07.008.

[60] Y Hu, E Christensen, F Restuccia, and G Rein, "Transient gas and particle emissions from smouldering combustion of peat", Proceedings of the Combustion Institute **37**, 4035–4042 (2019) 10.1016/j.proci.2018.06.008.

[61] Y Hu, N Fernandez-Anez, TEL Smith, and G Rein, "Review of emissions from smouldering peat fires and their contribution to regional haze episodes", **27**, 293–312 (2018) https://doi.org/10.1071/WF17084.

[62] CE Stockwell, T Jayarathne, MA Cochrane, KC Ryan, EI Putra, BH Saharjo, AD Nurhayati, I Albar, DR Blake, IJ Simpson, et al., "Field measurements of trace gases and aerosols emitted by peat fires in central kalimantan, indonesia, during the 2015 el niño", Atmospheric Chemistry and Physics **16**, 11711–11732 (2016) 10.5194/acp-16-11711-2016.

[63] Y Hu, W Cui, and G Rein, "Haze emissions from smouldering peat: the roles of inorganic content and bulk density", Fire Safety Journal **113**, 102940 (2020) 10.1016/j.firesaf.2019.102940.

[64] Y Liu, J Stanturf, and S Goodrick, "Trends in global wildfire potential in a changing climate", Forest Ecology and Management **259**, 685–697 (2010) 10.1016/j.foreco.2009.09.002.

[65] AC Watts and LN Kobziar, "Smoldering combustion and ground fires: ecological effects and multi-scale significance", Fire Ecology **9**, 124–132 (2013) 10.4996/fireecology.0901124.

[66] G Rein, "Smouldering Combustion Phenomena in Science and Technology", International Review of Chemical Engineering **1**, 3–18 (2009).

[67] R Hartford and W Frandsen, "When it's hot, it's hot... or maybe it's not! (surface flaming may not portend extensive soil heating)", International Journal of Wildland Fire **2**, 139–144 (1992) 10.1071/WF9920139.

[68] E Ranzi, A Cuoci, T Faravelli, A Frassoldati, G Migliavacca, S Pierucci, and S Sommariva, "Chemical Kinetics of Biomass Pyrolysis", Energy & Fuels **22**, 4292–4300 (2008) 10.1021/ef800551t.

[69] E Ranzi, M Corbetta, F Manenti, and S Pierucci, "Kinetic modeling of the thermal degradation and combustion of biomass", Chemical Engineering Science **110**, 2–12 (2014) https://doi.org/10.1016/j.ces.2013.08.014.

[70] H Yang, R Yan, H Chen, DH Lee, and C Zheng, "Characteristics of hemicellulose, cellulose and lignin pyrolysis", Fuel **86**, 1781–1788 (2007) 10.1016/j.fuel.2006.12.013.

[71] A Anca-Couce, N Zobel, A Berger, and F Behrendt, "Smouldering of pine wood: Kinetics and reaction heats", Combustion and Flame **159**, 1708–1719 (2012) 10.1016/j.combustflame.2011.11.015.

[72] T Kashiwagi and H Nambu, "Global kinetic constants for thermal oxidative degradation of a cellulosic paper", Combustion and Flame **88**, 345–368 (1992) 10.1016/0010-2180(92)90039-R.

[73] B Cagnon, X Py, A Guillot, F Stoeckli, and G Chambat, "Contributions of hemicellulose, cellulose and lignin to the mass and the porous properties of chars and steam activated carbons from various lignocellulosic precursors", Bioresource Technology **100**, 292–298 (2009) 10.1016/j.biortech.2008.06.009.

[74] G Rein, "Smouldering Combustion", in *SFPE Handbook of Fire Protection Engineering*, edited by Hurley M. J. et al. (Springer, New York, NY, 2016) Chap. 19, pp. 581–603, 10.1007/978-1-4939-2565-0_19.

[75] BD Smucker, TC Mulky, DA Cowan, KE Niemeyer, and DL Blunck, "Corrigendum to "effects of fuel content and density on the smoldering characteristics of cellulose and hemicellulose" [proc. combust. inst. 37 (2019) 4107-4116]", Proceedings of the Combustion Institute **38**, 6781–6783 (2021) 10.1016/j.proci.2020.11.004.

[76] EC Garlough and CR Keyes, "Influences of moisture content, mineral content and bulk density on smouldering combustion of ponderosa pine duff mounds", International Journal of Wildland Fire **20**, 589–596 (2011) 10.1071/WF10048.

[77] WH Frandsen, "The influence of moisture and mineral soil on the combustion limits of smoldering forest duff", Canadian Journal of Forest Research **17**, 1540–1544 (1987) 10.1139/x87-236.

[78] WH Frandsen, "Ignition probability of organic soils", Canadian Journal of Forest Research **27**, 1471–1477 (1997) 10.1139/x97-106.

[79] X Huang and G Rein, "Computational study of critical moisture and depth of burn in peat fires", International Journal of Wildland Fire **24**, 798–808 (2015) 10.1071/WF14178.

[80] BD Smucker and DL Blunck, Personal communication, 1 July 2019, 2019.

[81] C Lautenberger, *Gpyro v0.700*, http://reaxengineering.com/trac/gpyro, 2009.

[82] C Lautenberger and C Fernandez-Pello, "Generalized pyrolysis model for combustible solids", Fire Safety Journal **44**, 819–839 (2009) 10.1016/j.firesaf.2009.03.011.

[83] X Huang and G Rein, "Smouldering combustion of peat in wildfires: Inverse modelling of the drying and the thermal and oxidative decomposition kinetics", Combustion and Flame **161**, 1633–1644 (2014) 10.1016/j.combustflame.2013.12.013.

[84] KY Li, X Huang, C Fleischmann, G Rein, and J Ji, "Pyrolysis of medium-density fiberboard: optimized search for kinetics scheme and parameters via a genetic algorithm driven by kissinger's method", Energy & Fuels **28**, 6130–6139 (2014) 10.1021/ef501380c.

[85] C Huggett, "Estimation of rate of heat release by means of oxygen consumption measurements", Fire and Materials **4**, 61–65 (1980) 10.1002/fam.810040202.

[86] DA Cowan, BD Smucker, and DL Blunck, "Sensitivity of smoldering combustion to cellulose and hemicellulose content", in 10th us combustion meeting (2017).

[87] X Huang, Personal communication, 25 March 2017, 2017.

[88] R Moriana, Y Zhang, P Mischnick, J Li, and M Ek, "Thermal degradation behavior and kinetic analysis of spruce glucomannan and its methylated derivatives", Carbohydrate Polymers **106**, 60–70 (2014) 10.1016/j.carbpol.2014.01.086.

[89] NOSB TAP, *National Organic Standards Board Technical Advisory Panel Review on Cellulose Processing*, https://www.ams.usda.gov/sites/default/files/media/Cellulose%20TR%202001.pdf, Accessed: 2017-08-29, 2011.

[90] C-Therm Technologies, *Thermal Physical Properties Reference Library: Part II (L–R)*, http://ctherm.com/products/tci_thermal_conductivity/helpful_links_tools/thermal_physical_properties_conductivity_effusivity_heat_capacity_density2/, Accessed: 2017-08-29, 2017.

[91] EE Thybring, "Explaining the heat capacity of wood constituents by molecular vibrations", Journal of Materials Science **49**, 1317–1327 (2014) 10.1007/s10853-013-7815-6.

[92] RT Jacobsen, EW Lemmon, SG Penoncello, Z Shan, and NT Wright, "Thermophysical properties of fluids and materials", in *Heat transfer handbook*, Vol. 1 (John Wiley & Sons, 2003) Chap. 2, pp. 43–160.

[93] B Punmia and AK Jain, *Soil mechanics and foundations* (Laxmi Publication Pvt Limited, 2005).

[94] F Yu, G Wei, X Zhang, and K Chen, "Two effective thermal conductivity models for porous media with hollow spherical agglomerates", International Journal of Thermophysics **27**, 293–303 (2006) 10.1007/s10765-006-0032-7.

[95] Sigma-Aldrich, *α-Cellulose*, http://www.sigmaaldrich.com/catalog/product/sigma/c8002?lang=en&region=US, Accessed: 2017-08-29, 2017.

[96] M Schure, PA Soltys, DFS Natusch, and T Mauney, "Surface area and porosity of coal fly ash", Environmental Science & Technology **19**, 82–86 (1985) 10.1021/es00131a009.

[97] Parchem, *Glucomannan*, https://www.parchem.com/chemical-supplier-distributor/Glucomannan-007456.aspx, Accessed: 2017-08-29, 2017.

[98] F Richter, A Atreya, P Kotsovinos, and G Rein, "The effect of chemical composition on the charring of wood across scales", Proceedings of the Combustion Institute **37**, 4053–4061 (2019) 10.1016/j.proci.2018.06.080.

[99] RS Miller and J Bellan, "A generalized biomass pyrolysis model based on superimposed cellulose, hemicellulose and liqnin kinetics", Combustion Science and Technology **126**, 97–137 (1997) 10.1080/00102209708935670.

[100] LY Mwaikambo and MP Ansell, Journal of Materials Science Letters **20**, 2095–2096 (2001) 10.1023/a:1013703809964.

[101] C Qi, S Hou, J Lu, W Xue, and K Sun, "Thermal characteristics of birch and its cellulose and hemicelluloses isolated by alkaline solution", Holzforschung **74**, 1099–1112 (2020) 10.1515/hf-2019-0285.

[102] F Richter, FX Jervis, X Huang, and G Rein, "Effect of oxygen on the burning rate of wood", Combustion and Flame **234**, 111591 (2021) 10.1016/j.combustflame.2021.111591.

[103] TC Mulky, WJ Jayasuriya, and KE Niemeyer, *Input files, plotting scripts, and figures for "Smoldering combustion in cellulose and hemicellulose mixtures: examining the roles of density, fuel composition, oxygen concentration, and moisture content"*, Zenodo, 2019, 10.5281/zenodo.3358193.

[104] J Yang, N Liu, H Chen, W Gao, and R Tu, "Effects of atmospheric oxygen on horizontal peat smoldering fires: experimental and numerical study", Proceedings of the Combustion Institute **37**, 4063–4071 (2019) https://doi.org/10.1016/j.proci.2018.06.218.

[105] C Lautenberger, *gpyro:0.8171*, https://github.com/reaxfire/gpyro, version 0.8171, 2018.

[106] F vom Lehn, L Cai, and H Pitsch, "Sensitivity analysis, uncertainty quantification, and optimization for thermochemical properties in chemical kinetic combustion models", Proceedings of the Combustion Institute **37**, 771–779 (2019) 10.1016/j.proci.2018.06.188.

[107] KY Li, X Huang, C Fleischmann, G Rein, and J Ji, "Pyrolysis of medium-density fiberboard: optimized search for kinetics scheme and parameters via a genetic algorithm driven by kissinger's method", Energy & Fuels **28**, 6130–6139 (2014) 10.1021/ef501380c.

[108] A Anca-Couce, A Berger, and N Zobel, "How to determine consistent biomass pyrolysis kinetics in a parallel reaction scheme", Fuel **123**, 230–240 (2014) 10.1016/j.fuel.2014.01.014.

[109] A Anca-Couce and I Obernberger, "Application of a detailed biomass pyrolysis kinetic scheme to hardwood and softwood torrefaction", Fuel **167**, 158–167 (2016) 10.1016/j.fuel.2015.11.062.

[110] B Berg, K Hannus, T Popoff, and O Theander, "Changes in organic chemical components of needle litter during decomposition. long-term decomposition in a scots pine forest", Canadian Journal of Botany **60**, 1310–1319 (1982) 10.1139/b82-167.

[111] JJ McDermott, "Changes in chemical composition of twigs and buds of yellow poplar during the dormant period", Plant Physiology **16**, 415–418 (1941) 10.1104/pp.16.2.415.

[112] WJ Jayasuriya, TC Mulky, and KE Niemeyer, "Smouldering combustion in cellulose and hemicellulose mixtures: examining the roles of density, fuel composition, oxygen concentration, and moisture content", Combustion Theory and Modelling **0**, 1–25 (2022) 10.1080/13647830.2022.2071170.

[113] HT Sahin and OU Yalcin, "Chemical composition and utilization of conifer needles-a review", Journal of Applied Life Sciences International, 1–11 (2017) 10.9734/JALSI/2017/37076.

[114] DM Hamby, "A review of techniques for parameter sensitivity analysis of environmental models", Environmental Monitoring and Assessment **32**, 135–154 (1994) 10.1007/BF00547132.

[115] M Ye and MC Hill, "Global sensitivity analysis for uncertain parameters, models, and scenarios", in *Sensitivity analysis in earth observation modelling*, edited by GP Petropoulos and PK Srivastava (Elsevier, 2017) Chap. 10, pp. 177–210, 10.1016/B978-0-12-803011-0.00010-0.

[116] M Vincent, A Pometto, and JH van Leeuwen, "Simultaneous saccharification and fermentation of ground corn stover for the production of fuel ethanol using phanerochaete chrysosporium, gloeophyllum trabeum, saccharomyces cerevisiae, and escherichia coli k011", J. Microbiol. Biotechnol **21**, 703–710 (2011) 10.4014/jmb.1010.10044.

[117] MA Santoso, EG Christensen, J Yang, and G Rein, "Review of the transition from smouldering to flaming combustion in wildfires", Frontiers in Mechanical Engineering **5**, 49 (2019) 10.3389/fmech.2019.00049.

[118] J Yang, N Liu, H Chen, and W Gao, "Smoldering and spontaneous transition to flaming over horizontal cellulosic insulation", Proceedings of the Combustion Institute **37**, 4073–4081 (2019) 10.1016/j.proci.2018.05.054.

[119] R Koppmann, K Von Czapiewski, and JS Reid, "A review of biomass burning emissions, part I: gaseous emissions of carbon monoxide, methane, volatile organic compounds, and nitrogen containing compounds", Atmospheric Chemistry and Physics Discussions **5**, 10455–10516 (2005) 10.5194/acpd-5-10455-2005.

[120] RJ Yokelson, R Susott, DE Ward, J Reardon, and DWT Griffith, "Emissions from smoldering combustion of biomass measured by open-path Fourier transform infrared spectroscopy", Journal of Geophysical Research **102**, 18865–18877 (1997) 10.1029/97JD00852.

[121] C Liu, C Zhang, Y Mu, J Liu, and Y Zhang, "Emission of volatile organic compounds from domestic coal stove with the actual alternation of flaming and smoldering combustion processes", Environmental Pollution **221**, 385–391 (2017) 10.1016/j.envpol.2016.11.089.

[122] N Prat-Guitart, G Rein, RM Hadden, CM Belcher, and JM Yearsley, "Propagation probability and spread rates of self-sustained smouldering fires under controlled moisture content and bulk density conditions", International Journal of Wildland Fire **25**, 456–465 (2016) 10.1071/WF15103.

[123] BC Hagen, V Frette, G Kleppe, and BJ Arntzen, "Effects of heat flux scenarios on smoldering in cotton", Fire Safety Journal **61**, 144–159 (2013) 10.1016/j.firesaf.2013.08.001.

[124] BC Hagen, V Frette, G Kleppe, and BJ Arntzen, "Transition from smoldering to flaming fire in short cotton samples with asymmetrical boundary conditions", Fire Safety Journal **71**, 69–78 (2015) 10.1016/j.firesaf.2014.11.004.

[125] J Reardon, G Curcio, and R Bartlette, "Soil moisture dynamics and smoldering combustion limits of pocosin soils in North Carolina, USA", International Journal of Wildland Fire **18**, 326–335 (2009) 10.1071/WF08085.

[126] A Gani and I Naruse, "Effect of cellulose and lignin content on pyrolysis and combustion characteristics for several types of biomass", Renewable Energy **32**, 649–661 (2007) 10.1016/j.renene.2006.02.017.

[127] D Watkins, M Nuruddin, M Hosur, A Tcherbi-Narteh, and S Jeelani, "Extraction and characterization of lignin from different biomass resources", Journal of Materials Research and Technology **4**, 26–32 (2015) 10.1016/j.jmrt.2014.10.009.

[128] MJ de la Torre, A Moral, MD Hernández, E Cabeza, and A Tijero, "Organosolv lignin for biofuel", Industrial Crops and Products **45**, 58–63 (2013) 10.1016/j.indcrop.2012.12.002.

[129] J Yang, H Chen, W Zhao, and J Zhou, "TG-FTIR-MS study of pyrolysis products evolving from peat", Journal of Analytical and Applied Pyrolysis **117**, 296–309 (2016) 10.1016/j.jaap.2015.11.002.

APPENDICES

Appendix A: Influence of lignin on smoldering propagation

Benjamin D. Smucker, W. Jayani Jayasuriya, Kyle E. Niemeyer, and David L. Blunck

I contributed to support the computational analysis of this work, which included developing the computational model, running simulations, processing output data, providing results, and writing the computational model section in the manuscript

Target Journal: Combustion and Flame (In Preparation)

A.1 Abstract

Smoldering combustion during wildfires contributes significantly to emissions of pollutants, can burn for days or months, may damage roots and soil, and can transition to flaming combustion. To mitigate these hazards of smoldering combustion, it is necessary to understand how physical parameters that control smoldering combustion, such as the chemical composition. The main organic constituents within biomass are cellulose, hemicellulose, and lignin. Understanding how these constituents influence smoldering is an important step toward developing physics-based models and developing understanding that is applicable across multiple fuel sources. Previous studies have investigated how cellulose and hemicellulose influence smoldering behavior, but have not considered mixtures including lignin. The objective of this study is to identify the influence of lignin on smoldering propagation. This objective was achieved by experimentally and numerically studying the smoldering behavior of various concentrations of lignin in mixtures of cellulose and hemicellulose. These were tested at densities of 200 and 300 $\mathrm{kg/m^3}$. An infrared camera and thermocouples were used to determine the propagation of the smoldering front in the horizontal and vertical directions. A one-dimensional reactive porous media model with reduced chemistry was used to determine downward smoldering propagation. The horizontal and downward smoldering propagation velocities decrease when more lignin is present due to the slower pyrolysis rates and higher activation energy of lignin. Additionally, the computational downward propagation decreases with increased lignin content. At higher lignin contents, the effect of cellulose and hemicellulose on downward and horizontal smoldering decreases, indicating that lignin content has the largest impact on smoldering velocities of the three constituents. Increasing the density decreases both the horizontal and vertical propagation velocities due to lower oxygen diffusion and the additional mass being consumed.

A.2 Introduction

Smoldering combustion in wildland fires presents hazards that are important to the health of ecosystems and to humans. Compared to flaming combustion, smoldering is less complete combustion, resulting in relatively larger quantities of smoke, carbon monoxide, and volatile organic compounds (VOCs) [7, 8, 119–121]. Smoldering can

continue much longer than flaming combustion (i.e., days or months), or may transition to flaming combustion [5]. Smoldering has the potential to burn the entire organic soil layer, which can severely limit plant regrowth and damage roots [66].

Motivated by the detrimental effects of smoldering, numerous studies have investigated how smoldering behavior is influenced by physical conditions of the fuel (e.g., density, moisture content, inorganic content, etc.) affect smoldering propagation rates [1, 35, 38, 40, 78, 122–124]. A few representative findings are now highlighted. Both downward and horizontal smoldering propagation rates decrease with increasing density in a wide variety of fuels, including peat, cotton, and combinations of powderized cellulose and hemicellulose. This reduction in propagation rate is due to the additional fuel that must be consumed [1, 38, 40, 122–124]. Ignition limits in peat depend on both the inorganic content and moisture content of the fuel; the limiting moisture content decreases with increasing inorganic content, and vice versa [35, 78]. Horizontal propagation rates decrease with moisture content in peat because of heat losses. In contrast, downward propagation rates can increase with increasing moisture content [38] due to peat expanding with increasing fuel moisture content [122], resulting in lower organic bulk densities and faster propagation rates. Additionally, the sensitivity of propagation rates to density changes with moisture content, illustrating that there can be coupling between physical parameters [122].

Biomass can have different smoldering characteristics depending on its origin [77, 78, 125]. As an example, the limiting moisture content for sustained smoldering varied from 40% to greater than 100% in samples of biomass collected from different locations across North America [78]. Additionally, different fuels at the same density and moisture content have different propagation velocities. For example, cotton at $100\,\mathrm{kg/m^3}$ has a horizontal propagation velocity of 7.8-9 cm/hr [123], but peat at the same density has a propagation velocity of about 4.2 cm/hr [122]. Differences in smoldering behavior for various biomasses has been a challenge for the community because it limits the application of knowledge and models to fuels that have not been tested.

The chemical composition of biomass fuels changes depending on its origin. Hence, understanding how the chemical composition of fuels impacts smoldering behavior can potentially be used to help bridge the knowledge from fuels that have been studied to those that have not. The three most abundant organic chemical constituents in natural fuels are cellulose, hemicellulose, and lignin; the amount of these constituents varies significantly

with the fuel source [21]. A previous study of the sensitivity of smoldering propagation velocity to the ratio of masses of cellulose and hemicellulose showed that horizontal and downward propagation velocities increase with increasing hemicellulose content. This sensitivity results from the earlier pyrolysis and oxidation of hemicellulose when compared to cellulose. Additionally, higher cellulose content fuels have greater sensitivity to changes in the density due to cellulose having larger changes in permeability with density [40]. What is not understood is how lignin, the third primary organic constituent within biomass, impacts the smoldering characteristics when included with mixtures of cellulose and hemicellulose. The influence of lignin on smoldering behavior maybe significant considering that up to 55% of organic material in natural fuels (e.g., peat and duff) may be composed of lignin [21]. Thermogravimetric analysis (TGA) and differential scanning calorimetry (DSC) of cellulose, hemicellulose, and lignin have shown that lignin has a higher pyrolysis temperature and activation energy than cellulose and hemicellulose. Additionally, lignin reacts over a larger range of temperatures and has a higher char yield [11, 22, 126].

With this background and motivation, the objective of this study is to identify how the presence of lignin alters the smoldering behavior of mixtures of cellulose and hemicellulose, and ascertain the reasons for these changes. The knowledge gained from this study can be used to improve the understanding of smoldering behavior for fuels that include lignin. More long term, this work helps to establish the foundation for using mixtures of cellulose, hemicellulose, and lignin as surrogates in models of natural fuels.

A.3 Experimental Methods

Experiments were performed to identify how the lignin content and density of the fuel influence horizontal and downward smoldering propagation velocities. Both downward and horizontal smoldering behavior are considered because differences can exist in the controlling physics [38]. Different arrangements were used to allow for larger burn distances in the direction of interest and to avoid biasing from thermocouples when evaluation horizontal smoldering. The arrangement for the horizontal smoldering studies is shown in Figure A.1. The reactor box was composed of 1.3 cm-thick calcium silicate insulation board and was 20 cm by 20 cm by 5 cm deep. An infrared camera (FLIR SC6700) recorded top-down images reflected off of a polished stainless steel mirror placed 1 m from the

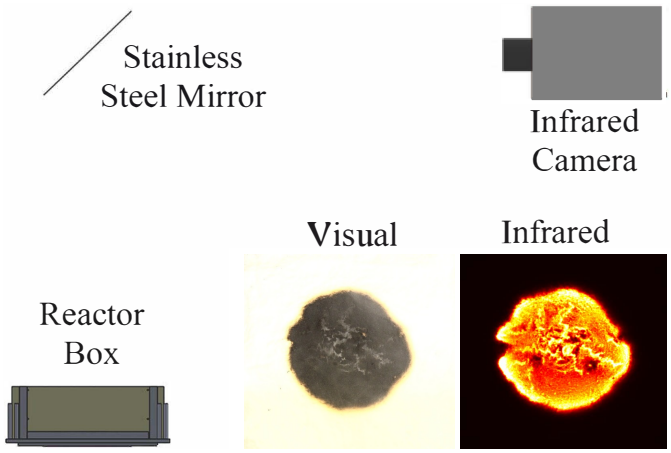

Figure A.1: Experimental arrangement for measuring the horizontal smoldering propagation velocities during smoldering combustion. The images in the bottom right corner are visual and infrared images of the same burn (75% cellulose, $\rho = 225\,\mathrm{kg/m^3}$) approximately 40 minutes after ignition. The burned area is approximately 10 cm across.

camera horizontally and 0.75 m above the fuel. The sampling frequency of the camera was 0.1 Hz, and the integration time was 0.48 µs. The spatial resolution of the camera was about 0.33 by 0.33 mm/pixel. The fuel was ignited using a 20 W cartridge heater placed at the surface in the center of the reactor. The heater was controlled such that the temperature of the heater was limited to 650 °C. The igniter was placed in the fuel for 3–10 minutes depending on when the smoldering was self-sustaining. Any fuel that adhered to the heater was scraped back into the middle of the reactor box. The burns typically lasted 1–3 hours.

The horizontal propagation velocities were determined from the infrared images. The burned area for each image was determined from the number of pixels above the threshold of photon counts corresponding to when the smoldering front was self-sustained (near 1800 counts). The burned area was assumed to be circular and the radius was obtained from the burned area. For reference, Figure A.1 shows representative visual and infrared images. After a transient period of 10-20 minutes, the change in radius of the smoldering front with time was nearly linear, as shown in Figure A.2. The horizontal propagation velocities reported in this work are determined from when the change in radius is linear with respect to the time; the transient period is not reported. The bias uncertainty of the mean propagation velocities is estimated near 2% based on the error in the calibration

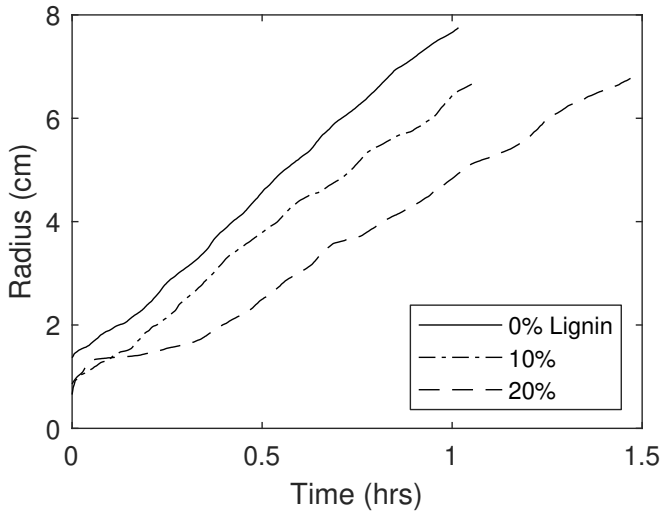

Figure A.2: The radius of the burned area with time for three different experiments. The non-lignin portion of the fuel is 75% cellulose (residual hemicellulose), and the density is 300 kg/m^3. Note the inflection in the radial growth after 0.3 hours in the 20% lignin case, as that is representative of the end of the transient time.

and linear fit.

The effect of lignin on downward propagation velocities was determined by burning samples in a second reactor box, with inside dimensions of 10 cm by 10 cm by 10 cm. The increased height allowed the smoldering propagation rate measurements to be measured over a longer distance and reduced heat losses through the bottom of the reactor box. Temperatures within the fuels were measured using sheathed type-K thermocouples. The thermocouples were spaced 1 cm apart with the tips of the thermocouples placed in the middle of the box. Temperature measurements were recorded at 1 Hz. The fuel was ignited using the same method as the horizontal smoldering tests. The burns typically lasted 4-12 hours. The fuel was considered ignited at a thermocouple location when the temperature reached 300 °C. This temperature threshold was estimated from when heat release occurs in cellulose and hemicellulose in an oxygenated environment using differential scanning calorimetry (DSC) [40]. Both cellulose and hemicellulose react at lower temperatures than lignin. The propagation velocity was determined by the distance between the thermocouples divided by the difference in ignition time corresponding to the two locations. Note that the specific temperature used to determine the propagation

rate is not as important as using a consistent threshold at each location, as was the case in this study. The propagation velocity reported were measured from 3 to 6 cm below the surface. Using this range reduced the biasing from the upper and lower boundary conditions on the propagation velocities. The reported downward propagation velocities for each fuel condition are the average of 4 to 7 tests unless stated otherwise.

The peak temperatures reported are the maximum temperature for an experiment at any thermocouple location. When the mean value is reported, it is the mean of the peak temperatures from a set of experiments (usually 8 or more tests).

The char thickness of downward propagation samples was estimated from temperature data. The char thickness was determined at the time when the thermocouple 5 cm below the surface reached the temperature where char begins to form (250 °C), setting the lower boundary of the char layer. Finding the top of the char layer at this time was a multi-step process. First, time when the top of the char layer was at a given thermocouple was determined from increased temperature fluctuations that occur once the thermocouples were exposed to air. Second, the location of the top of the char layer was interpolated from the times when the top of the char layer reached the various thermocouples. The variance in the char thickness was relatively large because of the imprecise nature of this measurement technique and variation in how the fuel burned around the thermocouples. However, this method was successful at capturing global trends.

The three physical conditions varied for the experiments were the lignin content, the density, and the percentage of cellulose and hemicellulose in the remainder (non-lignin) portion of the fuel. The lignin content was systematically varied from 0 to 30% by mass to isolate the effects lignin has on smoldering velocities. The fuels were tested over this range because it was the maximum range over which constant densities could be achieved with a constant fuel content. Admittedly this range of lignin content, doesn't cover all contents observed in biomass, as lignin content can be as high 55%. However, the lignin content for most lignocellulosic biomass is 10-25% [127]. The densities evaluated were 200 and 300 kg/m^3. The densities that could be achieved were limited because the cellulose has a loose density of about 170 kg/m^3, but the hemicellulose and lignin have a loose density of about 700 kg/m^3. Fuels with higher hemicellulose and lignin contents had higher bulk densities, so a process was developed to lower the density. Water was added to the fuel, the fuel was dried for at 103 °C, and then water was added to reach a moisture content of 5%. The bias uncertainty of the density is approximately 10 kg/m^3 based on

the error in the mass of the fuel and the dimensions of the reactor box. The percentage of cellulose and hemicellulose in the remainder (non-lignin portion) of the fuel was held constant to avoid varying the amount of cellulose and hemicellulose independently. The three conditions evaluated for the non-lignin fuel were 100% cellulose, 75% cellulose and 25% hemicellulose, and 50% cellulose and 50% hemicellulose by mass. The uncertainty in fuel content percentage is approximately 0.5% (as an absolute value).

The cellulose used in these experiments was α-cellulose (Sigma-Aldrich). Glucomman was used for the hemicellulose (Nutricost). The lignin was an organosolv lignin (Attis Innovations).

A.4 Computational Model

A one-dimensional transient numerical model was developed to study downward propagation of smoldering of cellulose, hemicellulose, and lignin mixtures using Gypro v0.8171 [105]. The cell size had a (Δz) of 1×10^{-4} m with an initial time step of 0.05 s. The modeling effort followed the approach of [1] used to study mixtures of cellulose and hemicelloluse.

A.4.1 Governing equations and Boundary conditions

The model solves equations for both condensed and gas phases. The governing equations include: condensed-phase mass conservation (A.1), condensed-phase species conservation (A.2), gas-phase mass conservation (A.3), gas-phase species conservation (A.4), condensed-phase energy conservation (A.5), gas-phase momentum conservation (A.6), gas-phase energy conservation (A.7), and the ideal gas law equation of state (A.8):

$$\frac{\partial \overline{\rho}}{\partial t} = -\dot{\omega}'''_{fg} \,, \tag{A.1}$$

$$\frac{\partial (\overline{\rho} Y_i)}{\partial t} = \dot{\omega}'''_{fi} - \dot{\omega}'''_{di} \,, \tag{A.2}$$

$$\frac{\partial (\rho_g \overline{\psi})}{\partial t} + \frac{\partial \dot{m}''}{\partial z} = \dot{\omega}'''_{fg} \,, \tag{A.3}$$

$$\frac{\partial (\rho_g \overline{\psi} Y_j)}{\partial t} + \frac{\partial (\dot{m}'' Y_j)}{\partial z} = -\frac{\partial}{\partial z}(\overline{\psi} \rho_g D \frac{\partial Y_j}{\partial z}) + \dot{\omega}'''_{fj} - \dot{\omega}'''_{dj} \,, \tag{A.4}$$

$$\frac{\partial(\overline{\rho}\overline{h})}{\partial t} = \frac{\partial}{\partial z}(\overline{k}\frac{\partial T}{\partial z}) - \dot{Q}'''_{s-g} + \sum_{k=1}^{K}\dot{Q}'''_{s,k} - \frac{\partial \dot{q}''_r}{\partial z} + \sum_{i=1}^{M}((\dot{\omega}'''_{fi} - \dot{\omega}'''_{di})h_i) - h_{vl}(T - T_\infty)\ , \tag{A.5}$$

$$\dot{m}'' = -\frac{\overline{K}}{v}\frac{\partial P}{\partial z}\ , \tag{A.6}$$

$$\frac{\partial(\overline{\psi}\rho_g\overline{h_g})}{\partial t} + \frac{\partial(\dot{m}''_z\overline{h_g})}{\partial z} = \frac{\partial}{\partial z}(\overline{\psi}\rho_g D\frac{\partial \overline{h_g}}{\partial z}) + \sum_{j=1}^{N}(\dot{\omega}'''_{s,fj} - \dot{\omega}'''_{s,dj})h^*_{g,j} + \dot{Q}'''_{s-g}\ , \text{ and} \tag{A.7}$$

$$P\overline{M} = \rho_g R T_g\ , \tag{A.8}$$

where ρ is the density; M is the number of condensed-phase species; X is the volume fraction; $\dot{\omega}'''$ is the reaction rate; T is the temperature; Y_j is the jth species mass fraction; ψ is the porosity; K is the permeability/number of reactions; h_{vl} is the volumetric heat transfer coefficient; $\overline{M}$ is the mean molecular mass obtained from local volume fractions of all gaseous species; $\dot{q}''_r$ is the radiative heat-flux; $\dot{Q}'''$ is the volumetric rate of heat release/absorption; R is the universal gas constant; D is the diffusion coefficient; h is the enthalpy; P is the pressure; subscripts f, d, i, j, k, s, and g represent formation, destruction, condensed-phase species index, gas-phase species index, reaction index, solid, and gas; and * indicates that gas-phase species enthalpy is calculated at condensed phase temperature. The overbars over ρ, ψ, K, and k indicate an averaged value weighted by condensed-phase volume fraction, and the overbar over h indicates an averaged value weighted by condensed-phase mass fraction. [82, 105] give detailed descriptions about the underlying model and solver.

At the top surface of the domain ($z = 0$) the convective heat transfer coefficient ($h_{c,0}$) was $10\,\mathrm{W/m^2K}$, simulating it as open to atmosphere with a mass-transfer coefficient ($h_{m,0}$) of $0.02\,\mathrm{kg/m^2s}$. The pressure and (ambient) temperature at the top surface were set as $1\,\mathrm{atm}$ and $300\,\mathrm{K}$, respectively. The bottom surface ($z = 10\,\mathrm{cm}$) was modeled as insulated to match the experimental setup used for validation.To account for losses through the insulation a heat-transfer coefficient ($h_{c,L}$) of $3\,\mathrm{W/m^2K}$ was used. Zero mass flux ($\dot{m}''$) occurred at the bottom surface [79]. To ignite the sample a heat flux ($\dot{q}''_e$) of $25\,\mathrm{kW/m^2}$ was applied for $20\,\mathrm{min}$ at the top boundary to establish a self-sustained smoldering front. These boundary conditions were used for all simulations.

In order to account for heat losses through the side faces of the reactor box, a volumet-

ric heat transfer coefficient (h_{vl}) is incorporated into the energy conservation equation as shown in Eq. A.5. The natural convection coefficient is converted to the volumetric term by multiplying the ratio of side area to volume ratio of the reactor box. Thus h_{vl} is calculated using Eq. A.9 , where the coefficient of natural convection is calculated using Eq. A.10 [33].

$$h_{vl} = \frac{1}{L} h_{face} \ , \tag{A.9}$$

$$h_{face} = \frac{\overline{k}}{L}\left(0.825 + \frac{0.387 Ra^{1/6}}{(1 + (0.492/Pr)^{9/16})^{8/27}}\right)^2 \ , \tag{A.10}$$

where L is 5 cm.

A.4.2 Chemical kinetics

A heterogeneous reaction (k) involving condensed- and gas-phase species is described by

$$\mathrm{A}_k + \sum_{j=1}^{N} v'_{j,k}\,\mathrm{G}_j \longrightarrow v_{B,k}\,\mathrm{B}_k + \sum_{j=1}^{N} v''_{j,k}\,\mathrm{G}_j \ , \tag{A.11}$$

where $v'_{j,k}$ and $v''_{j,k}$ are the reactant and product stoichiometric coefficients for gas-phase species G_j in reaction k, $v_{B,k}$ is the stoichimetric coefficient for condensed-phase species B in reaction k, and N is the total number of gas-phase species. The destruction rate of species A in the above reaction is given by following Arrhenius equation:

$$\dot{\omega}'''_{dA_k} = Z_k \frac{(\overline{\rho} Y_{A_k} \Delta z)_{\sum}}{\Delta z} \left(\frac{\overline{\rho} Y_{A_k} \Delta z}{(\overline{\rho} Y_{A_k} \Delta z)_{\sum}}\right)^{n_k} \times \exp\left(-\frac{E_k}{RT}\right) g(Y_{\mathrm{O}_2}) \ , \tag{A.12}$$

where

$$(\overline{\rho} Y_{A_k} \Delta z)_{\sum} = \overline{\rho} Y_{A_k} \Delta z|_{t=0} + \int_0^t \dot{\omega}'''_{fi}(\tau) \Delta z(\tau) d\tau \ , \tag{A.13}$$

Z is the pre-exponential factor, E is the activation energy, n is the order of reaction, subscript dA stands for destruction of species A, and subscripts k, f, and i are reaction index, formation, and condensed-phase species index. Inert atmosphere is defined with

$g(Y_{O_2}) = 1$ and oxidative atmosphere with $g(Y_{O_2}) = (1 + Y_{O_2})^{n_{O_2,k}} - 1$ in Eq. (A.12) [82].

A chemical kinetic scheme with five reactions for each constituent (cellulose, hemicellulose, and lignin) was used. The five reactions include a drying step, pyrolysis step for the fuel, and three oxidation reactions of fuel, β-char, and α-char [23, 83]. The model includes 15 global reactions, with 15 condensed-phase species and 4 gas-phase species, where the following five reactions are repeated for cellulose, hemicellulose, and lignin (Fuel_k):

$$\text{Fuel}_k \cdot v_{w,dr}\,\text{H}_2\text{O} \longrightarrow \text{Fuel}_k + v_{w,dr}\,\text{H}_2\text{O}\,(\text{g}) \tag{R26}$$

$$\text{Fuel}_k \longrightarrow v_{\alpha,cp}\,\alpha\text{-Char}_{\text{f}_\text{k}} + v_{g,cp}\,\text{Gas} \tag{R27}$$

$$\text{Fuel}_k + v_{\text{O}_2,co}\,\text{O}_2 \longrightarrow v_{\beta,co}\,\beta\text{-Char}_{\text{f}_\text{k}} + v_{g,co}\text{Gas} \tag{R28}$$

$$\alpha\text{-Char}_{\text{f}_\text{k}} + v_{\text{O}_2,c\alpha o}\,\text{O}_2 \longrightarrow v_{a,c\alpha o}\text{Ash}_{\text{f}_\text{k}} + v_{g,c\alpha o}\text{Gas} \tag{R29}$$

$$\beta\text{-Char}_{\text{f}_\text{k}} + v_{\text{O}_2,c\beta o}\,\text{O}_2 \longrightarrow v_{a,c\beta o}\text{Ash}_{\text{f}_\text{k}} + v_{g,c\beta o}\text{Gas} \tag{R30}$$

where v is the stoichiometric coefficient; α and β indicate char produced from fuel pyrolysis and fuel oxidation reactions, respectively; and subscripts w, g, O_2, a, f_k, dr, o, p, αo, βo are water, gas, oxygen, ash, fuel constitute, drying, oxidation, pyrolysis, α-char oxidation, and β-char oxidation, respectively. The chemical kinetic parameters (pre-exponential factor, activation energy, order of reaction, and heat of reaction) were obtained from [23], stoichiometric coefficients for cellulose from [72] and for hemicellulose and lignin from [34]. The consumption of oxygen is calculated using $v_{\text{O}_2,k} = \Delta H/(-13.1)$ MJ/kg [34, 85].

A.4.3 Physical properties

Table A.1 lists the physical properties of condensed-phase species: solid density ($\rho_{s,i}$), thermal conductivity ($k_{s,i}$), and heat capacity (c_i). The bulk density of char is calculated using $\rho_{\text{char}} \approx v_{\text{char}} \times \rho_{\text{fuel}}$ and the bulk density of ash using $\rho_{\text{ash}} \approx \text{AC}/100 \times 10 \times \rho_{\text{fuel}}$, where AC stands for ash content [1, 38]. The ash contents of cellulose, hemicellulose, and lignin are 0.3%, 1.2% and 1.4% respectively [1, 88]. It was assumed assumed that the physical properties of fuels do not depend on temperature [79].

Porosity (ψ_i) and effective thermal conductivity (k_i) are calculated using $\psi_i = 1 -$

Table A.1: Thermophysical properties of condensed-phase species, taken from the literature for water, cellulose, hemicellulose, char, ash [1], and lignin [2–4].

Species	Solid density, $\rho_{s,i}$ (kg/m^3)	Thermal conductivity, $k_{s,i}$ ($W/(m\,K)$)	Heat capacity, c_i ($J/(kg\,K)$)
Water	1000	0.6	4186
Cellulose	1500	0.356	1674
Hemicellulose	1365	0.34	1200
Lignin	1305	0.39	1147
Char	1300	0.26	1260
Ash	2500	1.2	880

$\rho_i/\rho_{s,i}$ and $k_i = k_{s,i}(1-\psi_i) + \gamma_i \sigma T^3$, where σ is the Stefan–Boltzmann constant and γ_i is an empirical parameter for radiation across pores. Pore size, γ_i, and permeability are calculated for each condensed-phase species using

$$d_{po,i} \approx d_{p,i} = \frac{1}{S_i \times \rho} \tag{A.14}$$

$$K_i = 1 \times 10^{-3} \times d_{p,i}^2 \tag{A.15}$$

$$\gamma_i = 3 \times d_{po,i}\ , \tag{A.16}$$

where ρ is the density of the fuel, S_i is the particle surface area for species i, $d_{p,i}$ is the particle size, K_i is the permeability, and $d_{po,i}$ is the pore size. For all simulations the moisture content (MC) was 10% to represent the natural moisture present in fuels; the bulk density of moist fuel is calculated as $\rho_{\text{wet fuel}} = \rho_{\text{dry fuel}} \times (1 + \text{MC})$.

A.5 Results and Discussion

A.5.1 Lignin selection

Organosolv lignin was used for this study after evaluation of 5 commercially available sources of lignin, as explained in this subsection. An organosolv lignin derived from pine was selected because it has low inorganic content (<1%), has propagation velocities that are relatively similar to combinations of cellulose and hemicellulose, and did not exhibit temperature decay at high lignin contents. The selection of lignin is important

because how the lignin is extracted can significantly affect the chemical structure of the compound and the smoldering behavior, as discussed in this subsection [127, 128].

A.5.1.1 Selection of lignin class

Two classes of lignins were evaluated prior to conducting the experiments: sulfonated or organosolv. The former is created by adding an alkali sulfonate to the biomass to make the lignin soluble [127]. The latter lignin is created by using using organic solvents to separate lignin from the rest of the biomass [128]. Three sulfonated lignins (Marasperse, Norlig, and Ufoxane) obtained from Borregaard and an two organosolv lignins obtained from Attis Innovations were evaluated to determine their suitability for smoldering tests. The sulfonated lignins were powders. The organosolv lignins were solid, with one was derived from pine, and the other from tobacco. The organosolv lignins had residual butanol (the organic solvent) that was removed by heating the lignins to 130 °C, which is above the boiling point of butanol, for at least 12 hours prior to testing. Once the butanol was removed the organosolv lignins were a porous solid, so they were then powderized and filtered with No. 14 (1.41 mm) mesh to remove larger particles.

Table A.2 shows the residual inorganic content and horizontal propagation velocities used to evaluate the suitability of the different lignins. The Marasperse and Ufoxane have relatively high inorganic contents (approximately 70% by mass), so a large portion of the fuel is not lignin. The Norlig had a lower inorganic content of 18%. The organosolv lignins have a relatively small inorganic content (<1%). Using one of the sulfonated lignins in burns with other fuels would mean that the inorganic content of the mixture would change as the lignin content was changed, arguably making it more difficult to identify the cause of differences in smoldering behavior.

Each of the aforementioned lignins were burned in combination with cellulose and hemicellulose to determine what impact the lignin type had on smoldering propagation. The fuel content for these burns was 20% lignin (including inorganic content), 60% cellulose, and 20% hemicellulose, and the density was 300 kg/m^3. The horizontal propagation rates for mixtures with Marasperse and Ufoxane had relatively fast propagation rates (10 and 8.4 cm/hr, respectively). The propagation velocities were significantly slower when the Norlig (3.8 cm/hr) or tobacco-derived organosolv lignin (4.5 cm/hr) was used. For reference, combinations of cellulose and hemicellulose at the same density ranged from

about 3.9 cm/hr for 100% cellulose to 6.3 cm/hr for 50% cellulose (and 50% hemicellulose) [40]. It is expected that the smoldering propagation rate would be similar to or less than corresponding tests with cellulose and hemicellulose because lignin has a higher activation energy and higher pyrolysis temperatures than cellulose and hemicellulose [11, 22, 126]. However, this trend was not observed for the Marsperse and Ufoxane lignin, which which had velocities roughly >50% greater than that expected. It is plausible that the other constituents within the Marasperse and Ufoxane lignin bias the smoldering velocity higher than pure lignin. It is noted that fuels with Norlig lignin had more appropriate propagation velocities. However Norlig still had a relatively high inorganic content, so the inorganic content would still change substantially as lignin content was varied. It was decided to use Organosolv derived lignins because of the small inorganic content and the appropriate horizontal propagation velocities.

Table A.2: Horizontal propagation velocities and inorganic content for multiple lignins in mixtures of 20% lignin, 60% cellulose, and 20% hemicellulose. The first three lignins are sulfonated lignins, and the last two are the organosolv lignin.

Lignin Type	Horizontal Propagation (cm/h)	Inorganic Content
Marasperse	10.0	71%
Ufoxane	8.4	66%
Norlig	3.9	18%
organosolv lignin (tobacco)	4.5	<1%
organosolv lignin (pine)	4.8	<1%

A.5.1.2 Comparing Organosolv Lignins

Figure A.3 shows downward propagation velocities for pine-derived and tobacco-derived organosolv lignins. The velocities were evaluated at varying lignin contents and three remainder (non-lignin) fuel contents. The data for the tobacco-derived lignin are the average of three tests because of limited quantities of fuel, and the data for the pine lignin are the average of four to seven tests. Due to the limited number of tests, the uncertainty for the tobacco lignin was very large (20-80%). The lignin from the two feedstocks have some similar global trends in propagation rates, as both show a decrease in velocity with

increasing lignin content and an increase going from a residual (non-lignin) fuel content of 100% cellulose to 75% cellulose (and 25% hemicellulose). However, only one of the tests (out of 18) with the tobacco lignin was larger than the mean value for the pine lignin. Thus, there is strong statistical evidence ($p < 0.001$, ANOVA) that the samples with pine lignin have higher propagation velocities than fuels with tobacco-derived lignin. This change is most evident in the results for the 100% cellulose case, as there is less of a decrease in velocity from 0 to 30% lignin when the pine lignin is used (∼20% decrease compared to a 60% decrease). Of note, several of the burns with the tobacco-derived lignin exhibited a decay in peak temperatures with the depth of the fuel, which caused some of the differences in downward propagation between the two lignins. The peak temperature decay was not observed with the pine lignin. This temperature decay has not been seen in natural fuels with high lignin such as peat at dry conditions [38]. Ultimately, the pine lignin was used for the remainder of this study. The rationale for this decision was twofold. First, the decrease in peak temperature with depth was observed in the tobacco-derived lignin but not in the pine lignin. Second, the pine lignin is more similar to lignin in smoldering fuels from trees relevant in wildland fire (ponderosa pine, douglas-fir, etc.).

A.5.2 Downward Propagation

Downward propagation velocities, as shown in Figure A.4, were determined at varying lignin content (using the organosolv lignin derived from pine) and constant densities. Corresponding calculations are included for comparison (open symbols) and are discussed shortly. The tests for plot on the left hand side had a density of $200\,\mathrm{kg/m^3}$, and tests for the plot on the right had a density of $300\,\mathrm{kg/m^3}$. For the non-lignin portion of the fuel, three fuel combinations were evaluated: 100% cellulose, 75% cellulose (and 25% hemicellulose), and 50% cellulose (and 50% hemicellulose). Each data point is the average of at least four tests. Uncertainty bars are the precision uncertainties reported with 95% confidence. The fuels at the lower density have propagation velocities that are about 1.3-1.5 times faster than the same mixtures at the higher density. This increase in propagation velocity is largely due to the additional fuel required to burn, as the higher density fuels has 50% more mass to burn in a given volume. Two trends are highlighted with regards to the fuel content. First, for all the fuel mixtures and densities,

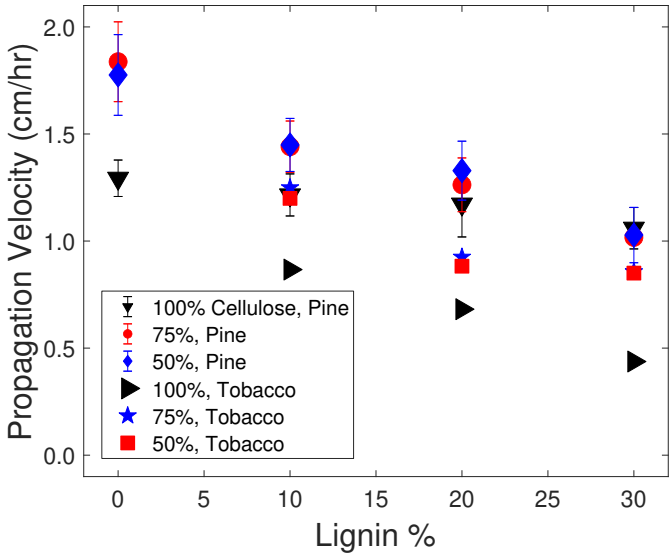

Figure A.3: Measured downward propagation velocities determined at varying lignin contents and hemicellulose, cellulose mixtures. The pine lignin markers are the estimated mean from 4 to 6 tests. The tobacco lignin markers are the average of three tests. Because of the limited number of tests at each condition, the error bars for the individual points for the tobacco lignin were large. Thus, the error bars were not shown for clarity, as only one test with the tobacco lignin (out of 18) had a propagation velocity greater than the average with the pine lignin

the downward propagation velocities decrease as the lignin content increases from 0 to 30%. These decreases result from the increased activation energy and slower reaction rates for lignin compared with cellulose and hemicellulose, as is described later with the computational results. Second, fuels with hemicellulose in the non-lignin portion have higher propagation velocities than those with just cellulose, but the sensitivity of propagation velocities to cellulose/hemicellulose decreases as lignin content increases. The reduced sensitivity suggests that the amount of lignin in the fuel can have the greatest influence on propagation rates, as evidenced by the propagation velocities at 30% and 40% lignin being within 5% of each other regardless of the non-lignin content for the 300 $\mathrm{kg/m^3}$ case.

Table A.3 shows a multiple linear regression model that was developed based on the experimental results shown in Figure A.4. The purpose of the model is to quantify

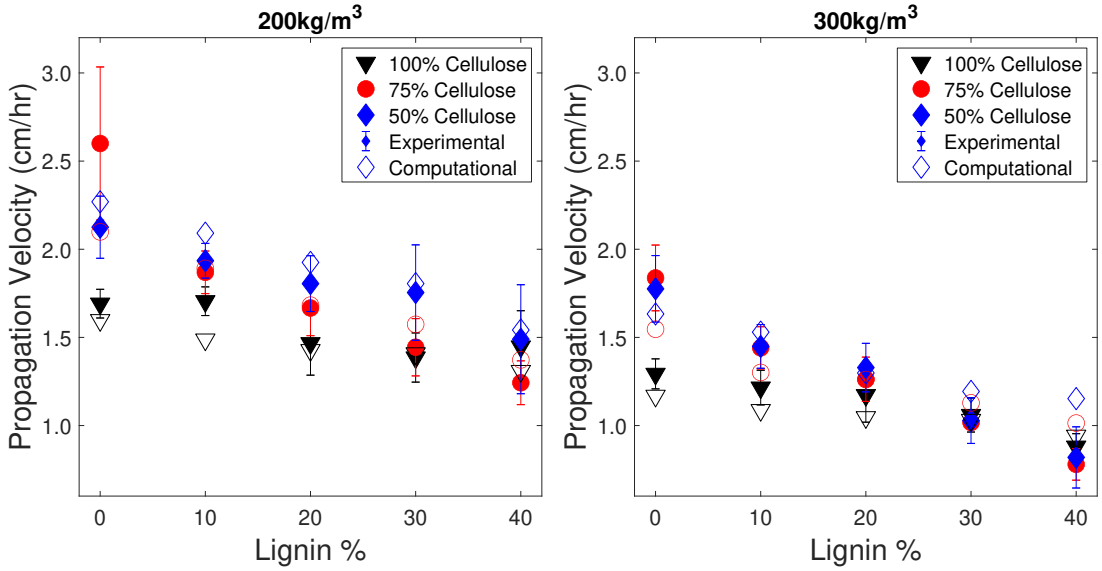

Figure A.4: Experimental and computational downward smoldering propagation velocities with varying lignin content at densities of 200 kg/m^3 (left) and 300 kg/m^3 (right).

the impact of lignin, cellulose/hemicellulose content, and density on the smoldering propagation velocity. In Figure A.4, the effect of hemicellulose on the propagation velocities is nonlinear. There is little evidence of an decrease (or increase) in propagation velocities when the cellulose content in the remainder fuel increases from 50% to 75% cellulose. However, there is a notable decrease in propagation velocity when increasing from 75% to 100% cellulose, as evidenced by the 25% difference in propagation velocity between the two fuel contents at 0% lignin. As such, a binary variable indicating the presence of hemicellulose was used. Additionally, a term of lignin*hemicellulose was used to account for the steeper slope observed in fuels with hemicellulose. All four of these values (lignin, density, hemicellulose, and lignin*hemicellulose) were strongly significant. Notably, the negative lignin*hemicellulose term confirms that the propagation velocities decrease with increasing lignin content and that the impact of hemicellulose on the propagation rates decreases with increasing lignin content. As a result, the model estimates a total decease of 1.05 cm/hr from 0 to 40% lignin for fuels with hemicellulose in the non-lignin portion, compared with 0.36 cm/hr for fuels with 100% cellulose in the non-lignin portion. The density causes a decrease of approximately 0.5 cm/hr from

200 to 300 kg/m^3. Having hemicellulose in the fuel increases the propagation velocity by approximately 0.56 cm/hr at 0% lignin, but because of the negative lignin*hemicellulose term the increase from hemicellulose is about 0 at >30% lignin. The adjusted R^2 = 0.84 for all velocity values, but there is a limit in how high R^2 can be because of the variability observed among all of the measurements. The value of R^2 increases to 0.91 when comparing the model to the mean propagation velocity values, indicating that the model is capturing much of the observed behavior. It is acknowledged that this model is limited at lignin contents greater than 40%. For instance, it predicts the propagation velocity to decrease when hemicellulose is present in fuels with lignin contents greater than 40%. Additionally, the affects of density may be nonlinear, so this model should not be used outside of this range (200-300 kg/m^3).

Table A.3: Multiple linear regression model for predicting the mean downward propagation velocity as a function of density, lignin, and hemicellulose.

Coefficient	Estimate	Standard Error	t-value	p-value	significance code
Intercept	2.750560	0.091726	29.987	< 2e-16	***
Lignin%	-0.008953	0.001913	-4.680	7.15e-06	***
Density	-0.004957	0.000310	-15.989	< 2e-16	***
Hemicellulose	0.561879	0.054455	10.318	< 2e16	***
Lig*Hemi	-0.017104	0.002301	-7.432	1.31e-11	***

The calculated computational propagation velocities are shown in Figure A.4 as the open symbols. There is generally good agreement between the computational and experimental velocities. With a few exceptions, the computational and experimental propagation velocities agree within 10% of each other, indicating that the model is capturing most of the physical processes. The computational propagation velocities capture the global trends of the experimental results; both the computational and experimental velocities decrease with increasing lignin content and increase with hemicellulose content. Additionally, the modeled results show the sensitivity of the smoldering propagation rates to the presence of hemicellulose decrease as the lignin content increases. It is noted that attaining this level of agreement only occurred after the model accounted for heat losses from the char layer, which will be discussed further below.

Calculated reaction rates were used to understand when and how fast reactions are

occurring in the different constituents. The left-hand plot in Figure A.5 shows the reaction rates for fuels composed of 10% and 30% lignin respectively at a depth of 5 cm. The non-lignin portion for both fuels is 75% cellulose (remainder hemicellulose), and the density is 300 kg/m^3. Of the three constituents, lignin pyrolyzes at higher temperatures and over a longer time. As a result, more heat and time are required to pyrolyze and oxidize the lignin, and the smoldering propagation slows. Unlike lignin, hemicellulose pyrolyzes at the lowest temperatures of the three constituents, as shown in the right-hand plot of Figure A.5, and the cellulose pyrolyzes rapidly at a more moderate temperature. The earlier pyrolysis of hemicellulose (and cellulose) results in less material needing to be heating, allowing other fuel constituents to pyrolyze and oxidize more readily. This effect is what causes the increase in the temperature with time when the cellulose pyrolyzes in Figure A.5. The increase in propagation from the earlier pyrolysis of hemicellulose has been noted previously in burns of just cellulose and hemicellulose [40].

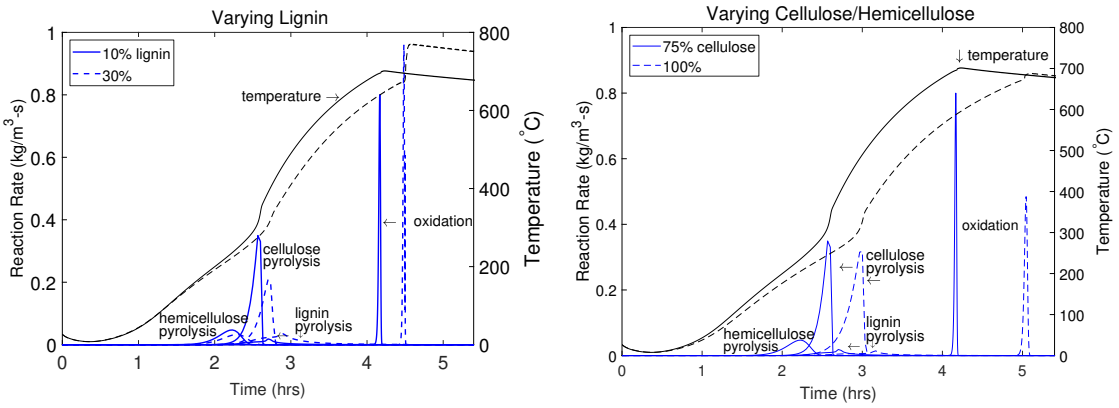

Figure A.5: Computational reactions rates with time at a depth of 5 cm. The density is 300 kg/m^3 for all cases. In the plot on the left, the fuel composed 10% and 30% lignin, and the non-lignin portion of the fuel is 75% cellulose (and 25% hemicellulose). In the plot on the right, the fuel is composed of 10% lignin with remainder fuel contents of 75% and 100% cellulose. The numbers on the plot refer to the following reactions: 1. hemicellulose pyrolysis 2. cellulose pyrolysis 3. lignin pyrolysis and 4. oxidation. The oxidation for all three constituents occurs is simultaneous.

The regression model is useful in quantifying the impact of fuel content and density, and the computational reaction rates give insights into the decrease in propagation velocities with lignin content. However, this analysis doesn't fully explain why the

sensitivity of propagation velocities to hemicellulose content is lower at higher lignin contents. It is plausible that this trend may be due to decreases in peak temperature and increases char thickness that occur with increasing lignin content, which counters potential increases in propagation rates because of hemicellulose. It is expected that the propagation velocities will tend to decrease with lower peak temperatures because of slower reaction rates. Additionally, the propagation velocities will tend to decrease with increasing char thickness all else being equal. The char layer occurs because of it takes a significant amount of time for the char to fully oxidize. The bottom of the char layer is pyrolysis front, where char is being formed. The top of the char layer is the top surface of the fuel for the tests in this study, as the ash layer is minimal. A thicker char layer would indicate that the char is being consumed slowly and that there are more heat losses to the surroundings due to the additional mass at an elevated temperature. To help evaluate sensitivities of the propagation rates to maximum temperatures, Figure A.6 shows the propagation velocities relative to maximum temperature for every test included in Figure A.4. The peak temperature reported was the maximum value that occurred in the thermocouples from 2 to 4 cm below the surface, as described in the Experimental Methods. Propagation velocities are plotted as a function of char thickness in Figure A.7. A full description of how the char layer thickness was determined can be found in the Experimental Methods section. Overall, there is very strong evidence ($p< 0.0001$) that propagation velocities increase with higher peak temperatures and decrease with increasing char thickness, although the scatter is relatively large, as $R^2 = 0.54$ and 0.41 for temperature and char thickness respectively. While neither is a great predictor on their own, a multiple linear regression model with maximum temperature, char thickness, and density has an R^2 value of 0.67, and R^2 increases to 0.78 when mean values are used. Figure A.6 and A.7 support hypothesis that propagation velocities increase with higher temperatures and decrease with thicker char layers.

In an effort to better understand the influence of the lignin content, Figures A.8 and A.9 show the mean maximum temperatures and char layer thickness respectively relative to the lignin content and density. For these tests, there is little statistical evidence of density having an impact maximum temperature and char layer thickness ($p> 0.15$). However, the plots are still separated based on the density, since density has been shown to impact maximum temperature [112]. In Figure A.8, the experimental temperatures agree within about 15 °C (and within error bars) between 0 and 20% lignin, but decrease

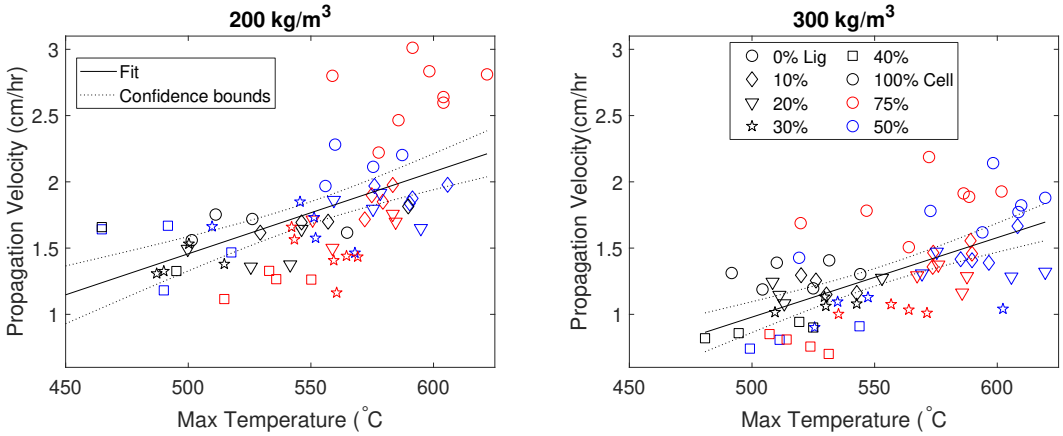

Figure A.6: Propagation velocity and maximum temperature for every test in Figure A.4. Marker shape corresponds to lignin content, and the color corresponds to the contents of the non-lignin portion.

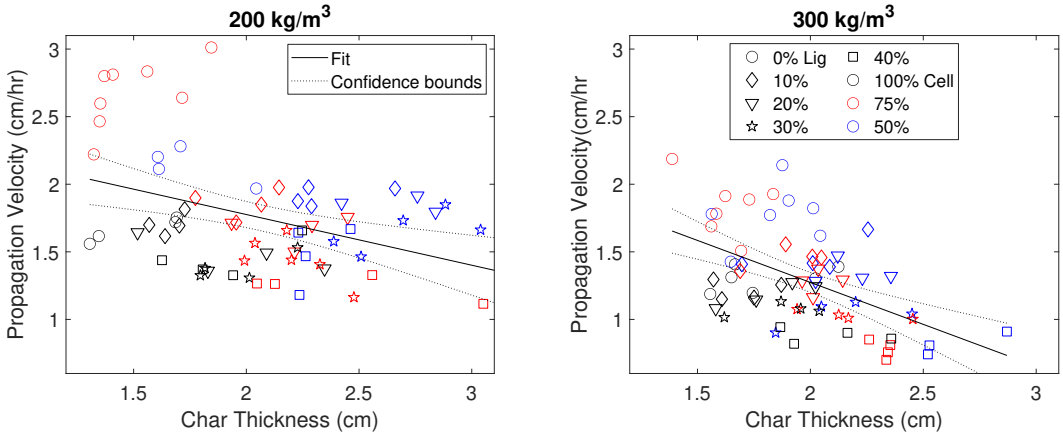

Figure A.7: Propagation velocity and char thickness for every test in Figure A.4. Marker shape corresponds to lignin content, and the color corresponds to the contents of the non-lignin portion.

by about 50 °C between 20% and 40% lignin. The decrease in temperature with lignin content is attributed to the slower reactions that occur in lignin when compared to cellulose and hemicellulose. In Figure A.9, the char thickness increases by about 25% from 0 to 40% lignin, with the largest increases between 0 and 20% lignin. The char thickness correlates strongly with char yield, as char lignin and hemicellulose have higher

char yields than cellulose [129]. When hemicellulose content increases, the increase in propagation velocities from higher temperatures offsets the potential decrease from higher char thickness. However, as lignin content increases, the maximum temperatures decrease and the char layer thickness increases. The slower burning rate and thicker char layer results in more total heat lost to the surroundings, and slower propagation velocities.

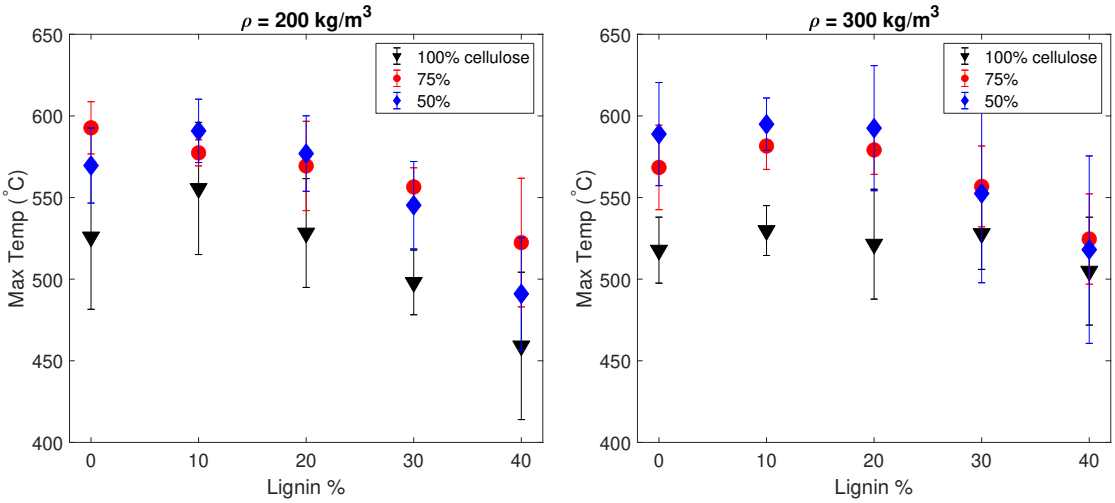

Figure A.8: Peak temperature with varying lignin content for three non-lignin fuel contents at 200 (left) 300 kg/m^3 (right). The experimental points are the mean from 4-6 tests with 95% confidence.

To further evaluate the role of heat losses through the char layer, Figures A.10 and A.11 show calculated propagation velocities and maximum temperatures with and without estimated heat losses through the char layer. These plots are used to illustrate the importance of accounting for heat losses through the sides of the reactor experimentally when developing 1-D models. Initially, the computational velocities had a much smaller decrease in velocity with increasing lignin content then the experimental propagation velocities, particularly when the density was 300 kg/m^3. As the velocities got to higher lignin contents, the computational values deviate further from the experimental values. This is at least partially due to differences in peak temperature, as illustrated in Figure A.11. To help account for these discrepancies, a heat loss term from the char was added to the model. The char layer thicknesses in Figure A.9 were used in the 1-D model to determine heat losses. After the heat losses were added to the model, there was notably

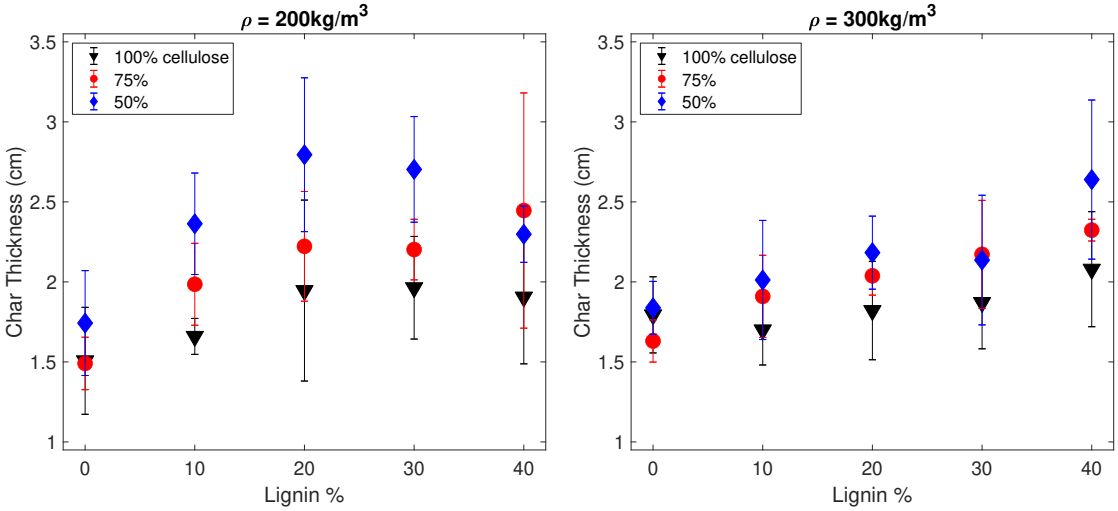

Figure A.9: Char thickness with varying lignin content for three non-lignin fuel contents. The points are the mean from 4-6 tests with 95% confidence. The tests represented in the plot on the left have a density of 200 kg/m^3, the those in the plot on the right have a density of 300 kg/m^3

better agreement between the computational velocities and the experimental velocities. In particular, the computational velocities with heat losses showed the larger decrease with lignin when hemicellulose is present, and showed that the impact of hemicellulose is smaller at higher lignin contents. While there is still an increase in maximum temperature even when adding heat losses to the model, the increase is smaller than when there are no heat losses. Additionally, the difference in peak temperature between the two computational models increases as lignin content increases, indicating that the heat losses increase as lignin content increases.

Comparing the computational and experimental temperature profiles can help determine if the computational model is capturing the physics controlling the smoldering experimentally. It is difficult to do this solely by comparing propagation velocities and peak temperatures. Figure A.12 shows the temperature profiles at 3 locations (3 cm, 5 cm, and 6 cm below the surface) for 8 tests under different fuel conditions. The computational and experimental profiles generally have a pretty similar shape for the cases 5cm and 6cm below the surface up to about 300 °C. It is noted that many of the tests were stopped once the thermocouple 6 cm below the surface reached 300 °C, which is why the profiles end

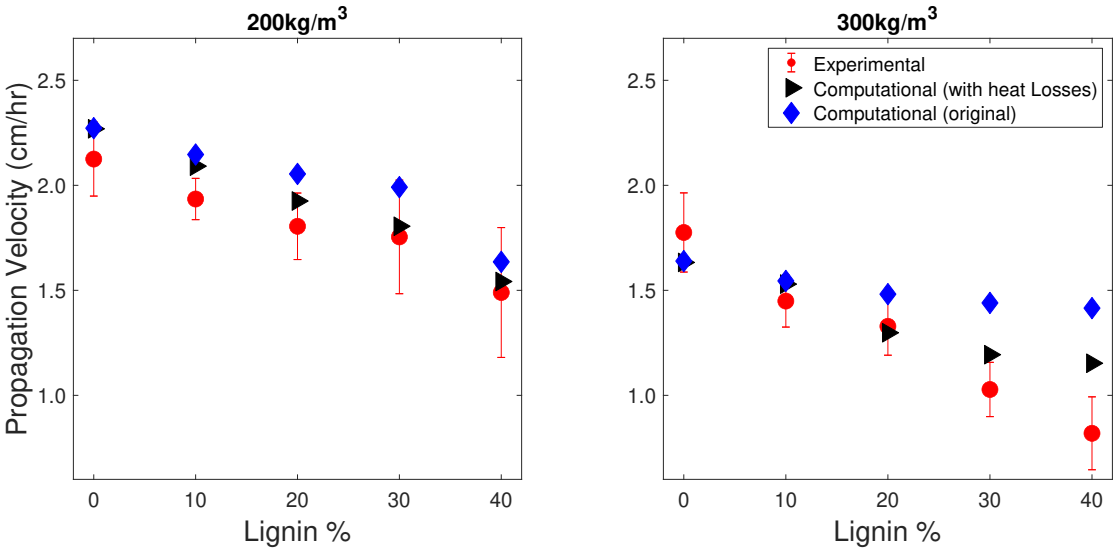

Figure A.10: Experimental propagation velocities compared to computational propagation velocities with and without heat losses. The non-lignin portion of the fuel for these tests was 50% cellulose and 50% hemicellulose.

abruptly. There are two notable differences between the model and experimental results. First, at 3cm, the model has a faster rise in temperature than the experimental results. This may be due to differences in ignition. Ignition occurs with a flux at the top in the computational model. However, in the experiments, the fuel is ignited with a cartridge heater in the center of the fuel, so 3-D effects may impact how quickly the thermocouple 3 cm below increases in temperature. Second, the peak temperatures are higher for the computational model than for the experimental values. This may be due, in part, to the thermocouples not measuring the maximum possible temperature. Most tests we'll fall below the maximum possible value, and the thermocouples themselves cause small heat losses due to their invasive nature. Despite these differences, the model captures the time it takes for the smoldering to propagation between 3cm and 6cm below the surface and the behavior 5-6 cm below the surface, making it a useful tool for evaluating smoldering behavior.

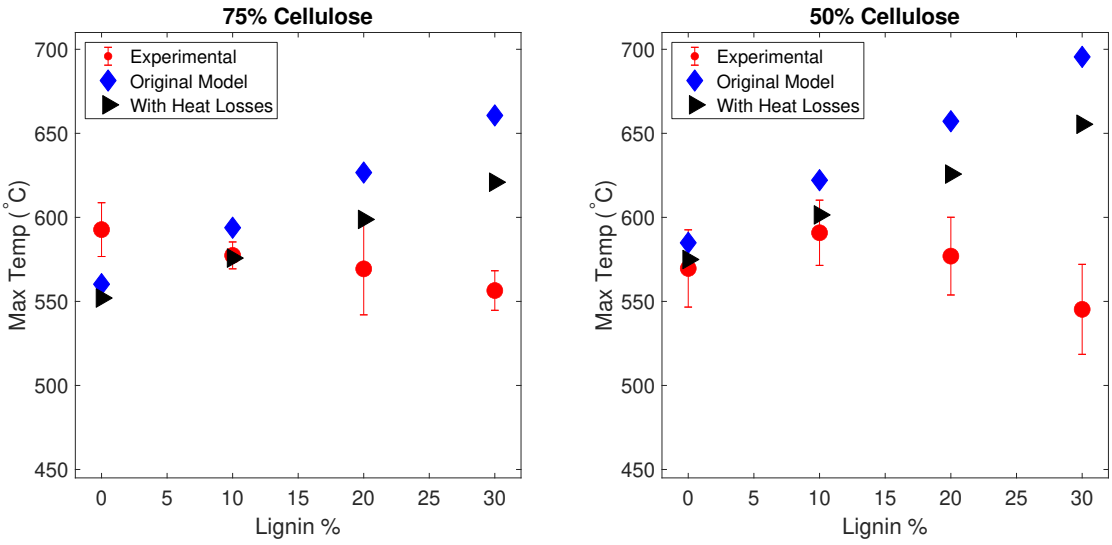

Figure A.11: Comparison of experimental peak temperatures to the computational peak temperatures with and without accounting for heat losses. The title represents the composition of the non-lignin portion of the fuel, with the remainder being hemicellulose. The density is 200 kg/m^3

A.5.3 Horizontal Propagation

Additional tests were performed to understand how the presence of lignin affects horizontal propagation velcoities. The density (200 kg/m^3) and content of the non-lignin components of the fuel were held constant. Considering horizontal propagation velocities is necessary because of differences in the physics controlling horizontal and downward smoldering propagation [38]. The measured horizontal propagation velocities are shown in Figure A.13. Each point is the average propagation velocity from three tests. For the case with 40% lignin and the remainder cellulose, a density of 200 kg/m^3, could not be obtained in the horizontal reactor, so the black "x" is the result of one test at a density of 220 kg/m^3. Overall, the horizontal propagation velocities are 2-3 times larger than the corresponding downward propagation velocities in Figure A.4. Two trends match the behavior of the downward propagation velocities: first, when the non-lignin portion is 75% or 50% cellulose (with residual hemicellulose), the propagation velocity decreases roughly linearly with increasing lignin content from about 6.0 cm/hr at 0% lignin to 4.0 cm/hr at 40% lignin, about a 33% decrease. Similarly, the downward propagation velocities in Figure A.4

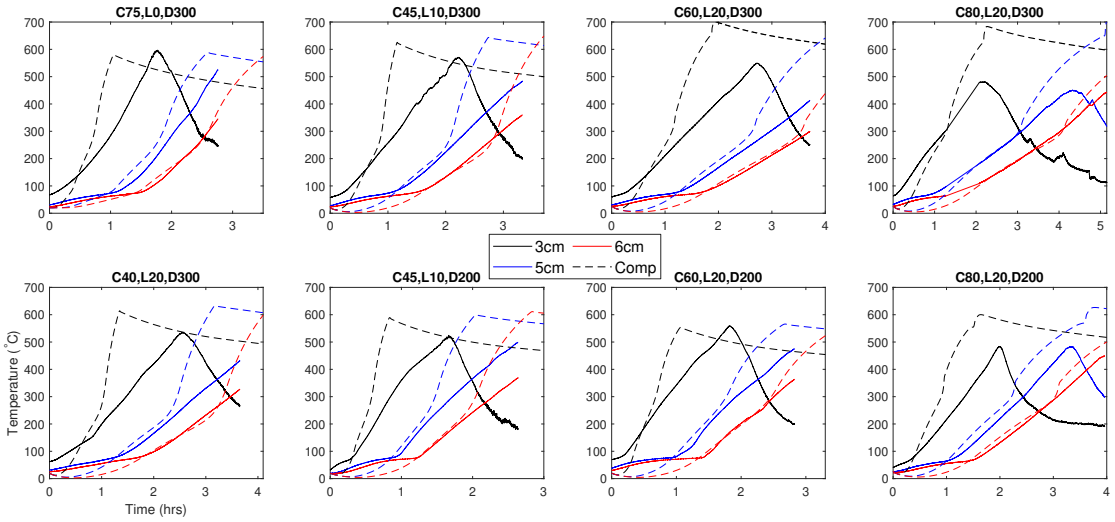

Figure A.12: Comparison of computational and and experimental temperature profiles at 3, 5, and 6 cm below the surface of the fuel. The experimental values are marked with solid lines, and the computational values are marked with dashed lines. The start time for the experimental values was adjusted to account for differences in ignition procedure. The experimental values are from one of the 4-6 tests at the listed condition. The values in the plot titles represent the percentage of cellulose, the percentage of hemicellulose, and the density in kg/m^3, respectively. The remainder of the fuel was hemicellulose.

decrease by about 30% from 0 to 40% lignin for the same fuels. Second, at lignin contents equal to or greater than 20%, the content of the non-lignin portion of the fuel makes relatively little difference in the propagation velocities, as all three cases have propagation velocities that agree with 10%. Likewise, the amount of cellulose/hemicellulose had little impact on the downward propagation velocities at higher lignin contents as well, as the values were within 5% of each other.

A third trend was not observed in the downward smoldering velocities. For the case with 100% cellulose in the non-lignin portion of the fuel, the propagation velocity increases by about 20% as the lignin content increases from 0 to 20%. Conversely, the downward propagation velocities only decrease with lignin content when the remainder is 100% cellulose (Figure A.4). The increase horizontal propagation from 0 to 20% lignin is attributed to structural effects. When the fuel shrinks as the smoldering front propagates, it can create cracks in the fuel that slow the horizontal smoldering spread. Cracks in

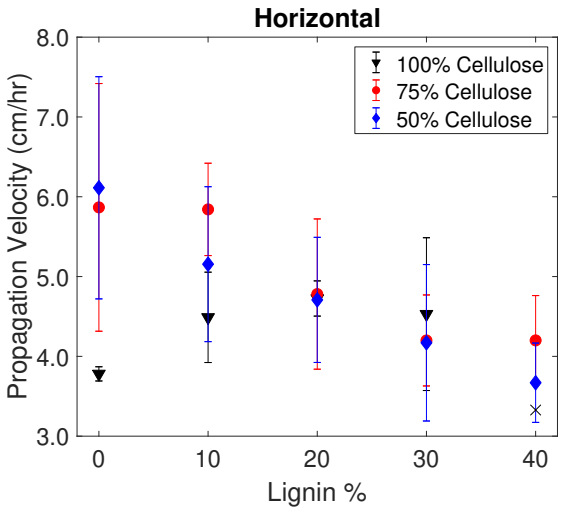

Figure A.13: Experimental horizontal propagation velocities with varying lignin content for three fuel contents in the non-lignin portion. The points are the average of three tests. The density was 200 kg/m^3. For the mixture of 40% lignin and 60% cellulose (100% of remainder), a density of 200 kg/m^3 in the horizontal reactor. The black "x" is for one test with this content at 220 kg/m^3.

the fuel bed will limit the heat conduction to unburned fuel, slowing the smoldering propagation, particularly if the cracks are near the pyrolysis front. The fuel composition can impact the cracking behavior, as illustrated in the visual images in Figure A.14. The image on the right (100% cellulose) has much longer and wider cracks than the image on the left (80% cellulose, 20% lignin). Cellulose has longer fibers that can bind together, resulting in larger cracks as the fuel shrinks. Having some lignin helps those cracks become smaller and more distributed. Comparing the 100% cellulose/0%lignin case to the 80%cellulose/20% lignin case, twice as many large (>2 mm across) cracks occurred in the 100% cellulose case, and the cracks were three times as long. Additionally, the cracks occurred further from pyrolysis front. The frequency, size, and location of the cracks ultimately result in slower propagation velocities.

Figure A.14: Images for burns with 100% cellulose (right) and 80% cellulose/20%lignin (left). Numerous large, dark cracks are visible outside the burned area in the 100% cellulose case.

A.6 Conclusions

Sensitivities of downward and horizontal propagation velocities were evaluated for fuels with varying contents of lignin, cellulose, and hemicellulose, and varying density. A multi-variable linear model was developed to quantify the impacts of fuel content and density. A one-dimensional computational model was used to determine corresponding downward propagation velocities and evaluate the chemical reaction rates. Peak temperatures and char thicknesses were determined to further evaluate the observed trends in the downward smoldering propagation velocities.

The specific conclusions from this work are as follows.

- Increasing lignin content causes a decrease in horizontal and downward smoldering propagation velocities at a fixed density and non-lignin fuel content. The reduction in propagation velocity is caused by slower pyrolysis and higher activation energy of lignin than cellulose and hemicellulose. It is expected that natural fuels with higher lignin contents will tend to smolder slower than similar fuels with lower lignin content, if other parameters (e.g., density, porosity) are equal.

- Once a minimum concentration of hemicellulose is present in the fuel, there is no

statistical evidence that additional hemicellulose increases the propagation velocity, regardless of lignin content. Having some earlier pyrolysis and oxidation from the hemicellulose increases the propagation velocities, but there are diminishing affects, as the higher temperatures associated with hemicellulose are offset by higher char thickness.

- As the lignin content increases, the impact of the relative amount of hemicellulose and cellulose decreases. With $\geq 20\%$ lignin content in the fuel, lignin is the dominant chemical component in determining smoldering propagation behavior.
- Fuels with lignin derived from pine had faster propagation velocities because of earlier pyrolysis and oxidation compared to lignin derived from tobacco. Additionally, some sulfonated lignins had higher horizontal propagation velocities than the organosolv lignins, but had high ash content (>60%). These findings indicates that the source of the lignin feedstock can have an impact on smoldering behavior, and may need to be considered when comparing these results to natural fuels.
- Experimentally, peak temperatures decrease with lignin. The decrease in peak temperature is caused the heat losses from the thicker char layer and the slower pyrolysis and oxidation of lignin. The computational peak temperatures increase with lignin because of the higher char yield of lignin. However, the heat losses resulting from the longer time required for lignin to burn counteract the higher char yield and heat of combustion of lignin, causing a decrease in temperature.
- Heat losses through the sides of the reactor have an impact on downward propagation velocities, and need to be taken into account in 1-D models. When heat losses were added to the 1-D model, there better agreement with experimental downward smoldering results.

Acknowledgements

This research was funded by the Strategic Environmental Research and Development Program (SERDP) under contract number (W912HQ-16-C-0045), project number RC-2651. The help of Attis Industries in supplying the organosolv lignin is gratefully acknowledged.

Disclaimer

The views, opinions, and/or findings contained in this report are those of the authors and should not be construed as an official Department of Defense position of decision unless so designated by other official documentation.